New Jersey Institute of Technology
Digital Commons @ NJIT

Theses | Electronic Theses and Dissertations

Spring 5-31-2010

Stochastic and deterministic dynamics investigation of the microstructure of granular materials

Vishagan Ratnaswamy
New Jersey Institute of Technology

Follow this and additional works at: https://digitalcommons.njit.edu/theses

 Part of the Mechanical Engineering Commons

Recommended Citation

Ratnaswamy, Vishagan, "Stochastic and deterministic dynamics investigation of the microstructure of granular materials" (2010). *Theses*. 69.
https://digitalcommons.njit.edu/theses/69

This Thesis is brought to you for free and open access by the Electronic Theses and Dissertations at Digital Commons @ NJIT. It has been accepted for inclusion in Theses by an authorized administrator of Digital Commons @ NJIT. For more information, please contact digitalcommons@njit.edu.

Copyright Warning & Restrictions

The copyright law of the United States (Title 17, United States Code) governs the making of photocopies or other reproductions of copyrighted material.

Under certain conditions specified in the law, libraries and archives are authorized to furnish a photocopy or other reproduction. One of these specified conditions is that the photocopy or reproduction is not to be "used for any purpose other than private study, scholarship, or research." If a, user makes a request for, or later uses, a photocopy or reproduction for purposes in excess of "fair use" that user may be liable for copyright infringement,

This institution reserves the right to refuse to accept a copying order if, in its judgment, fulfillment of the order would involve violation of copyright law.

Please Note: The author retains the copyright while the New Jersey Institute of Technology reserves the right to distribute this thesis or dissertation

Printing note: If you do not wish to print this page, then select "Pages from: first page # to: last page #" on the print dialog screen

NJIT
New Jersey's Science & Technology University

The Van Houten library has removed some of the personal information and all signatures from the approval page and biographical sketches of theses and dissertations in order to protect the identity of NJIT graduates and faculty.

ABSTRACT

STOCHASTIC AND DETERMINISTIC DYNAMICS INVESTIGATION OF THE MICROSTRUCTURE OF GRANULAR MATERIALS

by
Vishagan Ratnaswamy

Granular materials are ubiquitous in one's daily life. They can be found in the cereal you eat, the sugar you put in your coffee or the sand you walk on in the beach. The study of granular materials has a rich history dating back to the 17th century where Kepler studied the packing of particles. The compaction of granular materials is a problem that is studied by using theory, experiments and simulations. While these studies have yielded some important results, there still are many details about the mechanisms of granular compaction that are unknown.

In this thesis, the density relaxation phenomenon is modeled using both Monte Carlo and discrete element simulations to investigate the effects of regular taps applied to a vessel having a planar floor filled with monodisperse spheres. Results suggest the existence of a critical tap intensity which produces a maximum bulk solids fraction. A key result that is found in this thesis is the mechanism responsible for the relaxation phenomenon is an evolving ordered packing structure propagating upwards from the plane floor.

STOCHASTIC AND DETERMINISTIC DYNAMICS INVESTIGATION OF THE MICROSTRUCTURE OF GRANULAR MATERIALS

by
Vishagan Ratnaswamy

A Thesis
Submitted to the Faculty of
New Jersey Institute of Technology
In Partial Fulfillment of the Requirements for the Degree of
Master of Science in Mechanical Engineering

Department of Mechanical and Industrial Engineering

May 2010

APPROVAL PAGE

STOCHASTIC AND DETERMINISTIC DYNAMICS INVESTIGATION OF THE MICROSTRUCTURE OF GRANULAR MATERIALS

Vishagan Ratnaswamy

5-12-2010

Dr. Anthony Rosato, Thesis Advisor — Date
Professor of Mechanical Engineering, NJIT

4-26-2010

Dr. David Horntrop, Committee Member — Date
Associate Professor of Mathematical Sciences, NJIT

4-26-2010

Dr. Pushpendra Singh, Committee Member — Date
Professor of Mechanical Engineering, NJIT

4/26/10

Dr. Ian Fischer, Committee Member — Date
Professor of Mechanical Engineering, NJIT

BIOGRAPHICAL SKETCH

Author: Vishagan Ratnaswamy

Degree: Master of Science

Date: May 2010

Undergraduate and Graduate Education:

- Master of Science in Mechanical Engineering
  New Jersey Institute of Technology, Newark, New Jersey, USA 2010

- Bachelor of Science in Applied Mathematics
  New Jersey Institute of Technology, Newark, New Jersey, USA 2009

- Bachelor of Science in Mechanical Engineering
  New Jersey Institute of Technology, Newark, New Jersey, USA 2009

Major: Mechanical Engineering

Presentations and Publications:

A. D. Rosato, O. Dybenko, D. J. Horntrop, V. Ratnaswamy, L. Kondic,
"Microstructure development in density relaxation by tapping", to appear *Phys. Rev. E*

A. D. Rosato, V. Ratnaswamy, D. J. Horntrop, O. Dybenko, L. Kondic,
"Density Relaxation through Monte Carlo simulations", *Powders & Grains 2009* (eds. M.Nakagawa, S. Luding), p. 481 –484, American Institute of Physics (2009).

A. D. Rosato, V. Ratnaswamy, D. J. Horntrop, L. Kondic,
"A Concise Review of Tapped Density Relaxation and Recent Discrete Element Results", *IUTAM-ISIMM Symposium on Mathematical Modeling and Physical Instances of Granular Flows*, Sept. 14-18, 2009, Reggio-Calabria, Italy.

ACKNOWLEDGMENT

I would like to express my sincere thanks to my thesis advisor Dr. Anthony Rosato, for guidance and support throughout these five years in my research. In addition I would like to thank my committee members Dr. David Horntrop, and Dr. Pushpendra Singh, and Dr. Ian Fischer for their active participation in my thesis committee. Computing resources were provided by the NJIT Engineering Computing cluster KONG and an NSF-MRI grant (DMS-0420590) as well as the Open Science Grid. Additionally, I am glad to thank Mats Rynge who helped me set up and run my jobs on the OSG. I am also grateful to Dr. D. L. Blackmore, Dr. Lou Kondic, Dr. O. R. Walton, Dr. Xavier Tricoche and Nathan Andrysco for their interest and discussions of this work. I would like to thank the current as well as former students of the Granular Science Laboratory including Dr. Oleksandr Dybenko, Tai Anh Duong, Shawn Chester, Meng Cui, Luo Zuo, Jefferson Cuadra, Nathaniel Ching, Nick Matiescu, Aniel Parillo, and Beata Wec.

To my parents

TABLE OF CONTENTS

TABLE OF CONTENTS
(Continued)

LIST OF TABLES

LIST OF FIGURES
(Continued)

LIST OF FIGURES
(Continued)

LIST OF FIGURES
(Continued)

LIST OF SYMBOLS

d	Particle diameter
D	Diameter of the cylindrical vessel
R	Particle radius
ν	Solids fraction
N_T	Number of taps
μ_p	Limiting particle-particle friction coefficient
ρ	Particle mass density
γ	Vertical lift intensity in MC
g	Gravitational constant $\left(9.81 {}^{m}/_{\sec^2}\right)$
π	Mathematical constant (3.1415926)
f	Frequency of sine-wave tapping in DEM
b	Displacement amplitude of sine-wave tapping in DEM
Γ	Dimensionless acceleration in DEM
Δt	Time step
K_2	Normal unloading stiffness
α	Relative overlap between contacting bodies
$\underset{\sim}{x}_i$	Position vector of particle i

CHAPTER 1

INTRODUCTION AND LITERATURE SURVEY

1.1 Overview

The evolution of the bulk density of granular materials is a phenomenon that is heavily studied. The importance of those density studies have impacts in areas of industry such as pharmaceuticals, bulk process handling, as well as in the agricultural industry. Every year the bulk processing industry loses money because of the waste in handling granular materials, so there is a vast interest in understanding how these materials behave whether one needs to transport them, or pack them into dense configurations.

The way that granular materials arrive at various densities depends very much on their material parameters such as their restitution coefficient, inter-particle friction, size and geometry of the grain size and so forth. In addition to those properties, the type of vessel whether it is cylindrical or parallelepiped, along with the system size (how tall and wide the vessel is) plays a strong role in how dense the structure of the material becomes. The dryness of the material can also provide different effects on how these granular systems compact as well as the roughness of the base of the system. The way that one perturbs a system of granular material can also impact the way such systems arrive at their packed states. For example, one can perturb a vessel by continuously vibrating the floor of the vessel, or applying discrete taps to the vessel through the floor.

Continuous vibrations involve applying a sinusoidal pulse to a granular material repeatedly without any time of relaxation of the material. The bulk density, otherwise known as the solids fraction, of the system of particles is then measured after one decides

to stop vibrating the vessel. Discrete vibrations are perturbations in which the system of particles is perturbed by a sinusoidal pulse; however, there is a period of relaxation of the media in between pulses and the solids fraction is measured after the system is measured in the time after the system is relaxed and before the next tap is applied.

The compaction of granular materials has been studied in the three typical ways: experiments, theory, and simulations. Experiments have covered vibrating as well as discrete perturbations to a vessel of material [23, 26]. The theory that has been developed has come from a statistical mechanics approach and has looked at the compaction of granular systems from a 1-D view [71]. In addition to theory and experiments, researchers have studied the compaction process through both stochastic as well as deterministic means. Such stochastic means are through Monte Carlo method and for the deterministic methods; researchers have used dissipative molecular dynamics.

1.2 Evolution of Solids Fraction in Published Literature

The compaction process of the granular matter has an extensive history and the time evolution of bulk solids fraction is widely represented in the literature. The formation of regular and irregular configurations of particles during granular compaction is naturally accompanied by study of the microstructure geometry. The following sections and subsections are constructed to provide an overview of the experimental, and simulation approaches that have been applied to the problem of density relaxation. More specifically, experiments involving discrete taps and continuous vibrations of particulate systems will be reviewed, following by related numerical simulations involving Monte Carlo and discrete element methods.

1.3 Experimental Work

This subsection provides a concise review of the experimental results reported in the literature in which continuous vibrations and discrete taps have been used.

1.3.1 Continuous Vibration

An early study was done by Stewart [15] where they found a maximal improvement in the solids fraction by continuously vibrating a bed of particles with a low amplitude-high frequency protocol. Results obtained by Stewart were also found by Evans [16]. Those results gave why to a dimensionless parameter that is used widely in density compaction called the dimensionless acceleration, which will be called Γ throughout this thesis. The dimensionless acceleration is characterized by Equation 1.1 shown below where f is the frequency of the tap, a is the amplitude of the tap, g is the gravitational acceleration.

$$\Gamma = \frac{4\pi^2 f^2}{g} a \tag{1.1}$$

Studies in continuous vibration of granular media were also performed by Zhang et al [20], where a cylindrical vessel of acrylic monodispersed spheres were vibrated for approximately ten minutes, where after the solids fraction was measured. In their studies, they performed a wide variety of amplitudes and frequencies to investigate which amplitude-frequency pair gave the most dense solids fraction. Experiments in [20] looked at the improvement in solids fraction which is the ratio of the difference in the final and initial solids fraction to the initial solids fraction.

1.3.2 Discrete Tapping of Granular Matter

Ribiere et al [61] experimentally studied granular dynamics subjected to gentle mechanical taps. They determined the compactivity using the fluctuations in the packing fraction in the equilibrium (stationary state). Their experiments consisted of a cylindrical vessel of diameter 10 cm filled with glass spheres of diameter 1 mm. A picture of the experimental setup is shown in Figure 1.1 below.

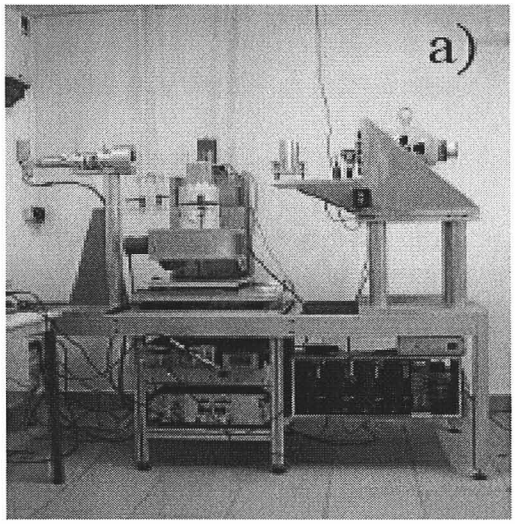

Figure 1.1 Experimental setup to apply discrete taps to a cylindrical vessel taken from [61].

The tapping is brought about by an electromagnetic exciter that is connected to a voltage that induces vertical displacements to the moving part of the container and the beads. Each tap is an entire cycle of a sin wave at a fixed frequency of 30 Hertz. After every tap, there is a period of one second of relaxation. The authors compare their results to those experiments using flow pulses [66]. The experiments conducted in [61] produced a steady state and may correspond to a balance between convection and compaction. In the Ribiere's experiments [61], they ran cases for different dimensionless accelerations

by varying the amplitude of the tap with a constant frequency of 30 Hz. It was observed in their results that to reach a high value of solids fraction, a small tapping intensity should be used.

Ribiere et al [61] then discussed the influence of the initial state (poured state). To investigate the influence of the initial state, they looked at two states: one with a high packing fraction ($\rho_0 \approx 0.63$) and one with a low packing fraction ($\rho_0 \approx 0.582$). They showed that both states reach essentially the same bulk equilibrium state as shown in Figure 1.2. In [61], the authors observed that the number of taps is larger for decompaction (going from high density to lower density) than for compaction which is because compaction is aided by gravity.

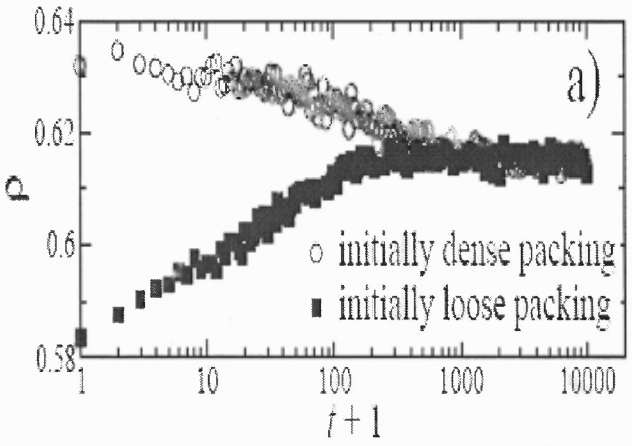

Figure 1.2 Plot of the evolution of the solids fraction of two different states. It can be seen that the final state is the same even though the initial state is different taken from [61].

Another aspect in their studies that was discussed in [61] was the influence of the tap duration. For the tap duration analysis the authors looked at frequencies of 30, 60 and 90 Hertz and their corresponding gammas. They looked at the equilibrium packing

fraction versus the corresponding gamma for each frequency and showed that the equilibrium packing fraction decreases for each frequency as the gamma increases.

The authors in [61] plotted the fluctuations as a function of the stationary solids fraction, and showed that it produced a single master curve implying that the fluctuations and the stationary solids fraction are linked and do not depend on the values of frequency and gamma. Their results are in agreement with Ciamarra et al [66] where they used numerical simulations of granular packings using flow pulses.

The results obtained in [61] strongly support the idea that the stationary state can be described by one parameter, the packing fractions. The preceding statement is only true for the stationary state. In [61], the authors use the fluctuations and the stationary packing fraction to obtain the compactivity described by Edwards. Ribiere et al [61] plotted the compactivity versus the stationary solids fraction, and showed that the compactivity decreases as the stationary solids fraction increases. The compactivity for tapping intensities for a frequency = 30 Hertz was plotted and the authors showed that the compactivity is linked to the tapping intensity.

They note that an increase in gamma increases the average solids fraction for an acceleration less than three. For accelerations larger than three, there is a slow decrease. The authors only recovered the reversible branch (frequency used is 30 Hertz) as shown in Figure. 1.3. They explained it because the number of taps used was large enough to allow the system to reach the stationary stage.

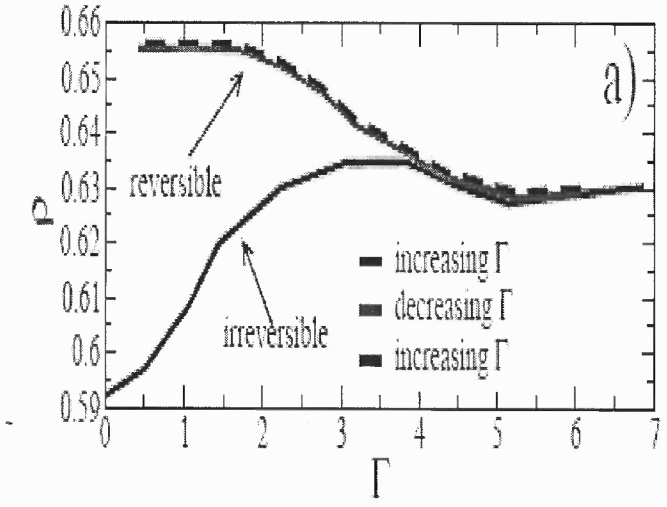

Figure 1.3 Plot of the equilibrium solids fraction versus the acceleration Γ. The authors were able to obtain the reversible branch by reducing the acceleration taken from [61].

1.4 Simulation Studies

In what follows, a succinct review of Monte Carlo and Discrete Element simulations of the density relaxation phenomenon is given. Both simulation methods have been used extensively to study the compaction of granular materials. While, Monte Carlo (stochastic) simulations and the discrete element method (DEM) are based on very different principles, both methods give results that have been verified by experiments. There sometimes is a stronger preference to use DEM simulations because the method is governed by Newton's equations of motion and would hence provide a realistic portrait of the dynamics taking place in the particle system being investigated.

1.4.1 Monte Carlo Simulation

The Monte Carlo simulation method has been used to study granular systems by randomly applying displacements to particles which results in similar "dynamics" that

can be obtained by using Newton's laws of motion. However, one important point to note is that for the Monte Carlo simulation method, there is no real concept of time or forces because the algorithm is not based upon deterministic dynamics.

Another use of the Monte Carlo simulation was done by Rosato et al [46] where he studied the size segregation of a system of polydispersed particles which undergoes vibration. Mehta and Barker [52] also used the Monte Carlo simulation to study granular packings where they used a linear expansion for the system of particles along with lateral displacements.

Ribiere et al [60] also performed MC numerical simulations where they have the following parameters: 4096 monodispersed spheres of radius R. Container is a box with a flat square bottom measuring 32 particle radii's in each of the lateral dimension. Periodic Boundary conditions are imposed on the horizontal directions. There is a free interface at the top of the packing. A tap is simulated in two stages, the first stage is where the packing is dilated vertically given by Equation 1.2, where ε is the dilation parameter that is proportional to the square of Γ.

$$(z-R) \rightarrow (z-R)(1+\varepsilon) \tag{1.2}$$

The next stage simulates the gravitational re-deposition using a nonsequential algorithm. The model only takes into account the steric constraints because that's important for compaction to occur. They found that their simulations as well as their experiments show the cage motions as well as the jumps. Cage motion is where a grain is always surrounded by the same neighbors. A jump is a displacement where the grain

moves significantly more than the mean square displacement of a grain. The simulations in [60] confirm that jumps as well as caging occurs. The characteristics of the caging motion change during the simulation due to the evolution of the packing fraction.

The authors in [60] found that jumps always yield a large displacement in the direction of gravity. The above statement corresponds to the fall of a bead in a hole located beneath it. This is correlated to the compaction mechanism. In Ribiere et al's [60] simulation of 10000 taps only about 100 jumps occurred which happened during the beginning of the simulation. That corresponds to when the packing fraction is farm from the steady state value. They then seek to understand the evolution of the jumps by comparing the jumps that are inhibited in the simulations to normal jumps. In [60] the authors modified their algorithm to inhibit jumps, and then checked their results to that obtained using molecular dynamics. The results showed that when without significant jumps, the increase of packing fraction was slower.

The packing obtained after a large number of taps is less dense with jumps than one without jumps. The authors in [60] explained the above using energy landscape in which two states are separated by potential barriers that cannot be avoided by many slow events.

Jumps play an important role in the evolution of media. The number of jumps decreases as the system compacts. In [60], the effect of jumps was studied by looking at the mean squared displacement of a grain. The authors looked at a modified random walk model to describe the cage motion to look at the diffusive properties without jumps, in which cage motions are the only allowed displacement. Their conclusions are that jumps play an important role in the macroscopic behavior of media. Their simulations showed

that compaction is slower and that the state reached after long time is less dense if the jumps are inhibited.

That observation is surprising because such rare behavior in an equilibrium system have little effect on the overall evolution. The above results for out-of-equilibrium granular media can also be valid for out-of-equilibrium systems such as glasses, colloids, etc, and can be useful when studying granular media under shearing.

In addition to tapping using the Monte Carlo simulation, there was also the use of flow pulses where a system of particles were submerged and then tapped using the pulses to measure the solids fraction as one of the quantities of interest. Such cases have been done by Ciamarra et al [66].

1.4.2 Discrete Element and Molecular Dynamics Modeling

The use of the discrete element method (DEM) that was developed in 1971 took shape from molecular dynamics that is used the statistical physics community. The DEM is used to model the behavior of bulk solids. The main premises of the DEM is to solve Newton's equations of motion for a system of particles where such particles are modeled using a dissipative force model. Unlike molecular dynamics, DEM accounts for the dissipation in energy in the collisions between particles.

The studies that have been conducted using DEM can be seen in Luding [46], Roasto [49], and Liu [47]. In addition, studies done by An et al [58] where they studied three dimensional systems subjected to vibrations. The focus of their work was to look at how the vibration conditions such as the amplitude and frequency as well as inter-particle friction play a role in the packing of the system of particles. They showed that increasing the amplitude or frequency of the vibration will cause the packing fraction to increase

then decrease. Also, the sliding and rolling friction had an effect of decreasing the density of the packings. In addition, they found that a loose packing had a smaller coordination number, a less peaked radial distribution function.

1.5 Objective

In this thesis, the study of density relaxation of granular materials will be investigated through simulations. The simulations that will be used are broken into two categories: stochastic and deterministic. For the stochastic simulation, we will use a Monte Carlo method with a Metropolis approach to simulate a three dimensional system of spheres subjected to several uniform expansions. To measure how dense the system is the use of a combination of techniques such as the solids fraction, vertical center distribution and coordination number will be employed.

Dissipative molecular dynamics was also used to model the compaction of granular materials by using a discrete tapping protocol. For that method, the discrete element method was used where the interactions of particles are modeled using a spring-dashpot model, and the equations of motion are integrated to obtain velocities and accelerations. Then, the same quantities such as the solids fraction, coordination number distribution and vertical center distribution is computed as they were for the Monte Carlo simulations. The investigation was performed for various amplitudes as well as frequencies to determine how the systems of particles behave.

1.6 Thesis Outline

The remainder of this thesis is organized as follows. Chapter 2 describes the Monte Carlo simulation method and the results that were obtained by employing it. Chapter 3 describes the discrete element method along with a kinetic energy analysis of the tapping parameters. Chapter 4 describes the results that were obtained using the DEM simulations. In Chapter 5, the summary of the results as well as the conclusion is presented. Additionally, suggested future directions with regard to the research done are presented in chapter 5.

CHAPTER 2

MONTE CARLO SIMULATION METHODOLOGY AND RESULTS

2.1 Introduction

In this chapter, the behavior of granular materials will be modeled by using a stochastic simulation technique, the Monte Carlo method. In [96], the Monte Carlo method was used to investigate the expansion of a system of monodisperse spheres in a parallelepiped using various lifting protocols such as a linear expansion, or a combination of a linear and uniform expansion. The purpose of this work is to investigate the process by which the system density increases, and in parallel to carefully examine the evolving microstructure using techniques such as coordination number, radial distribution function as well as the vertical center distribution, and solids fraction analysis.

The results described in this chapter represent a continuation of what was done in [96], where tapping is modeled by uniformly lifting the particle assembly. In this chapter, the behavior of such systems will be analyzed using a global measure such as the solids fraction, as well as by the vertical center distribution, a local measure.

2.2 Bulk Solids Fraction of a Granular Assembly

The solids fraction of a vessel of particles is defined as the ratio of the volume of particles that occupy a vessel to the volume of the vessel itself as define in Equation 2.1.

$$\nu = \frac{Volume_{solids}}{Volume_{occupied}} \tag{2.1}$$

The value of such a measurement allows one to determine how dense a structure of particles is. In determining how dense a system is one could now gain insight into which structures would give have the densest formation depending on what tapping procedures are used whether they are continuous vibrations or discrete taps.

Figure 2.1 below shows four typical crystal structures, e.g., body-centered cubic (BCC), face-centered cubic (FCC), cubic and hexagonal close-packed (HCP).

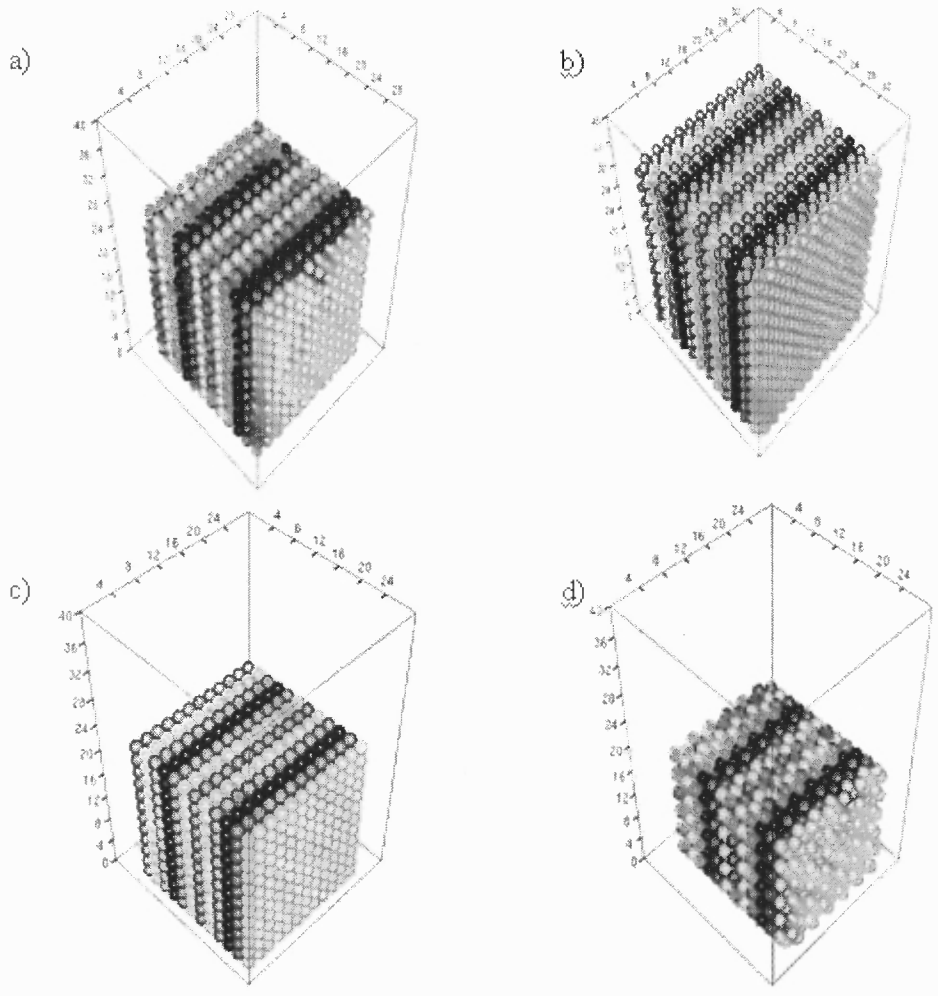

Figure 2.1 a) BCC crystal b) FCC crystal c) Cubic crystal d) HCP crystal

The two structures having the densest packing are the Hexagonal Close Pack (HCP) and the Face Centered Cubic (FCC) crystals with a solids fraction of $\frac{\pi}{3\sqrt{2}} \approx 0.74$. However, it has been reported in [51] that while both have the densest structures, it is the FCC structure that is the most stable because of how the structure is ordered.

2.3 Vertical Center Distribution

The solids fraction analysis is an indicator of the bulk density of the assembly. However, that does not lend insight into microstructure of the assembly of particles. For example, although HCP and FCC have the same solids fraction, each has a different crystal structure. Thus, a local measure is needed to observe differences in the arrangement of the spheres.

The vertical center distribution is such a measure because it allows one to see the distribution of particle centers in a given layer thickness. The control is partitioned volume in the vertical direction into layers of thickness δ as shown in Figure. 2.2, after which the number of particle centers in each layer in calculated.

$$n(y,\delta H) = \frac{1}{N_p}\sum_{k=1}^{N_p} \delta(y - y_k)\delta H \tag{2.2}$$

The number of centers in each layer is then normalized by the total number of particles in the system N_p. The exact computation is given in Equation (2.2).

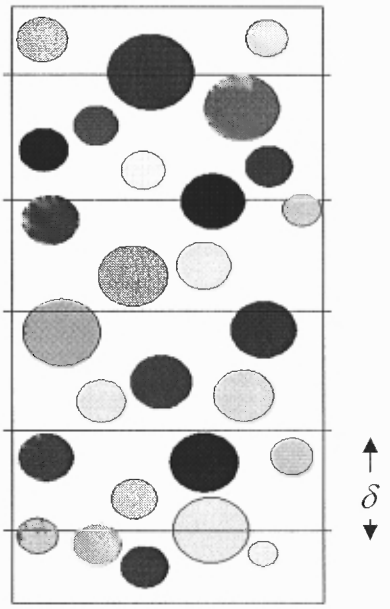

Figure 2.2 Partition of a Control Volume in calculating the VCD

The VCD of some common crystals such as cubic crystals, face centered crystals, body centered crystals, and hexagonal closed pack crystals, which are shown in Figures. 2.3 – 2.6 below. For each VCD for the aforementioned crystals, one should note that there is a periodicity with regard to the peaks that are present. That result is not a surprise because there is a definitive pattern when it comes to creating those structures.

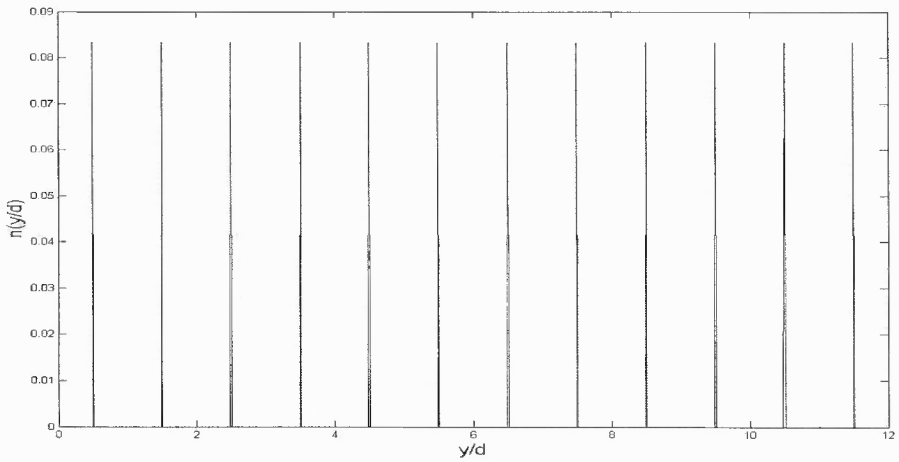

Figure 2.3 VCD of Cubic Crystal – 1728 particles

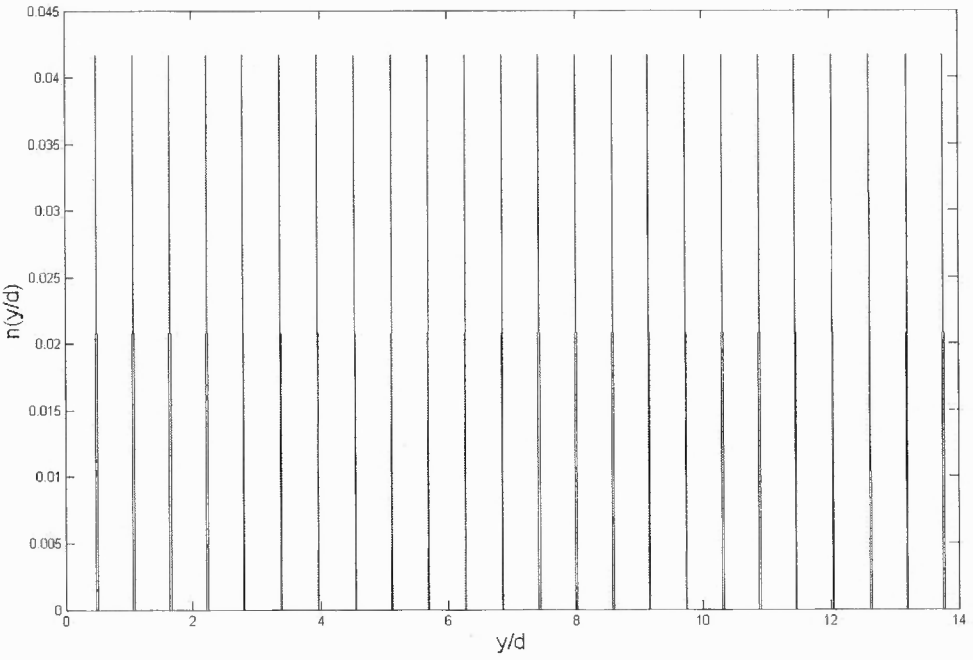

Figure 2.4 VCD of Body Centered Crystal – 3456 particles

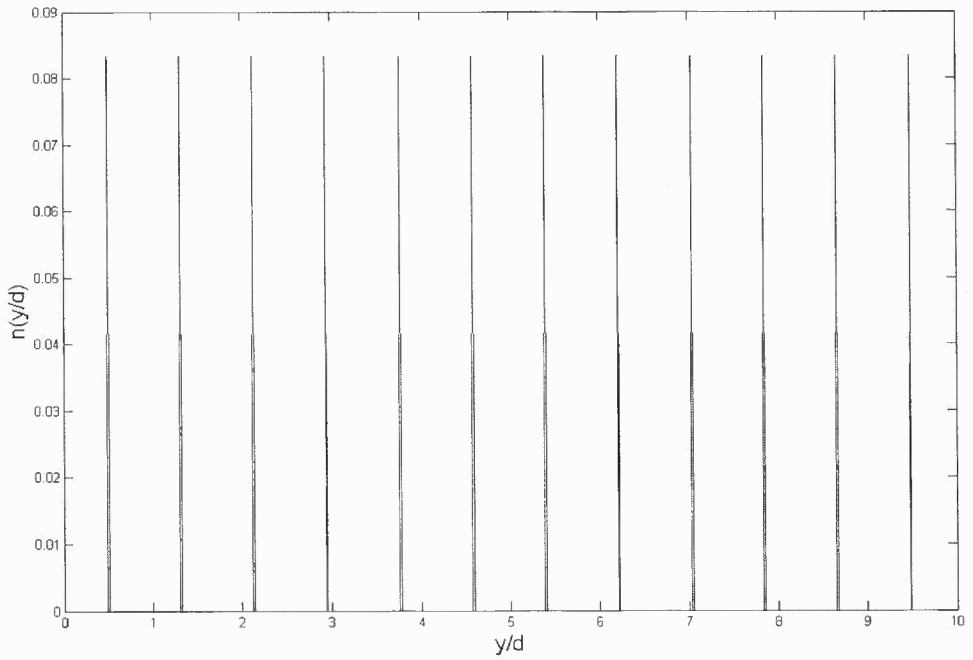

Figure 2.5 VCD of HCP Crystal – 1728 particles

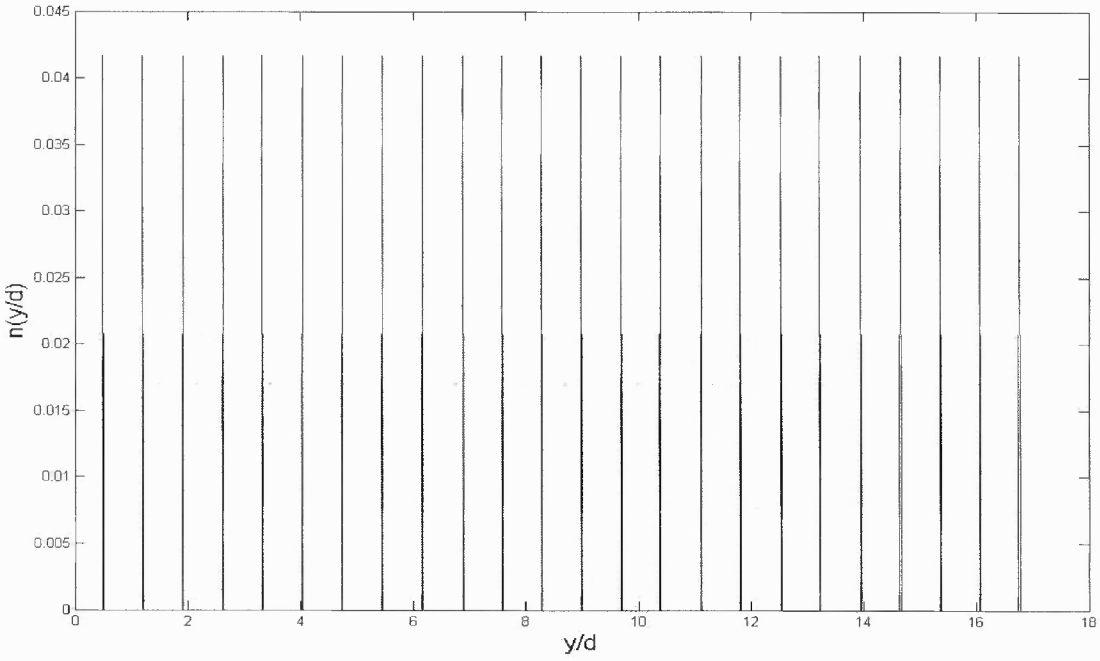

Figure 2.6 VCD of Face Centered Crystal – 6912 particles

2.4 Monte Carlo Simulation Model

The Monte Carlo simulation consists of first generating a random initial configuration of spheres. In this configuration, the spheres are hard spheres meaning that they are not allowed to overlap. After the initial configuration is determined, the system of particles is allowed to move down to the floor of the vessel by means of gravity. To ensure that there are no overlaps, the following criterion is used:

1) Compute the distance between particle centers given in Equation 2.3:

$$d(i,j) = \sqrt{(x_i - x_j)^2 + (y_i - y_j)^2 + (z_i - z_j)^2} \tag{2.3}$$

2) Check that the distance between particles is greater than the diameter, i.e. $d(i,j) \geq 2r + \delta$ where r is the radius of the particle, and δ is equal to 10^{-4}.

The computational domain used for the simulations is a box having a solid plane floor, and periodic boundary conditions in the lateral directions (x and z; $12d$ x $12d$). These periodic conditions are used to eliminate the ordering effect of the side walls, as commonly done. The poured assembly is then subjected to a series of taps of intensity γ. A typical assembly after the application of several taps is depicted in Figure. 2.7.

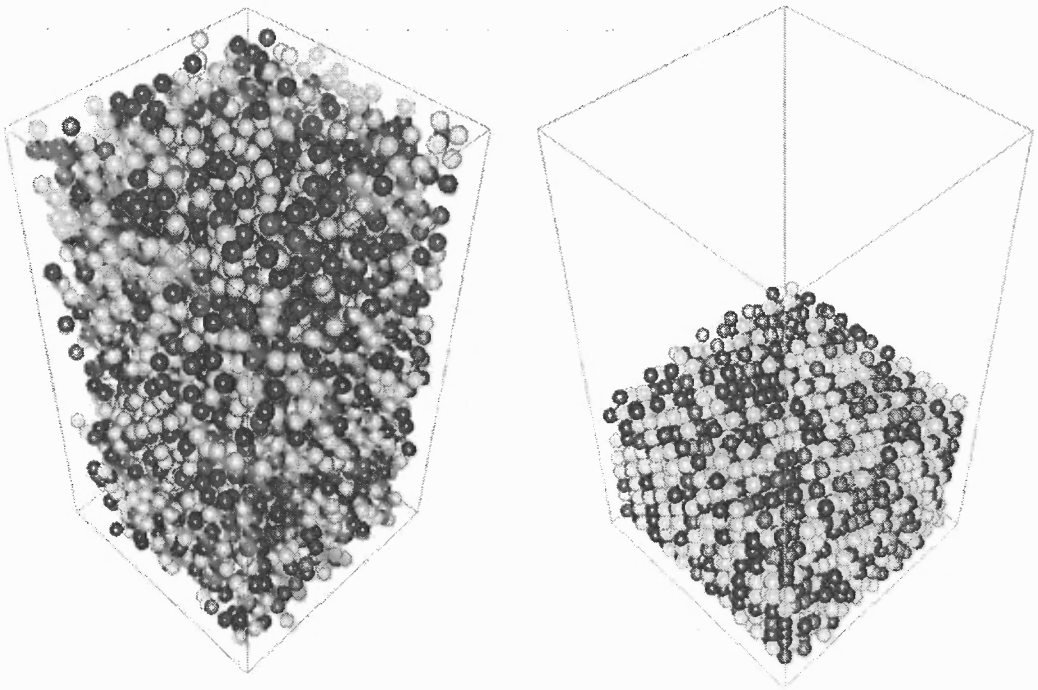

Figure 2.7 a) Poured Assembly. b) System after many taps.

In the MC simulation, a single step in the algorithm consists of the random selection of a particle $\mathbf{x}_i = \left(x_i, y_i, z_i\right)$, followed by its assignment to a trial position given by Eq. 2.4, where ξ is a random vector with each component sampled from a uniform distribution on (0,1) and δ is the maximum allowed displacement.

$$\mathbf{x}_i' = \mathbf{x}_i + \delta(1-2\xi) \tag{2.4}$$

The trial position is accepted unconditionally (provided that an overlap does not occur) as the new location if the change in the system energy given in Eq. 2.5 below.

$$\Delta E \equiv mg\sum_{i=1}^{N}(y_i' - y_i) \le 0 \tag{2.5}$$

Otherwise, if the change in energy is positive ($\Delta E > 0$), the trial position is accepted with probability $e^{-\beta\Delta E}$. For the macroscopic particles under study, β is very large so that the likelihood of an accepted upward displacement is small. Another particle is then selected at random, and the above procedure is repeated. As this settling process advances through many thousands of MC steps, the mean free path decreases resulting in a drastically slowed rate of approach to a local equilibrium. Therefore, the parameter δ is modified every 10^4 MC steps in accordance to $\delta' = 0.995\delta$ if fewer than half of these steps are accepted.

The effect of a single tap applied to a containment vessel filled with spherical particles of diameter d is idealized by lifting the entire particle assembly from the floor by an amount Δ, whose normalized value is $\gamma \equiv \Delta/d$. The assumption here is that a tap is sufficiently energetic to cause a small separation of the assembly from the floor. That is, γ physically represents the lift that a granular mass will experience as it is energetically tapped. Within a single tap n of intensity γ, the bulk solids fraction $\nu_j(n;\gamma)$ was monitored (i.e., the fraction of volume occupied by spheres) at MC step j every 10^6 steps. The settling process was terminated when the difference in the bulk solids

fractions $\left|\nu_{(k+1)10^6}(n;\gamma)-\nu_{10^6 k}(n;\gamma)\right| < 0.001,\ k=0,1,2,\ldots$. This protocol was validated by enforcing the latter criterion twice to ensure that premature termination could not occur.

2.5 Solids Fraction Computation

The solids fraction as was previously defined in this chapter is the ratio of the volume of matter occupied to the volume of that contains the particles. In this process, the solids fraction is computed by measuring the solids fraction from the base of the vessel until 80 percent of the height of the stack of particles. Measuring the solids fraction that way ensures that the "top effect" is removed from the evolution of the solids fraction.

The "top effect" is where one has disordered layers of particles on the top of the stack. If such a measure were included, then one would lose information about the evolution of the majority of the stack of particles. To calculate the solids fraction, 80 percent of the control volume is partitioned into slices and the volume distribution is found in each slice. Then the volumes in each slice is summed up and divided by the total control volume. A more detailed analysis is done in [96].

2.6 Monte Carlo Results

In all cases reported here, poured assemblies consisting of 3,456 particles with solids fractions ν_0 in the range 0.56 to 0.58 filled the periodic box to a depth of approximately $22d$. For each tap n, the ensemble averaged bulk solids fraction $\langle \nu(n;\gamma) \rangle$ over M realizations(where M is 100) is computed, and its standard deviation is given by Eq. 2.6 where $\langle \nu(n;\gamma) \rangle$ is given by Eq. 2.7

$$\left\langle \sigma(n;\gamma)\right\rangle = \sqrt{\frac{1}{M}\sum_{k=1}^{M}\left[\nu_k(n;\gamma)-\left\langle \nu(n;\gamma)\right\rangle\right]^2} \tag{2.6}$$

$$\left\langle \nu(n;\gamma)\right\rangle = \frac{1}{M}\sum_{k=1}^{M}\nu_k(n;\gamma) \tag{2.7}$$

The equilibrium bulk solids fraction $\nu_\infty(\gamma)$ was found by increasing the number of realizations over a sufficient number of taps N_T until the condition $\left\langle \sigma(N_T;\gamma)\right\rangle < 0.001$ was satisfied.

The MC tapping procedure differs from that used in [34], where vertical position-dependent displacements of the particles ($y' = \lambda y$) were applied in sync with random lateral perturbations. In an earlier paper [26], it was reported that statistically equivalent solids fractions were obtained with or without application of these random lateral displacements. Furthermore, for the packings (~22*d* high) reported here, application of taps consisting of the vertical position-dependent displacements produced little or no increase in solids fraction in the upper portion of the bed, so that the bulk solids fraction remained relatively low. This behavior is attributed to an overly aggressive vertical displacement of the particles with distance from the floor, so that after each tap, the system tends to lose memory of its previous microstructure. Physically, this corresponds to the situation in which vigorous taps or shakes are applied so that the system relaxes to nearly the same or lower bulk density.

The simulated mean coordination number (i.e., average number of contacts per particle) versus solids fraction is shown in Figure. 2.8.

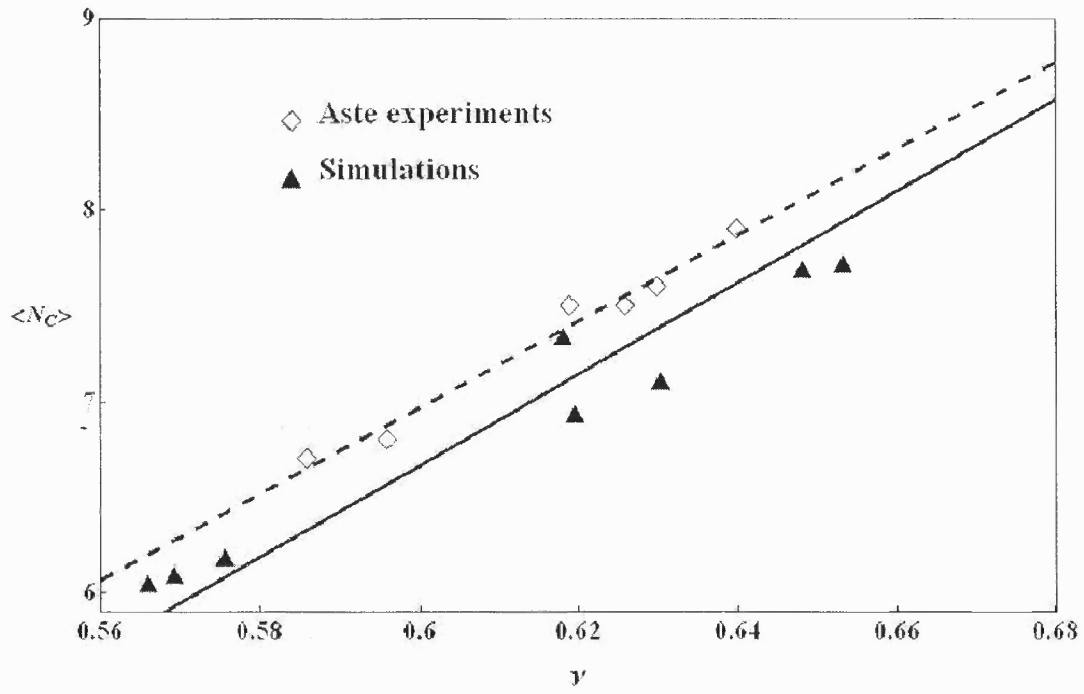

Figure 2.8 Mean Coordination Number for Uniform Expansion

The behavior of these simulation results is in reasonably good agreement with the experimental measurements of Aste et al. [1], showing the same trend over a range of ν. Since the error of the experimental results was not reported, one can not comment on the significance of the slight shift of the two lines shown in Figure. 2.5. Additionally, results were found that further corroborated (reported in [26]) the simulation results in the fit of the solids fraction evolution data at low tap intensities to the inverse log phenomenological law reported in [5-8].

In addition to the bulk density analysis, fits to a stretched exponential were also done to corroborate the data with that of those that were performed in experiments by [26] . The fits that were done were primarily the KWW (Kohlrausch-Williams-Watts) fit given in Equation 2.8 below.

$$\nu_n = \nu_\infty - (\nu_\infty - \nu_0)e^{-[(t/\tau)^\beta]} \tag{2.8}$$

The parameters of Equation 2.8 are summarized in Table 2.1 below. The KWW fit is one that is widely used in many studies for granular packings when it comes to fitting the time evolution of the solids fraction.

Table 2.1 Summary of the Fit Parameters of the KWW Law

Parameter	Description of Parameter
ν_n	Solids fraction at a particular time.
ν_∞	Equilibrium Solids fraction predicted by the KWW fit.
ν_0	Initial Solids fraction of the poured state.
t	Time corresponding to the tap, or lift etc.
τ	Compaction Time.
β	A fitting parameter from the KWW law.

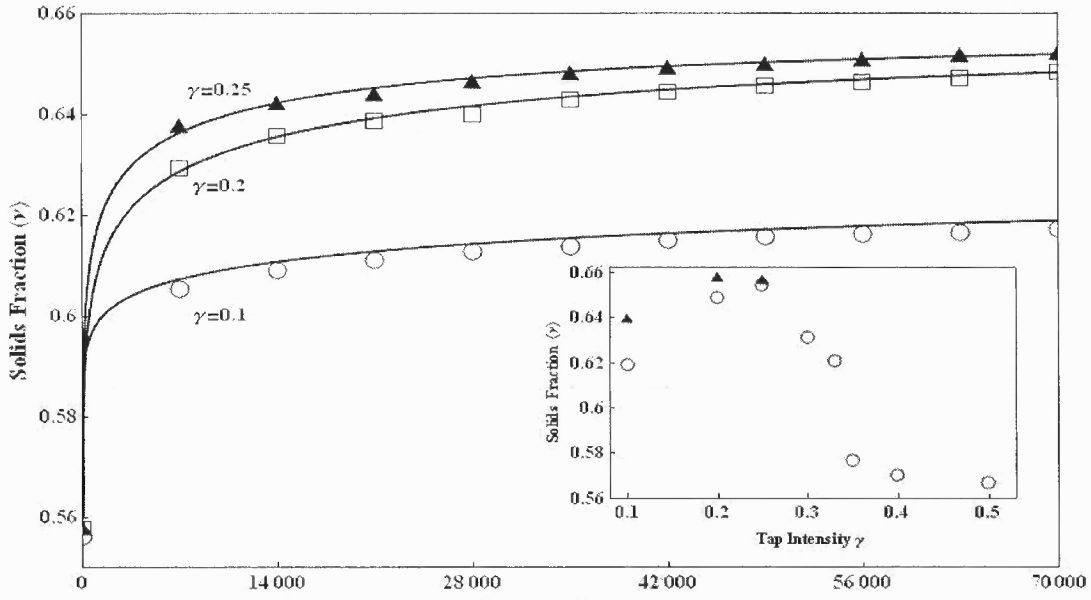

Figure 2.9: Fits to the Unifrom Expansion Curves for a poured structure

In Figure. 2.9, the main plot consits of the MC evolution for $\gamma = 0.1, 0.2, 0.25$ along with the KWW fit for each of the aforementioned lifts. In addition, there is an inset figure for Fig. 2.9 which shows the predicted final solids fraction from the fits. The trend of the data in the inset suggests that there is an optimal lift intensity that yields a dense structure. The parameters that were done with the fits are shown in Table 2.2 below.

Table 2.2 Fitting Parameters of the Data for the KWW Law

γ	ν_∞	ν_0	t_f (taps)	β
0.1	0.6396	0.5705	27180	0.2
0.2	0.658	0.5416	1985	0.2558
0.25	0.6567	0.55	1083	0.2715

An important aspect of the simulations is that the low tap intensities $\gamma = 0.1,\ 0.2,\ 0.25$ have not reached equilibrium. One way in which one can see this is to rewrite the stretched exponential in the form given in Equation 2.10 below.

$$\frac{\nu_\infty - \nu_n}{\nu_\infty - \nu_o} = e^{-(t/\lambda)^\beta} = f\left(-(t/\tau)^\beta\right) \tag{2.10}$$

A graph of the normalized solids fraction $\frac{\nu_\infty - \nu_n}{\nu_\infty - \nu_o}$ versus $(t/\tau)^\beta$ would then show if the data follows a decaying exponential law. Figure. 2.7 shows the result for $\gamma = 0.1,\ 0.2,\ 0.25$.

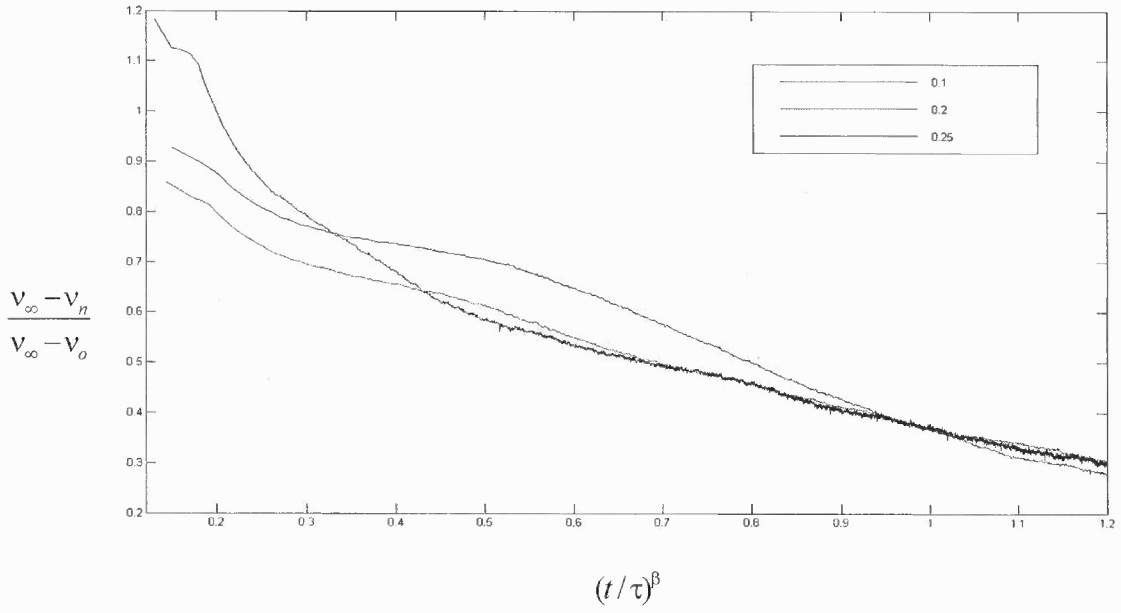

Figure 2.10 Graph of versus $(t/\tau)^\beta$ for $\gamma = 0.1,\ 0.2,\ 0.25$.

For the γ's shown in Figure. 2.10, it is clear that the graphs have not leveled out so that more taps are needed to reach equilibrium values. Another observation from the graph is that for smaller γ values, the time scale to attain equilibrium is longer.

2.7 Independence of the Initial Configuration

To further explore the hypothesis of the equilibrium solids fraction's dependence on the initial state, the simulation process was reversed by starting with a hexagonal crystal structure ($\nu_0 \cong 0.74$), which was subsequently tapped at the same intensities ($0.1 \le \gamma \le 0.5$) previously used. After only a few taps, the dense crystal structure is disrupted thereby causing a significant reduction in solids fraction. This is shown in the inset of Figure. 2.11. After many thousands of taps, the solids fraction graphs flatten as shown for intensity values $\gamma = 0.20, 0.25$ of Figure. 2.11.

For large intensities, equilibration is attained for less than 10^4 taps. The results of this study which are summarized in Figure. 2.12 reveal a trend very similar to that visible in Figure. 2.9. That is, the graph peaks at roughly the same range of intensity values as in Figure. 2.9. This finding regarding the existence of a critical intensity is also supported by experiments reported elsewhere [28] and by the conjecture [30] that bulk density is related to impact velocity.

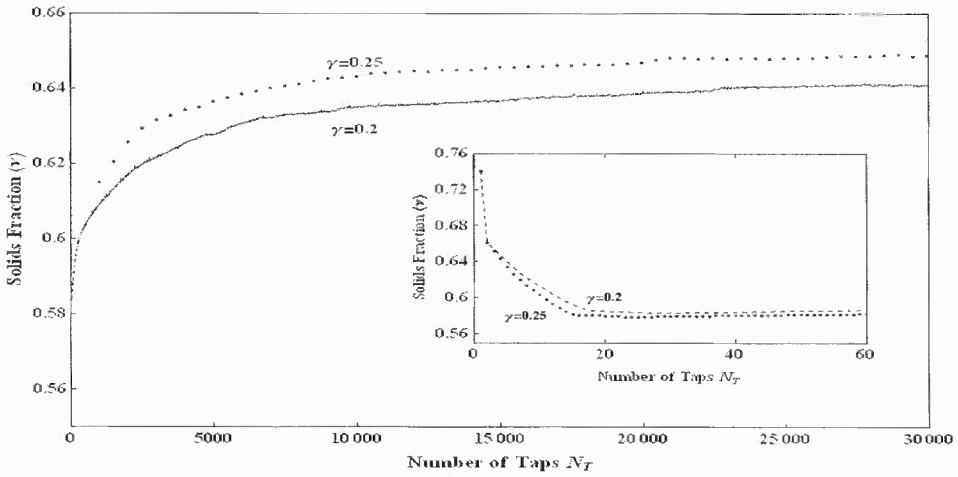

Figure 2.11 Density evolution in which the initial state was an HCP crystal.

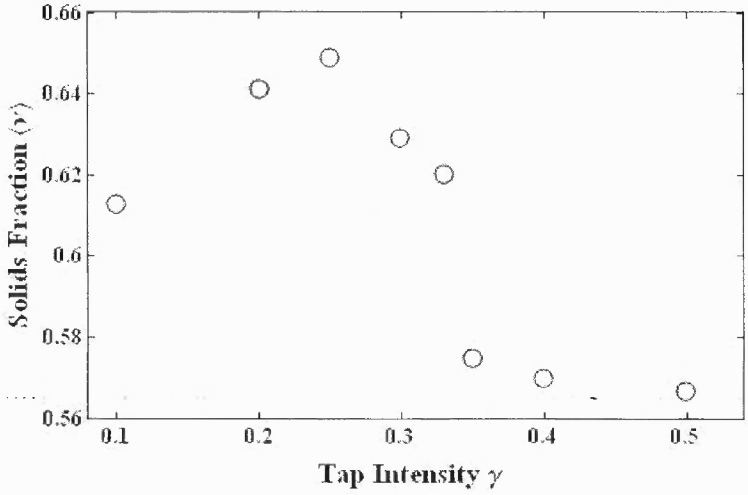

Figure 2.12 Final solids fraction as a function of tap intensity γ.

The behavior of the solids fraction versus number of tap for $\gamma \in [0.3,\ 0.5]$ are shown in Figures. 2.13 to 2.17. Here, one observes that equilibrium is reached quickly in contrast to what took place for the smaller values of γ (=0.1, 0,2 and 0.25).

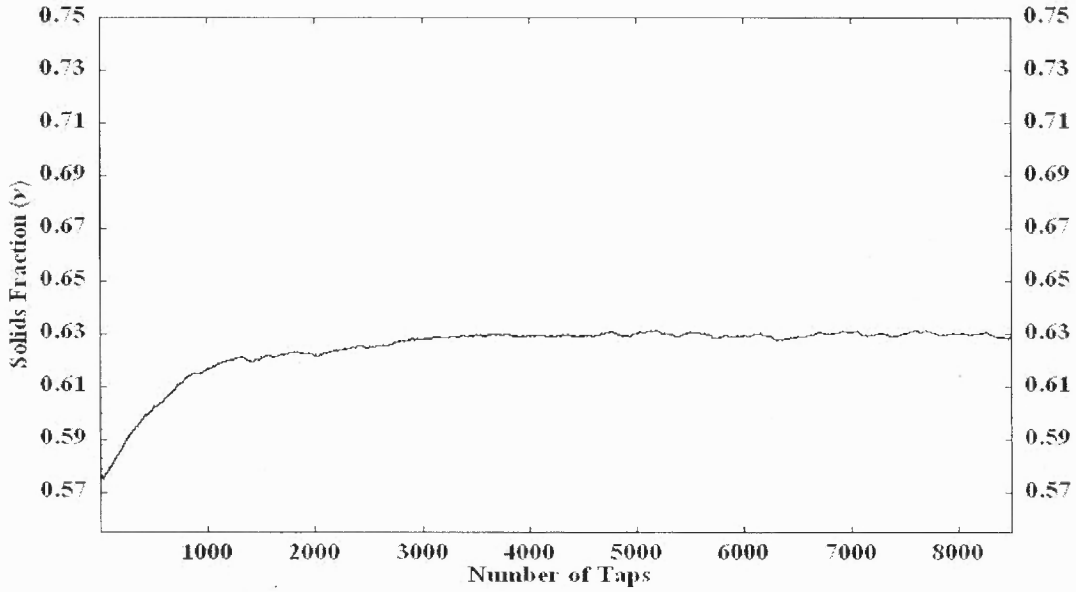

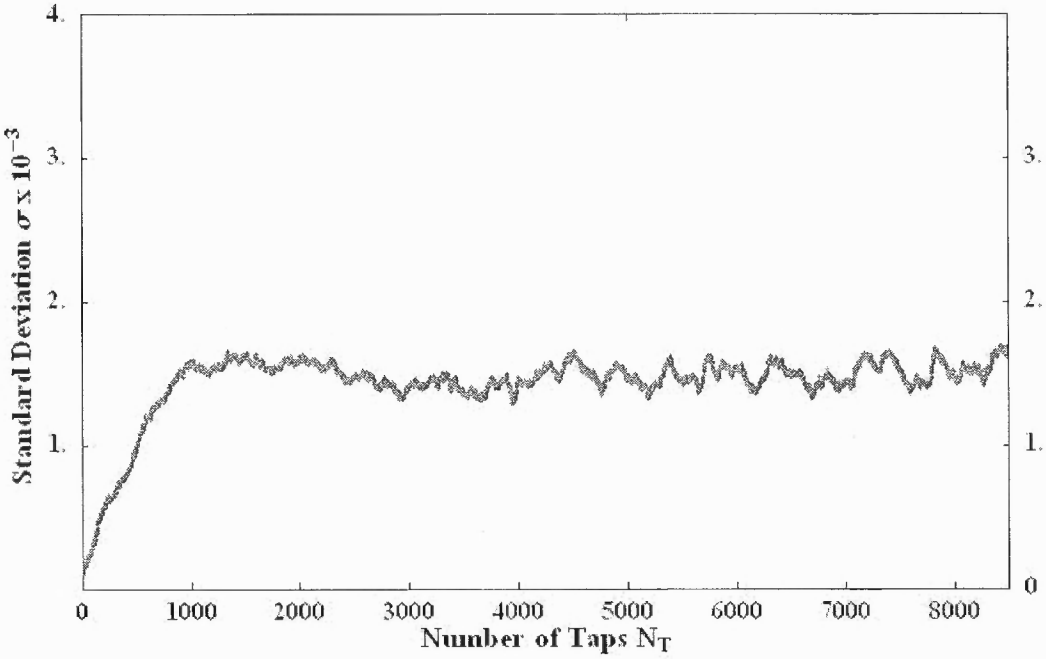

Figure 2.13: Density and Standard Deviation curve for $\gamma = 0.3$.

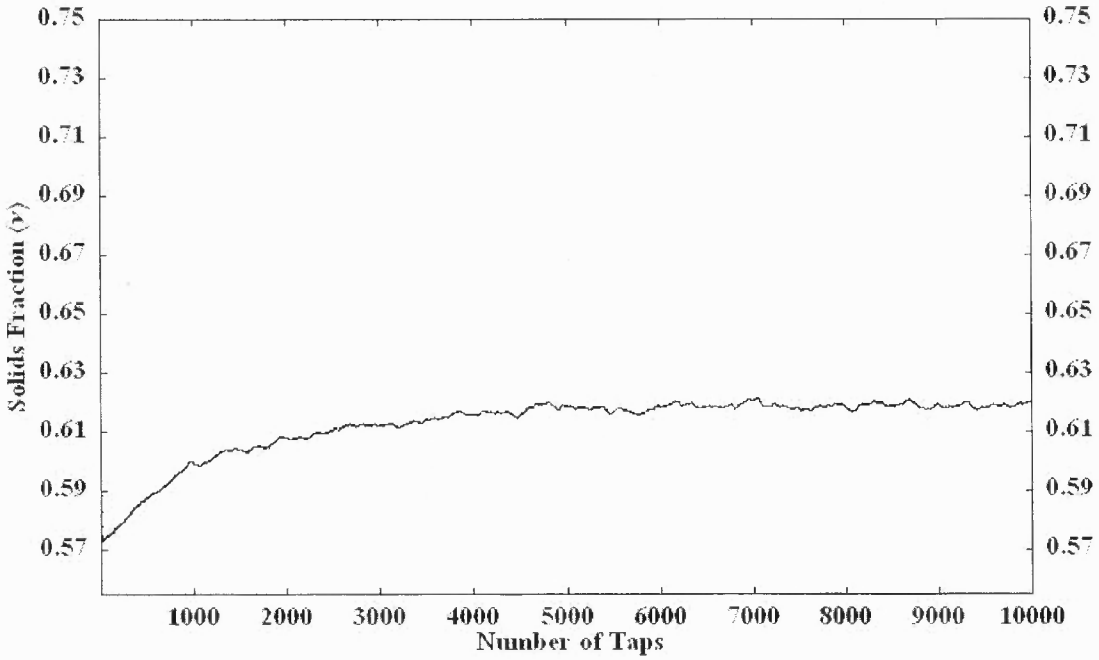

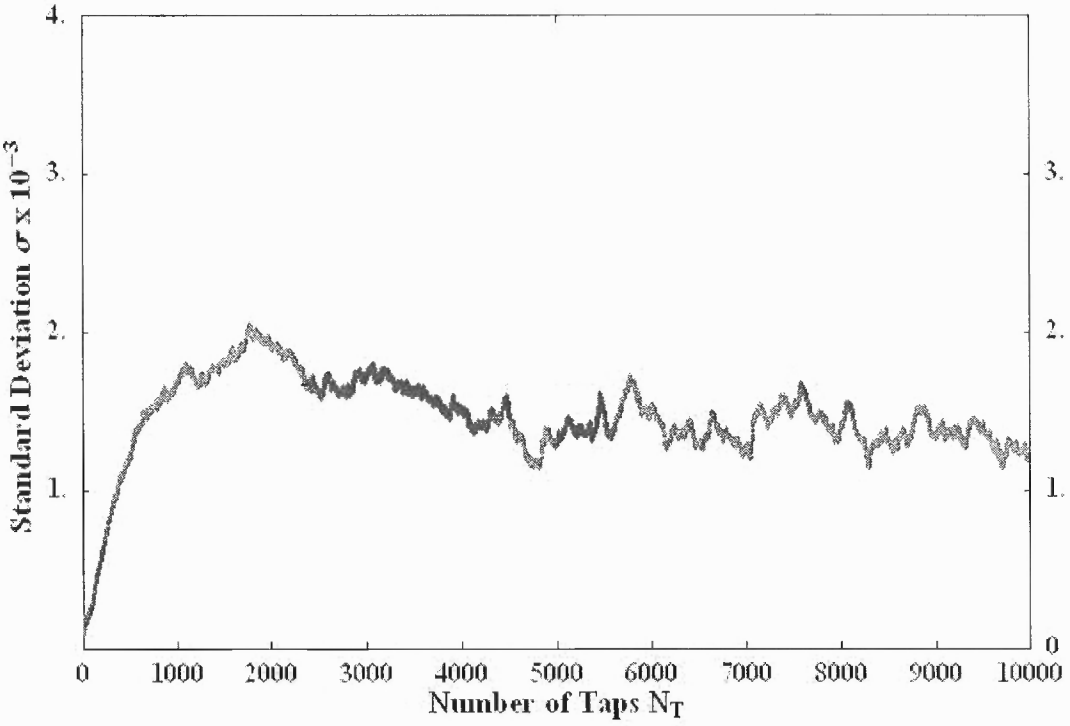

Figure 2.14: Density and Standard Deviation curve for $\gamma = 0.33$.

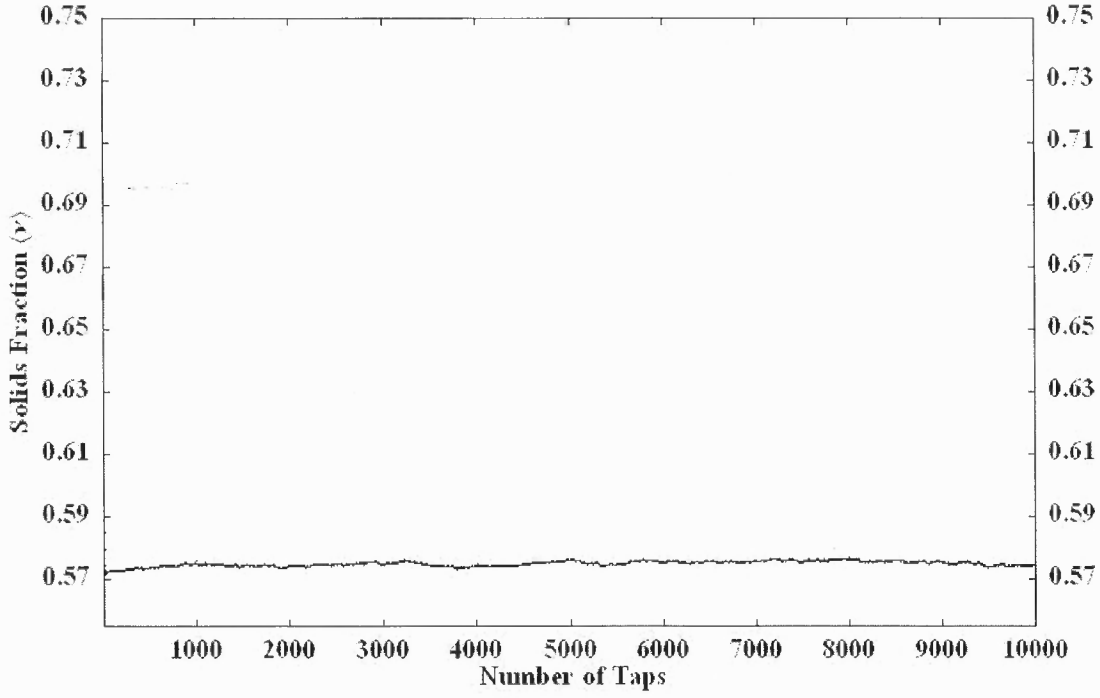

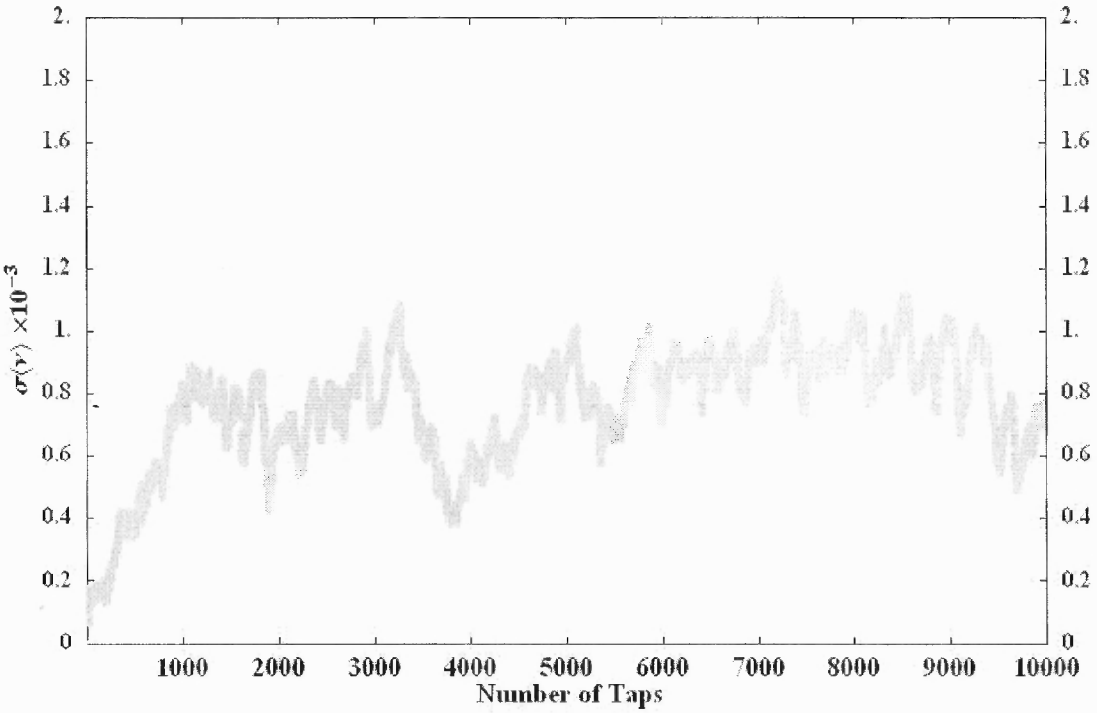

Figure 2.15: Density and Standard Deviation curve for $\gamma = 0.35$.

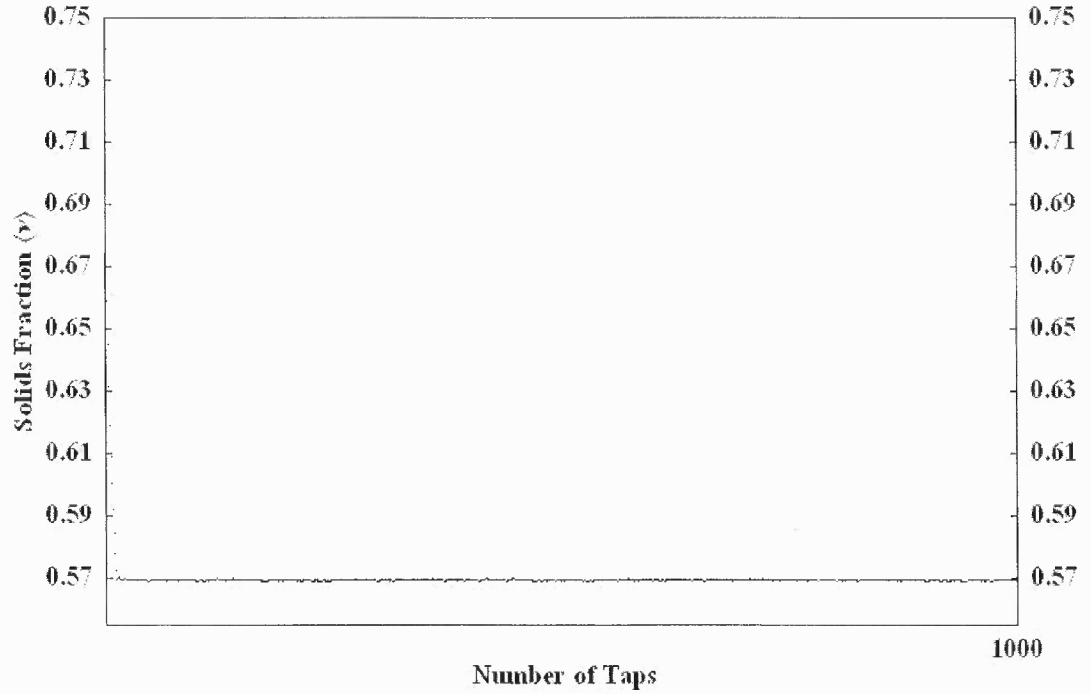

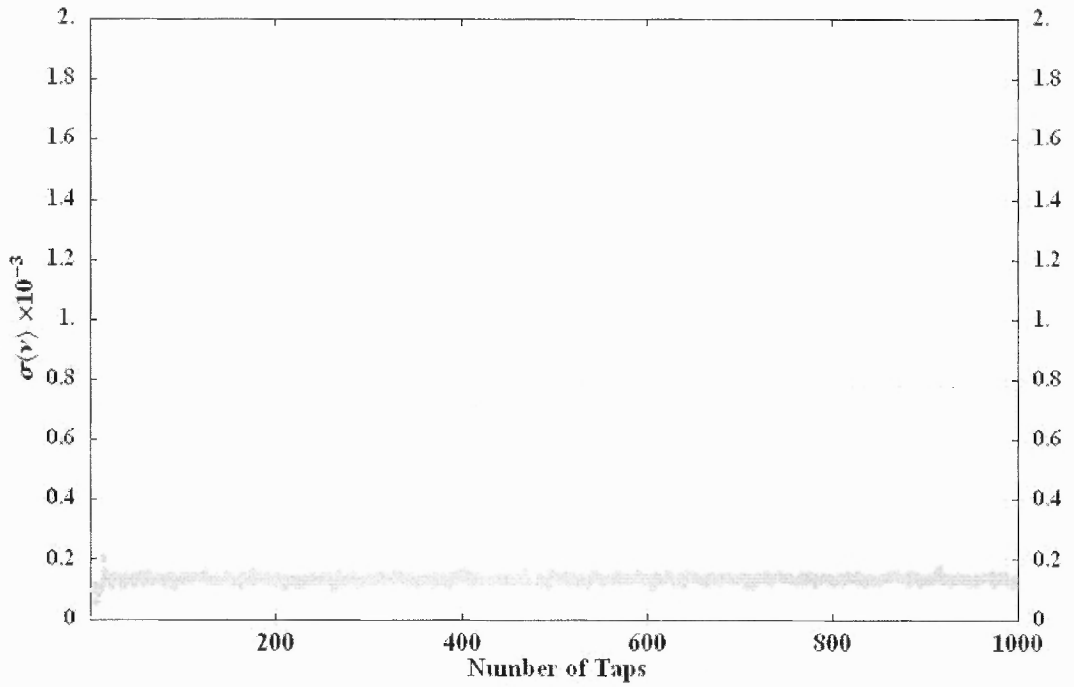

Figure 2.16: Density and Standard Deviation curve for $\gamma = 0.4$.

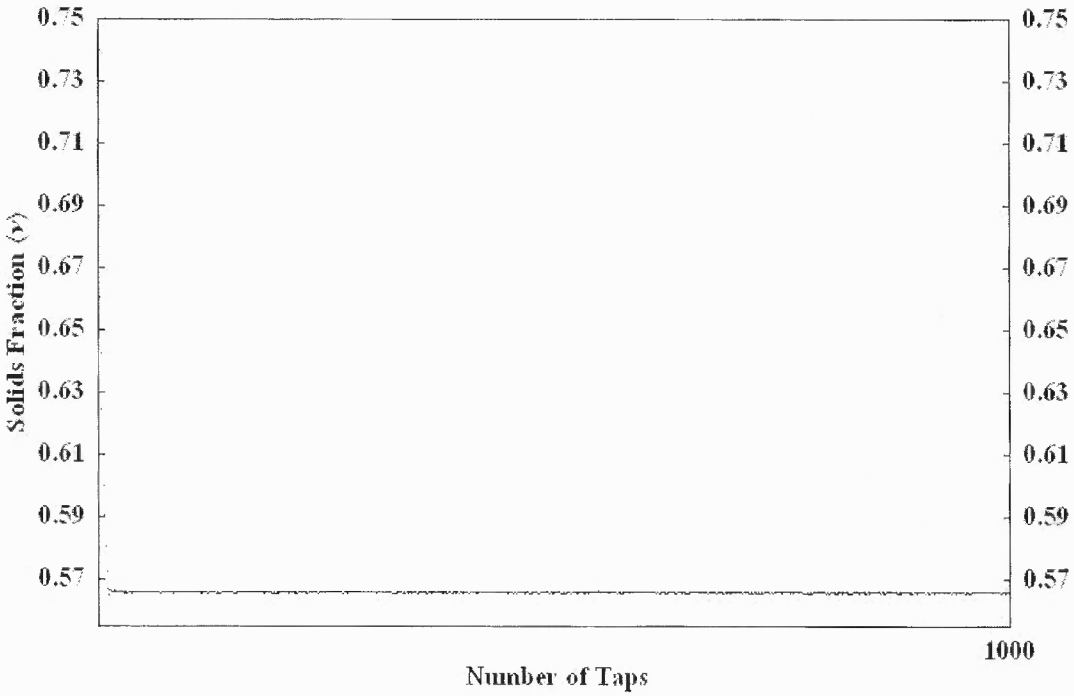

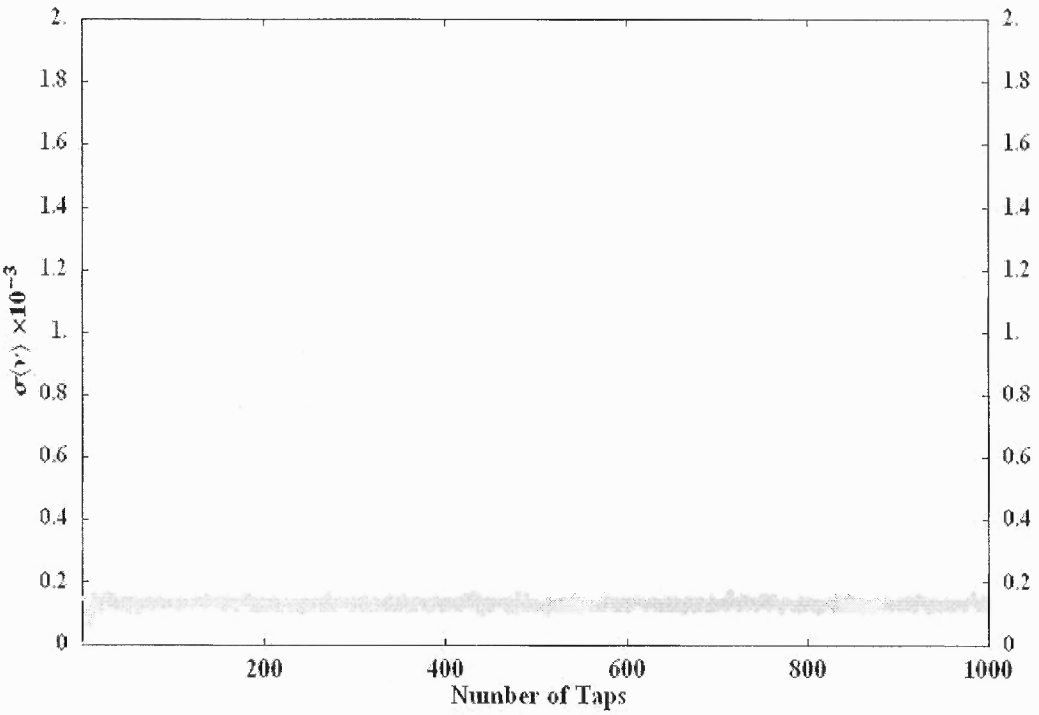

Figure 2.17: Density and Standard Deviation curve for $\gamma = 0.5$.

To gain some insight into the structure of the two densest configurations which correspond to $\gamma = 0.2$ and $\gamma = 0.25$, a VCD analysis is carried out using the configuration data. Figure. 2.18 to 2.19 show the distributions for $\gamma = 0.2$ and $\gamma = 0.25$ for 20,000 and 30,000 taps respectively . In both cases, there is an ordering that starts from the floor and propagates upwards. A similar effect was observed when starting from a poured configuration and applied the same uniform lift expansion parameters as seen in [28].

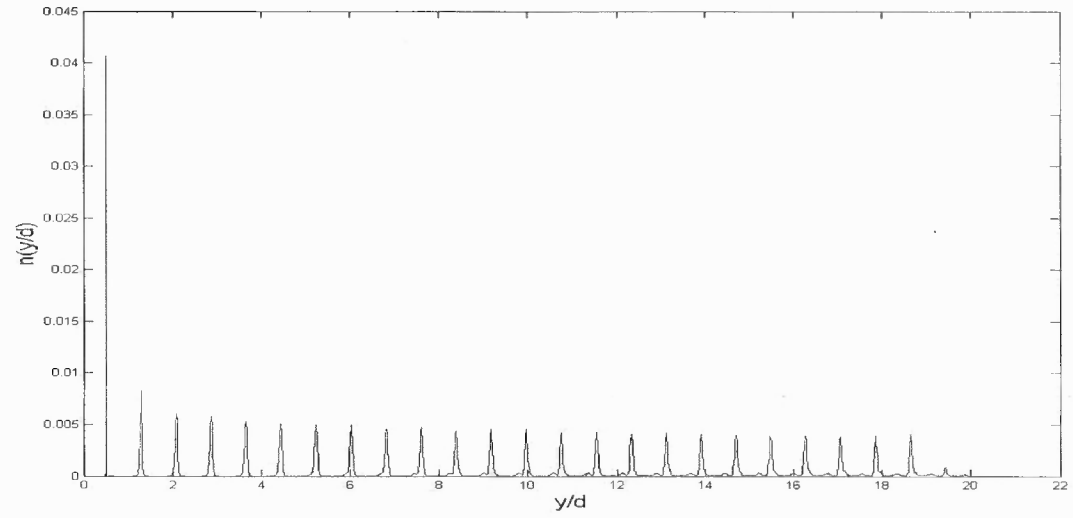

Figure 2.18: VCD for $\gamma = 0.2$

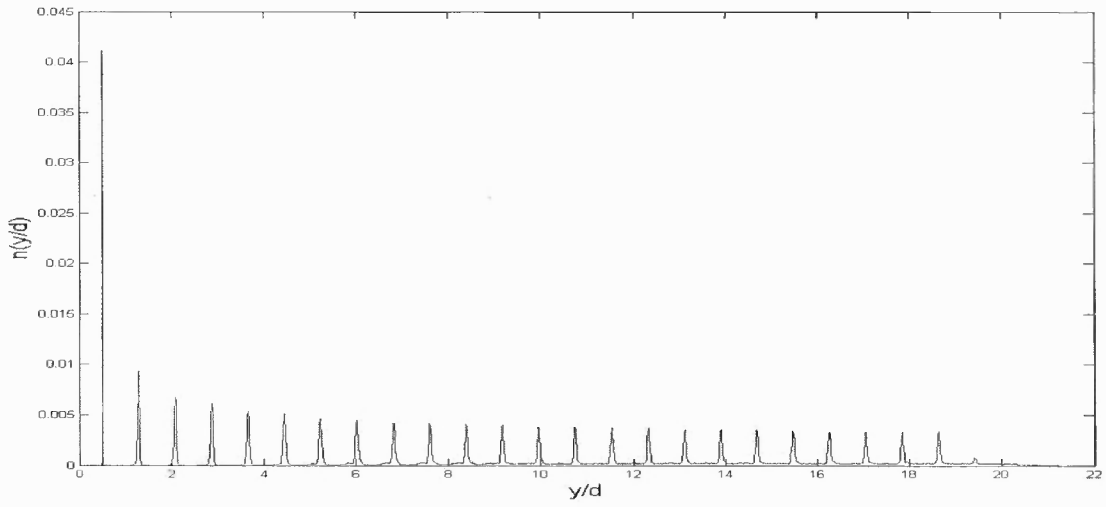

Figure 2.19: VCD for $\gamma = 0.25$

2.8 Perturbation of the Tap Intensity

In this study, the effect of perturbing an equilibrated system by changing the tap intensity γ was examined. For this purpose, $\gamma = 0.33$ was chosen, which equilibrated to a bulk

density $\langle \nu \rangle_\infty = 0.6195$ in 30,000 taps. Then, the intensity was decreased to 0.3 and another 20,000 taps were applied, resulting in approximately 1.6% increase in bulk solids fraction to $\langle \nu \rangle_\infty = 0.6295$. The ensemble-averaged density and its standard deviation versus the number of taps for this process are shown in Figure. 2.20a and 2.20b, respectively.

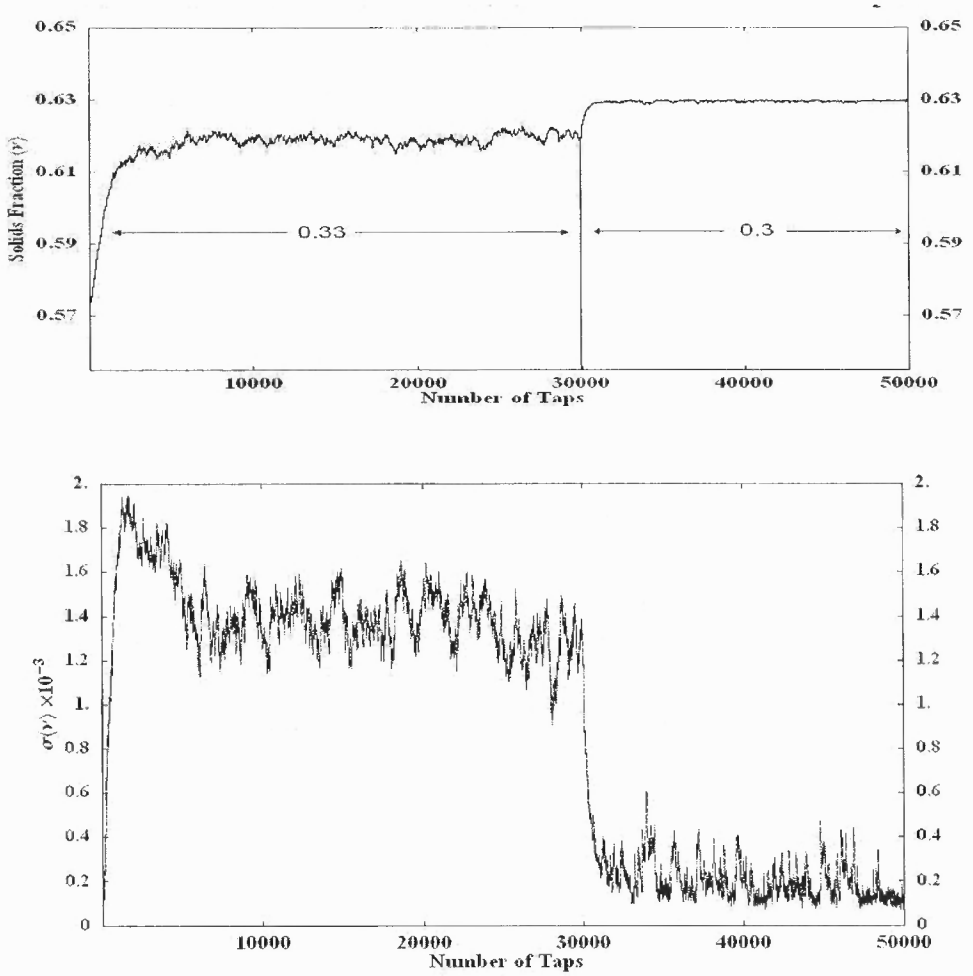

FIGURE 2.20. (a) Monte Carlo evolution of the ensemble-averaged solids fraction <ν> versus the number of taps: $\gamma = 0.33$, $\langle \nu \rangle_\infty = 0.6195$; $\gamma = 0.3$, $\langle \nu \rangle_\infty = 0.6295$; (b). Standard deviation versus number of taps.

A substantial jump in solids fraction (Figure. 2.20a) takes place where the γ was reduced to 0.3, accompanied by a corresponding pronounced reduction in the standard deviation and its fluctuations (Figure. 2.20b). A further reduction in γ to 0.25 at 50,000 taps produces a substantially reduced rate of increase in solids fraction to 0.6425 as shown in Figure. 2.21, after the application of 110,000 additional taps. Although not shown here, the standard deviation in this case indicated that the system had not yet equilibrated.

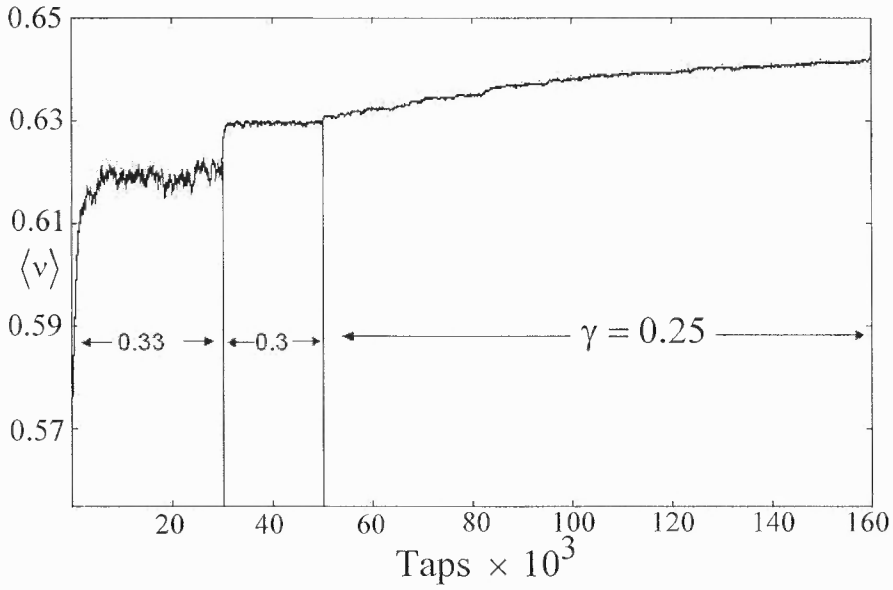

FIGURE 2.21: MC evolution of $\langle \nu \rangle$.

CHAPTER 3

DESCRIPTION OF THE DISCRETE ELEMENT MODEL

3.1 Introduction

This chapter contains a description of the Discrete Element simulation model, beginning with a concise background on the method itself and the force models used. This is followed by introducing the physical properties of system. Details of the modifications made to an existing discrete element code are described, consisting of how discrete taps were implemented. Finally, the analyses of the particle layer responses to the taps via maximum displacements are provided.

3.2 Background

The discrete element method (DEM) is based on the numerical solution of Newton's laws for a set of discrete, interacting particles. A recent and detailed review of this method and applications can be found in [46, 47]. In the study discussed here, particles were inelastic, frictional, monodisperse spheres obeying binary, soft-sphere interactions [48] in which normal and tangential impulses are functions of a small overlap between colliding particles. Energy loss in the normal direction (i.e., along center line of contacting spheres) is produced by linear loading (K_1) and unloading springs (K_2), corresponding to a constant restitution coefficient $e = \sqrt{K_1/K_2}$. This model has been shown to reproduce the nearly linear loading behavior for a spherical surface that experiences plastic deformation of the order of 1% of a particle diameter. In the tangential direction, a

Mindlin- Deresiewicz-like model [49] is used in which tangential stiffness, given by Equation 3.1 below,

$$. K_T = \begin{Bmatrix} K_o\left[1-\left(T-\hat{T}\right)/\mu N-\hat{T}\right]^{1/3}, \text{ increasing } T \\ K_o\left[1-\left(\hat{T}-T\right)/\mu N+\hat{T}\right]^{1/3}, \text{ decreasing } T \end{Bmatrix} \tag{3.1}$$

(where $K_O = 0.8K_1$), decreases with tangential displacement until full sliding occurs at the friction limit μ [50]. Here, $\hat{T}$ is initially equal to zero; subsequently, it is set to the value of the total tangential force when the tangential displacement changes direction.

The computational domain is again a laterally periodic box ($12d$ x $12d$) in which particles randomly placed at t = 0 within the box are allowed to settle under gravity to a fill height of approximately 22 particle diameters as shown in Figure. 3.1. The different color particles that are present have the sole purpose of aesthetics.

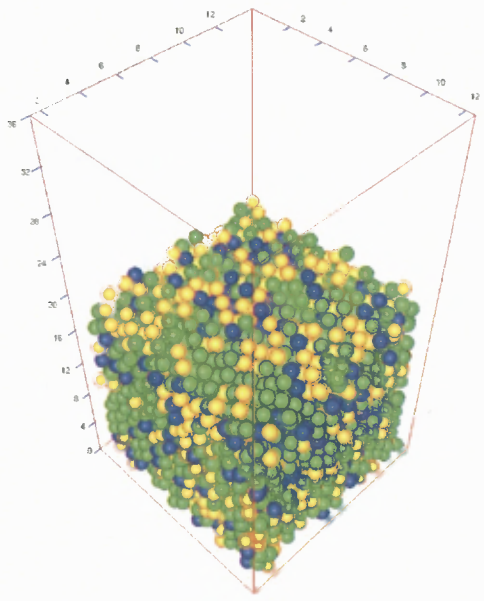

Fig. 3.1. A snapshot of a system of particles as described above with a fill height of approximately 22d.

The number of spheres in these studies was the same as for the MC simulations. By tuning the value of the friction coefficient μ, it is possible to obtain a wide range of solids fractions. This is demonstrated in the simulation results summarized in Figure. 3.2, which were obtained by averaging twenty independent realizations of poured particles.

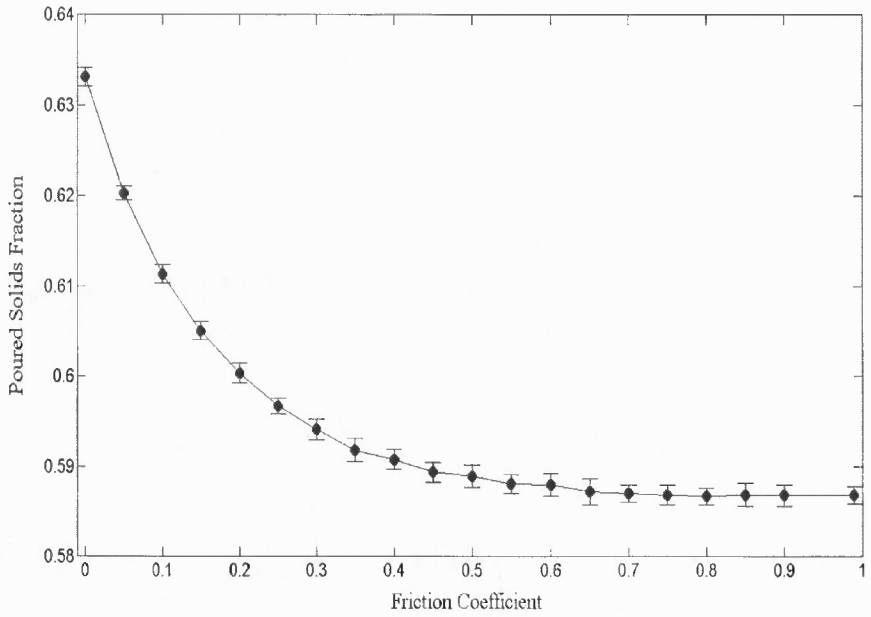

Fig. 3.2. A wide range of bulk densities can be obtained by changing particle friction properties. Each point on the graph represents an average taken over 20 discrete element realizations, with the vertical lines representing the deviation from the average.

For large friction coefficients, less dense systems are produced after pouring due to the formation of bridges and arches within the structure. For smooth particles ($\mu = 0$), the bulk solids fractions obtained are in good agreement with the value (0.6366 ± 0.0005) normally attributed to a random packing of spheres [28]. It should be noted that the dependence of the solids fraction on friction coefficient has been reported for spheres [9] and for disks [71].

For the remainder of the discussion, the focus of the simulation studies will be primarily on spheres for which $e = 0.9$ $\mu = 0.1$ and $\rho \approx 1200$ kg/m^3. It is understood that these material properties may also have significant influence on system behavior.

3.3 Tapping Protocol

The assembly of spheres is tapped by prescribing impulses to the floor. In particular, a half-sine displacement wave of frequency f is applied to the floor, so that the period t_b is $(1/2f)$. The equation for the velocity of the impulse particle is by equation (3.2), where v_{amp} is maximum magnitude of the velocity of the floor, t_p is the relaxation time, Ω is angular frequency ($2\pi f$), ir is the tap number, and t_C is the time duration of a "cycle". Here, the term "cycle" refers to the period of the tap plus the time required for the system to relax to a quiescent state, i.e., $t_c = t_b + t_p$.

$$v_f(t) = v_{amp} \cdot \cos\left(\Omega\left(t - t_p + (ir-1)t_C\right)\right) \tag{3.2}$$

When the system of particles is tapped, the impulse from the floor is transmitted to the particles resting on the floor. The resulting impulse then engenders collisions between particles in the system thereby causing an increase in the kinetic energy of the system. The system then settles down during the relaxation time scale t_p so that the kinetic energy of the system is zero for all practical purposes. An example of the floor motion is shown in Figure. 3.3 for the case $f = 5$ Hz, $t_b = 0.1$ sec, $t_p = 0.3$ sec and t_C is 0.4 sec.

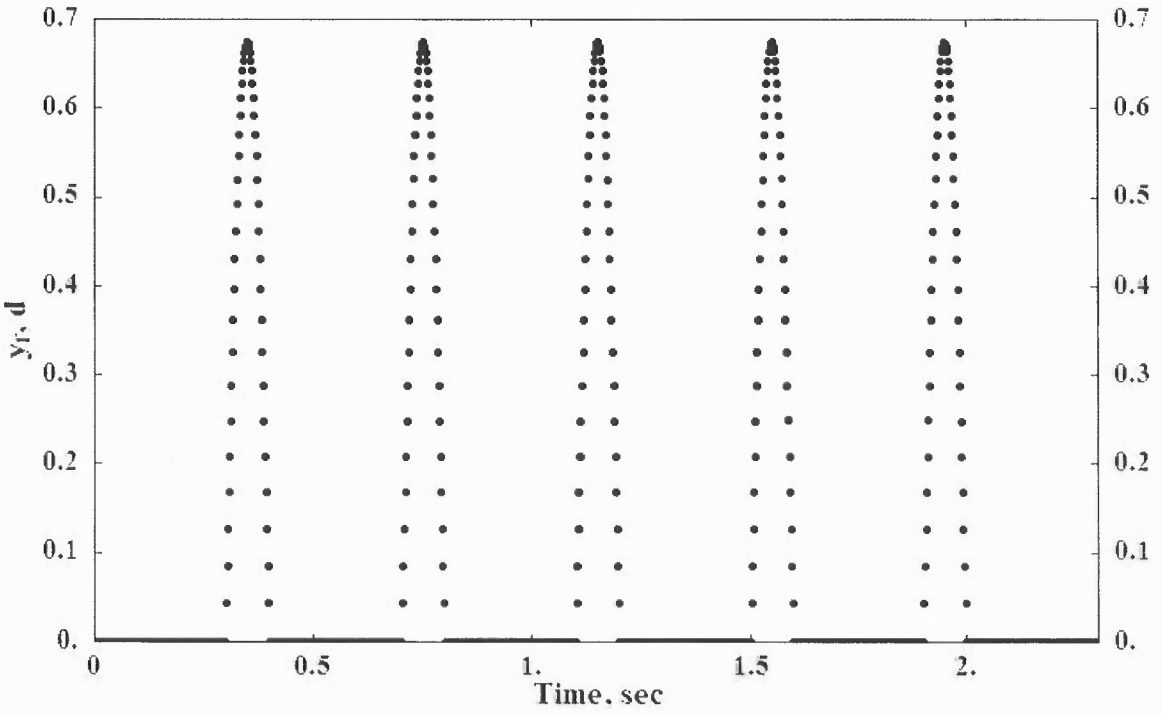

Figure 3.3. The evolution of the vertical position of the floor level y_f. The floor particle is positioned below y_f at one particle radius taken from [93] .

3.4 Kinetic Energy Analysis

The behavior of a system of particles is influenced by a number of parameters that includes the restitution coefficient *e*, inter-particle friction coefficient μ, mass overburden, frequency *f*, dimensionless displacement amplitude of the floor (*a*/*d*) and aspect ratio (L/d) of the vessel. Because of the size of the parameter space and the availability of computing resources, it was necessary to fix some of these parameters while varying others that were deemed to have a more substantial influence on system behavior.

A kinetic energy study was done to determine the role that *e*, *f* and *a*/*d* played on the behavior of a system, for which the aspect ratio was 12*d* x 12*d* for the lateral

dimensions of the vessel and the fill height was $H \sim 12d$ (1728 particles). While the study was not exhaustive, interesting trends were identified.

From the first case of $f = 30$ Hz and $e = 0.3$, one can see in Figure. 3.4 the formation of a secondary peak in the kinetic energy distribution at the large a/d values. However, there is quite a bit of energy dissipation since the restitution coefficient is somewhat small ($0 < e \leq 1$).

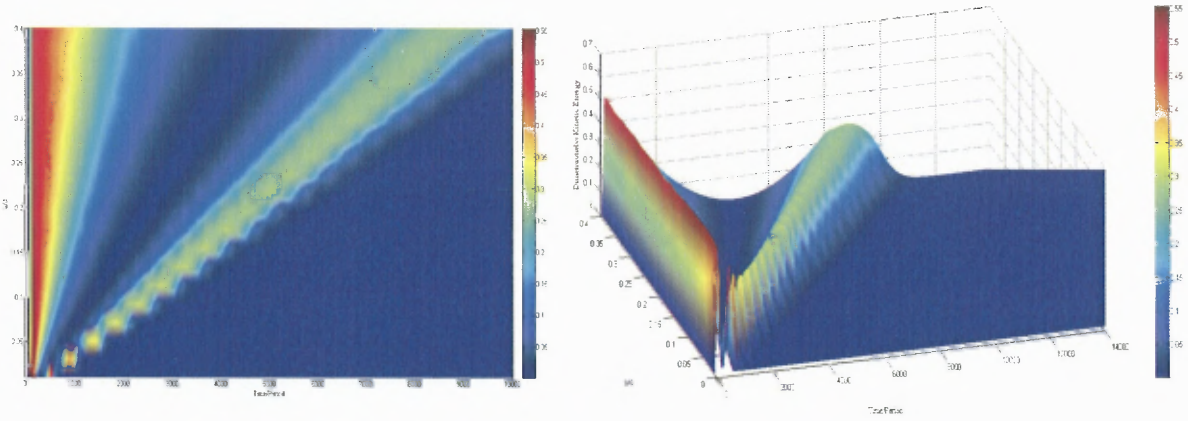

Figure 3.4: Kinetic Energy Distribution for a frequency of 30 Hz and restitution coefficient of 0.3.

The second case is for a frequency of 30 Hz and restitution coefficient of 0.5 in Figure. 3.5, one can see that there is a secondary peak in the kinetic energy distribution forming for larger a/d ratios. The secondary peaks in the energy distribution are more prominent compared to the case of a restitution coefficient of 0.3 since the restitution coefficient is higher in this case.

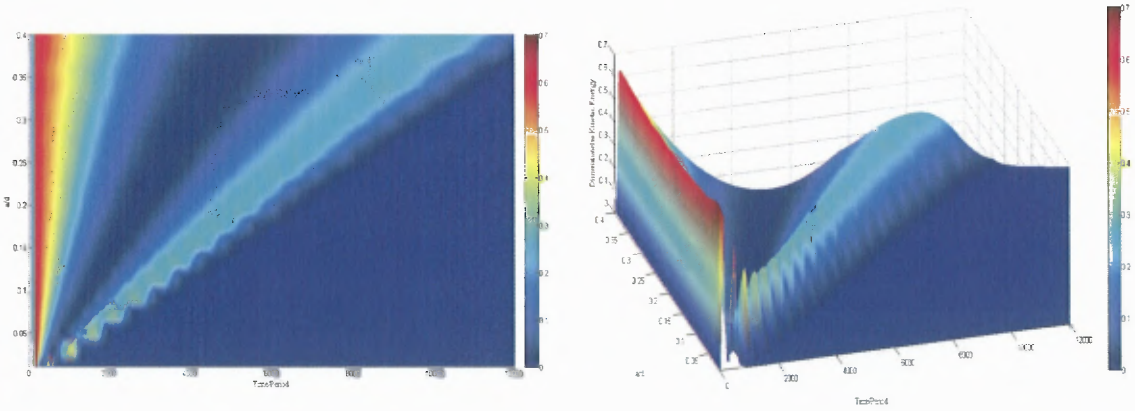

Figure 3.5: Kinetic Energy Distribution for a frequency of 30 Hz and restitution coefficient of 0.5.

The third case is for a frequency of 30 Hz and restitution coefficient of 0.7 in Figure. 3.6, one can see that there is a secondary peak in the kinetic energy distribution forming for larger a/d ratios. The secondary peaks in the energy distribution are seen in this case.

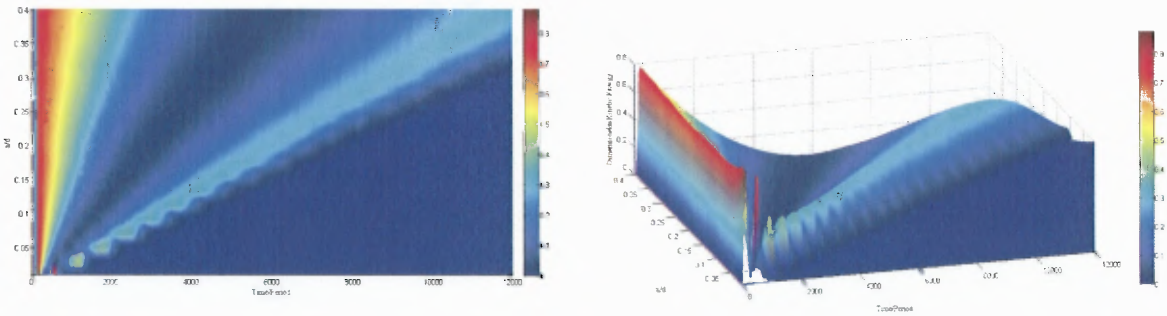

Figure 3.6: Kinetic Energy Distribution for a frequency of 30 Hz and restitution coefficient of 0.7

Figure 3.7 below is for a frequency of 30 Hz and restitution coefficient of 0.9. One can see that there is a secondary peak in the kinetic energy distribution forming for

larger a/d ratios. Compared to the cases of $e = 0.3$, 0.5 and 0.7 the secondary peak for 0.9 is larger, which can be attributed because there is not as much energy loss since 0.9 is the highest restitution coefficient that was investigated.

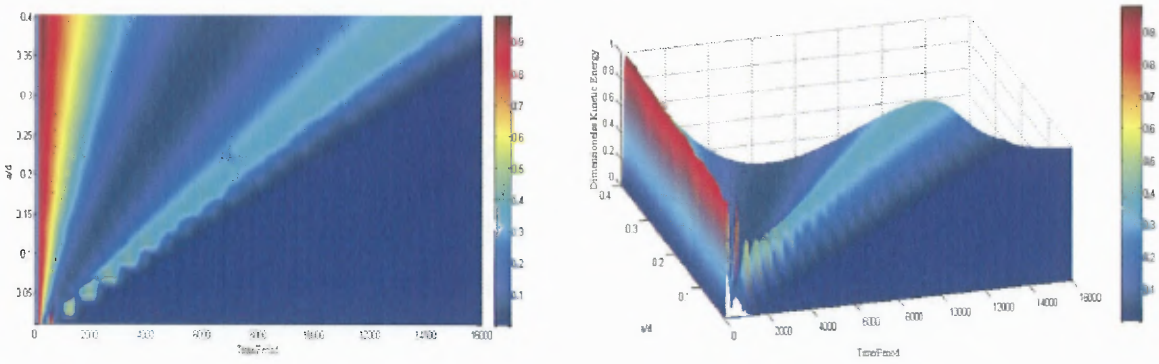

Figure 3.7: Kinetic Energy Distribution for a frequency of 30 Hz and restitution coefficient of 0.9.

In Figure 3.8 below, the kinetic energy distribution is represented as a surface and contour plot for a frequency of 40 Hz and restitution coefficient of 0.3. One can see that there is a secondary peak in the kinetic energy distribution forming for larger a/d ratios. Additionally, the secondary peaks still form even with a different frequency.

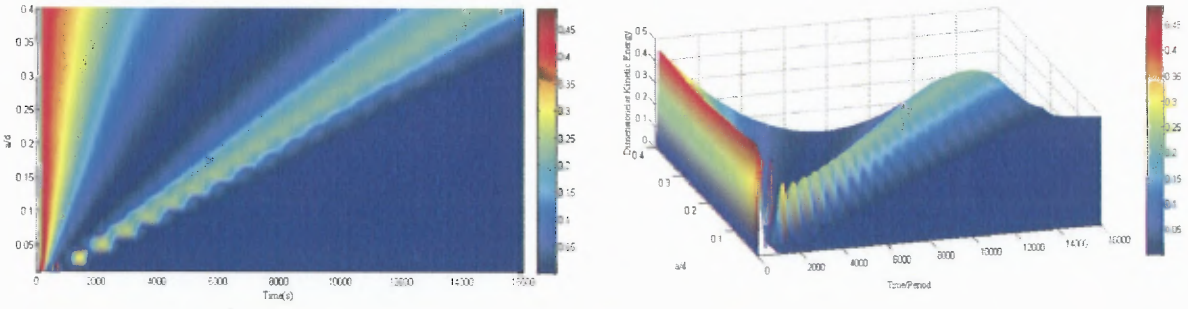

Figure 3.8: Kinetic Energy Distribution for a frequency of 40 Hz and restitution coefficient of 0.3.

Figure 3.9 below is for a frequency of 40 Hz and restitution coefficient of 0.5. In that figure, can see that there is a secondary peak in the kinetic energy distribution forming for larger a/d ratios. Secondary peaks are more prominent for a restitution coefficient of 0.5 than 0.3 for 40 Hz just as was seen for 30 Hz.

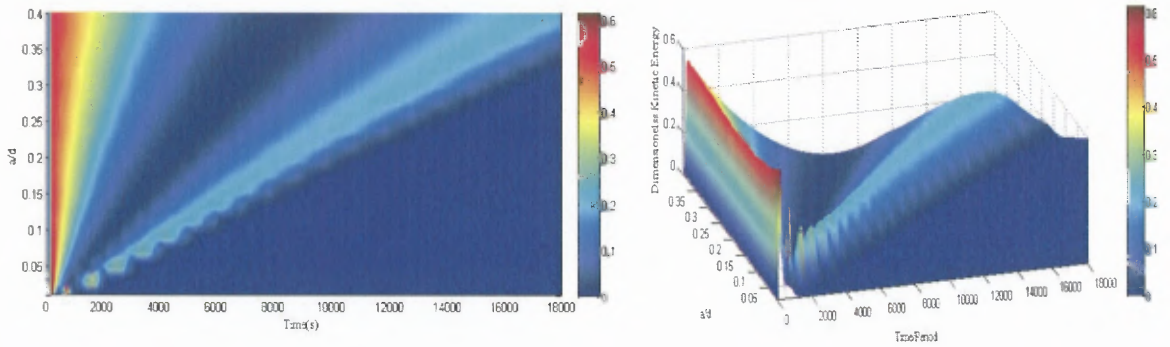

Figure 3.9: Kinetic Energy Distribution for a frequency of 40 Hz and restitution coefficient of 0.5.

In Figure 3.10, the kinetic energy distribution is done for a frequency of 40 Hz and restitution coefficient of 0.7. It should be noted again that there is a secondary peak in the kinetic energy distribution forming for larger a/d ratios.

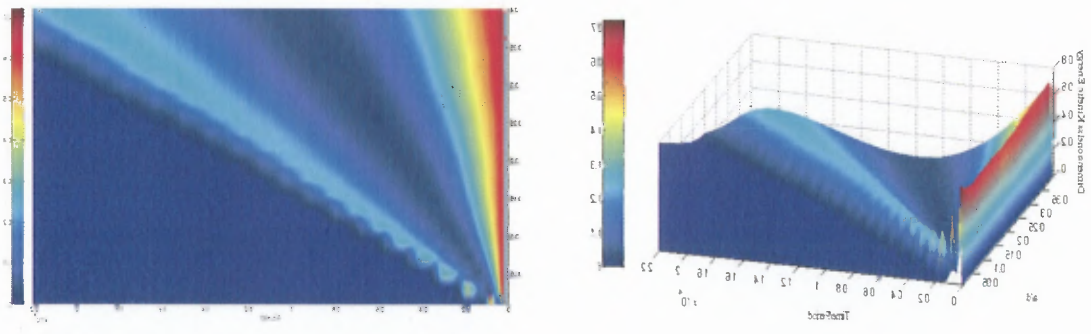

Figure 3.10: Kinetic Energy Distribution for a frequency of 40 Hz and restitution coefficient of 0.7.

Figure 3.11 represents the kinetic energy distribution for a frequency of 40 Hz and restitution coefficient of 0.9 in Figure. 3.10, one can see that there is a secondary peak in the kinetic energy distribution forming for larger a/d ratios. Additionally, as was seen for a frequency of 30 Hz, the restitution coefficient of 0.9 had the largest secondary peak in the kinetic energy distribution because there is less energy dissipation for the higher restitution coefficient.

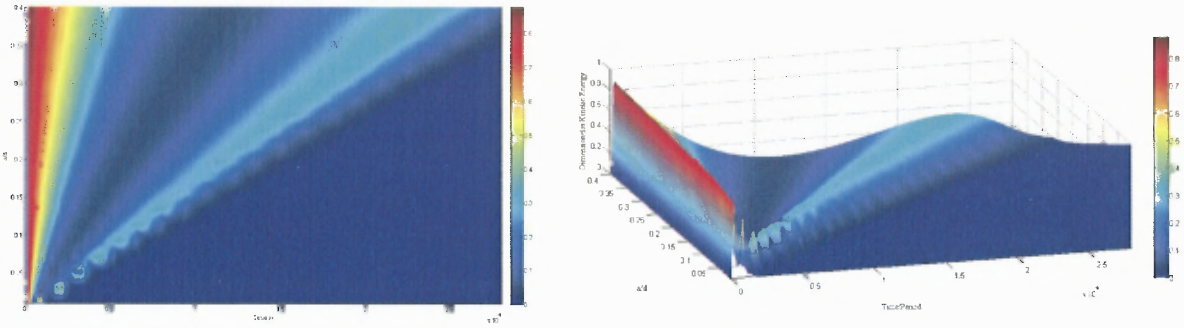

Figure 3.11: Kinetic Energy Distribution for a frequency of 40 Hz and restitution coefficient of 0.9.

CHAPTER 4

DEM CASE STUDIES OF DENSITY RELAXATION IN GRANULAR MATERIAL

4.1 Introduction

In this chapter, the results that are presented are obtained by using the DEM method to simulate a system of particles that are subjected to the aforementioned tapping protocol. The system of particles will be tapped using two different accelerations and in one case the mass overburden will be doubled to determine how the bulk density behaves for a larger fill height. In addition, microstructure tools will be presented and applied to analyze the behavior of such system of particles that are subjected to tapping.

4.2 Motivation of Analysis

The process of how disorganized systems of particles become dense is one that is not thoroughly understood. Even with widely used techniques that include the solids fraction as well as the nearest neighbor distribution and the free volume distribution, there still remain many questions on how a system reorganizes to arrive at dense structures. Tools that have been developed to analyze that problem have included the vertical center distribution which has been inspired by P. Singh et al [98, 99]. In addition another tool will be used that is called the local density evolution of the system which makes use of the Voronoi tessellation.

4.3 Dependence on Amplitude and Frequency for Single Realizations

The phase space of the parameters in the DEM simulation is quite large. To understand how each parameter plays a role in the behavior of the system of particles, a study was done to investigate how the amplitude, and frequency affect the way a system organizes from a loose to a dense state. The cases were run at different frequencies and different amplitudes for only one realization.

The first case that was run for an acceleration of $\Gamma = 1.0$. The results are shown below for each frequency in Figures 4.1 and 4.2.

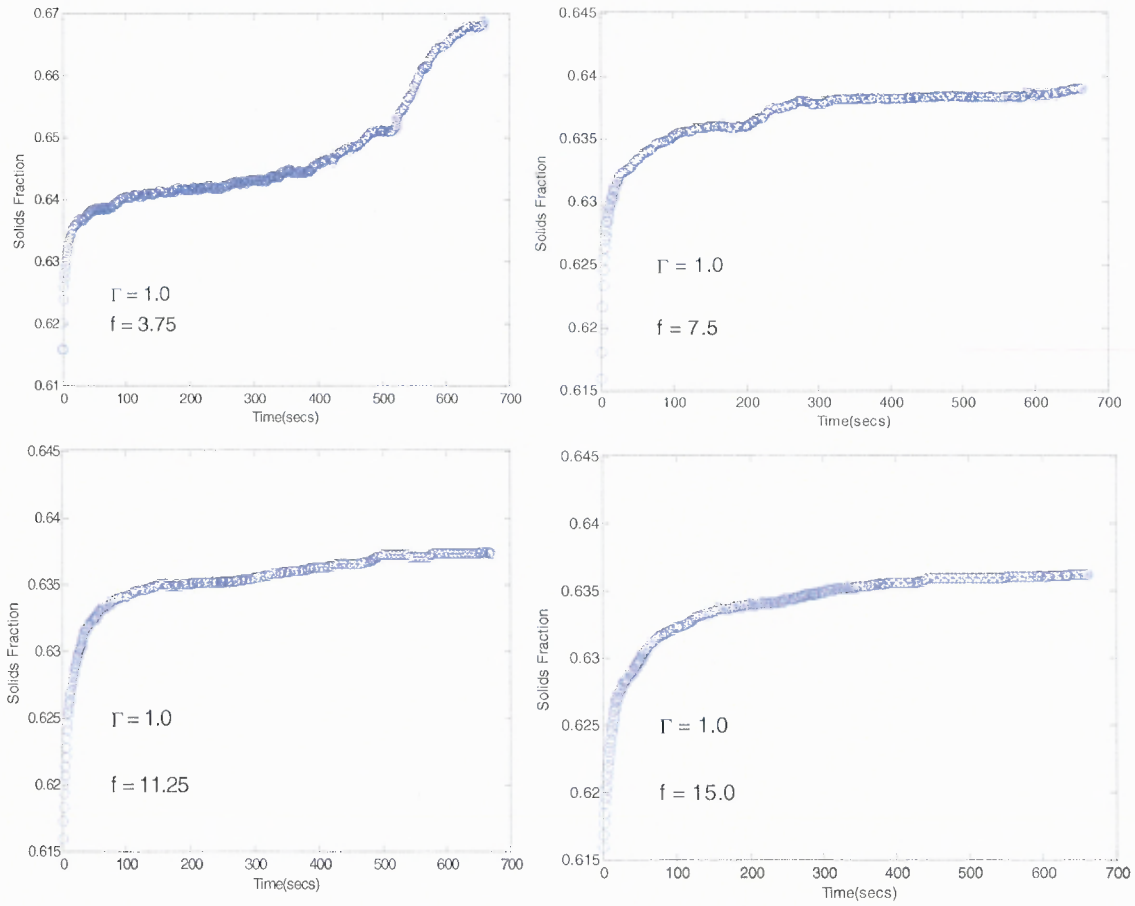

Figure 4.1: Single Realizations for $\Gamma = 1.0$ for frequencies of 3.75, 7.5, 11.25 and 15.0 Hz.

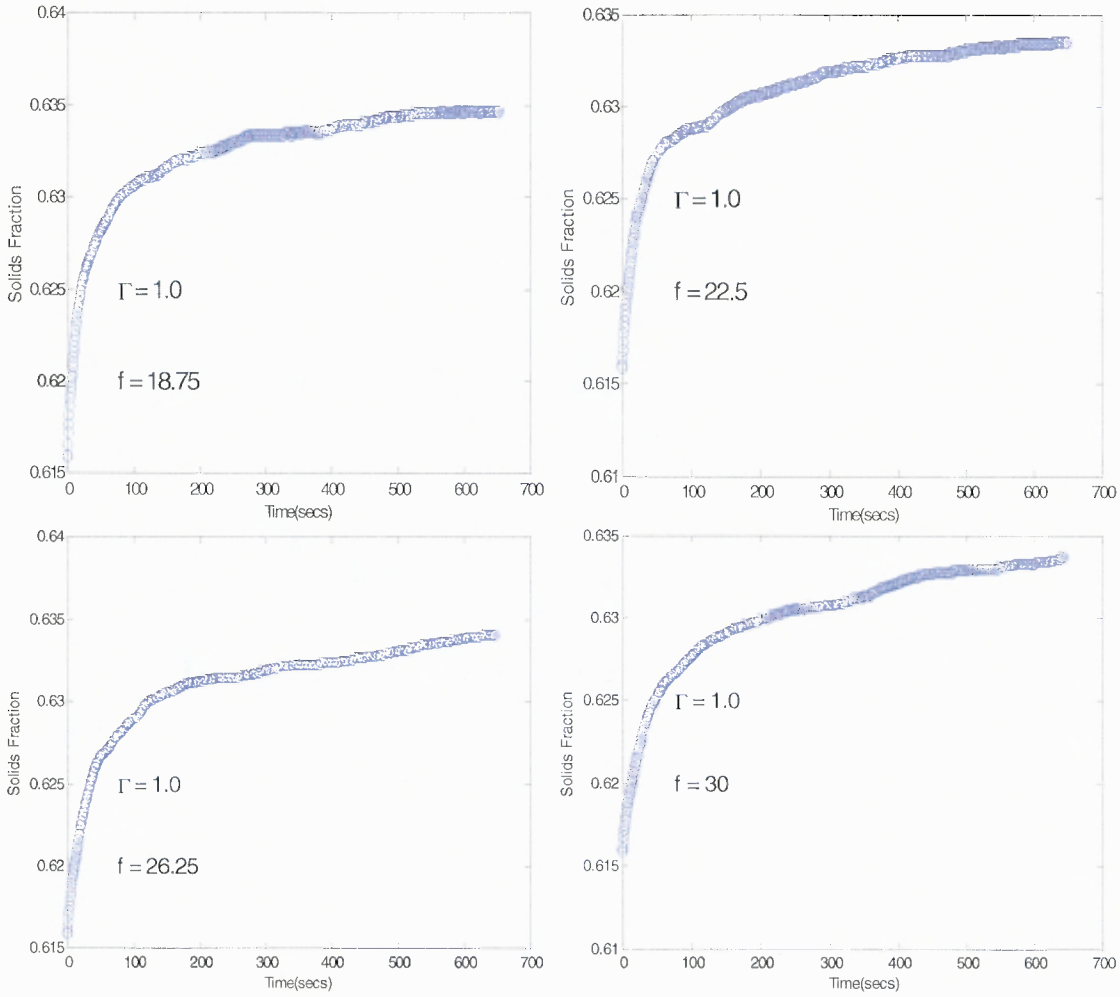

Figure 4.2: Single Realizations for $\Gamma = 1.0$ for frequencies of 18.75, 22.5, 26.25 and 30.0 Hz.

For $\Gamma = 1.0$, the solids fraction evolution as a function of time indicates that the system of particles hasn't reached its equilibrium solids fraction since the curves in Figures 4.1 and 4.2 are still increasing.

The next acceleration that was investigated was for $\Gamma = 1.5$ at different frequencies. The results of the solids fraction are displayed in the plots below in Figures 4.3, 4.4 and 4.5. For a frequency of 3.75 Hz, there is a gradient that occurs that causes a "jump" in the solids fraction from 0.68 to approximately 0.705.

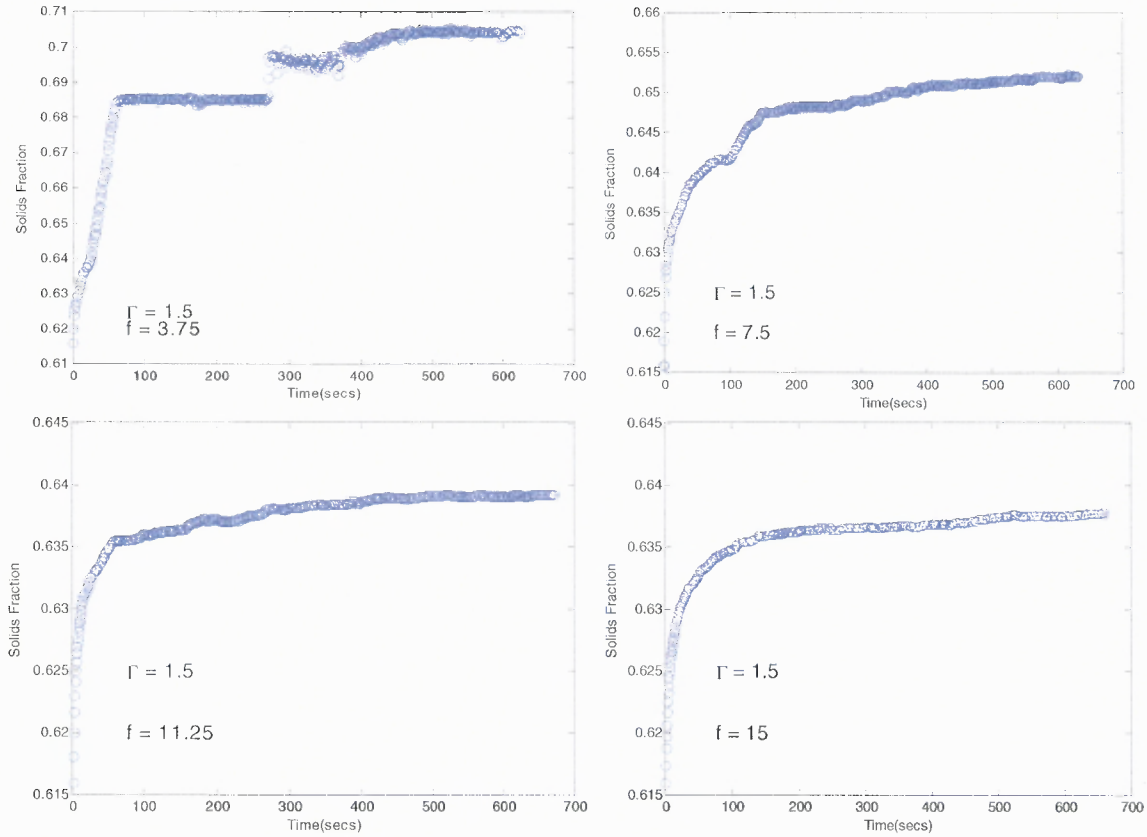

Figure 4.3: Single Realizations for $\Gamma = 1.5$ for frequencies of 3.75, 7.5, 11.25 and 15.0 Hz.

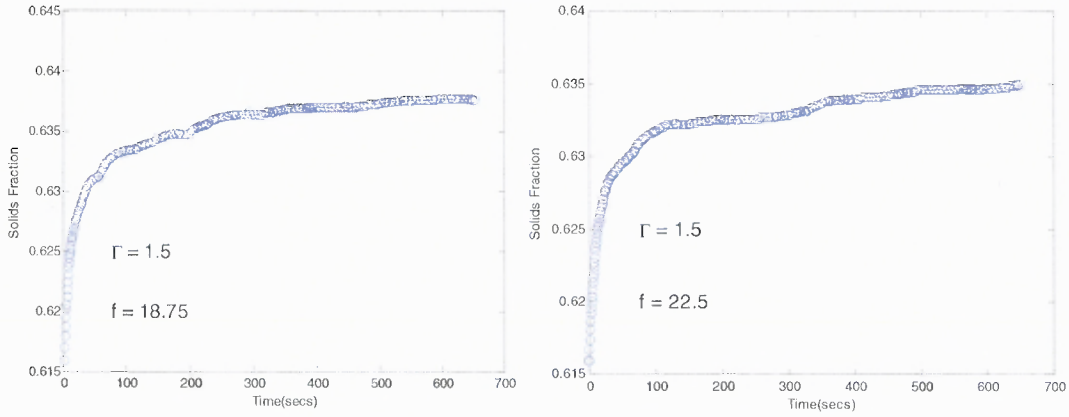

Figure 4.4: Single Realizations for $\Gamma = 1.5$ for frequencies of 18.75 and 22.5 Hz.

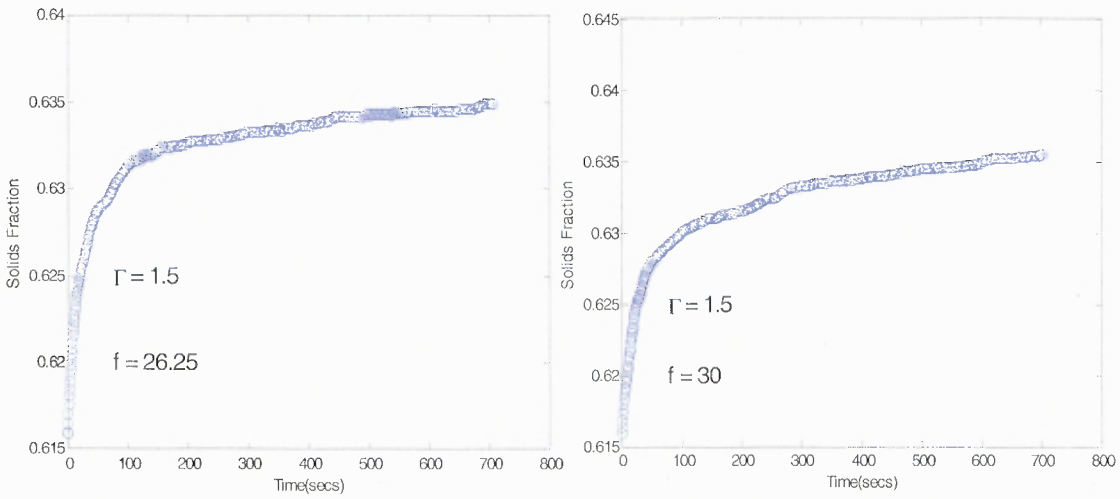

Figure 4.5: Single Realizations for $\Gamma = 1.5$ for frequencies of 26.25 and 30 Hz.

An acceleration of 2.0 is presented in the following results in Figures 4.6 and 4.7. It should be noted that a frequency of 3.75 Hz produces a somewhat noisy density evolution because the system was not quiescent during the long time scale due to the insufficient time that was used for the relaxation phase. In addition, a frequency of 7.5 Hz produces a large gradient in the solids fraction evolution.

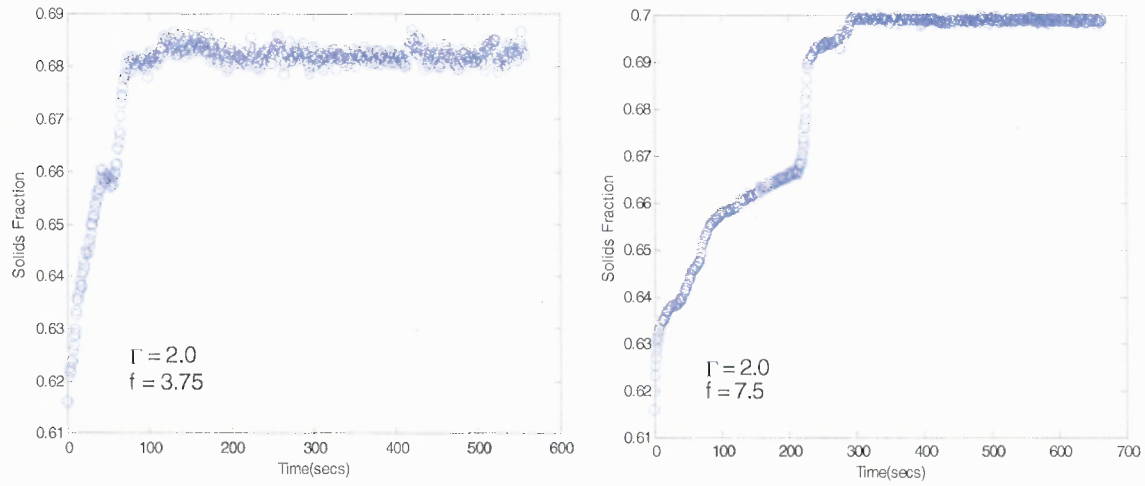

Figure 4.6: Single Realizations for $\Gamma = 2.0$ for frequencies of 3.75 and 7.5 Hz.

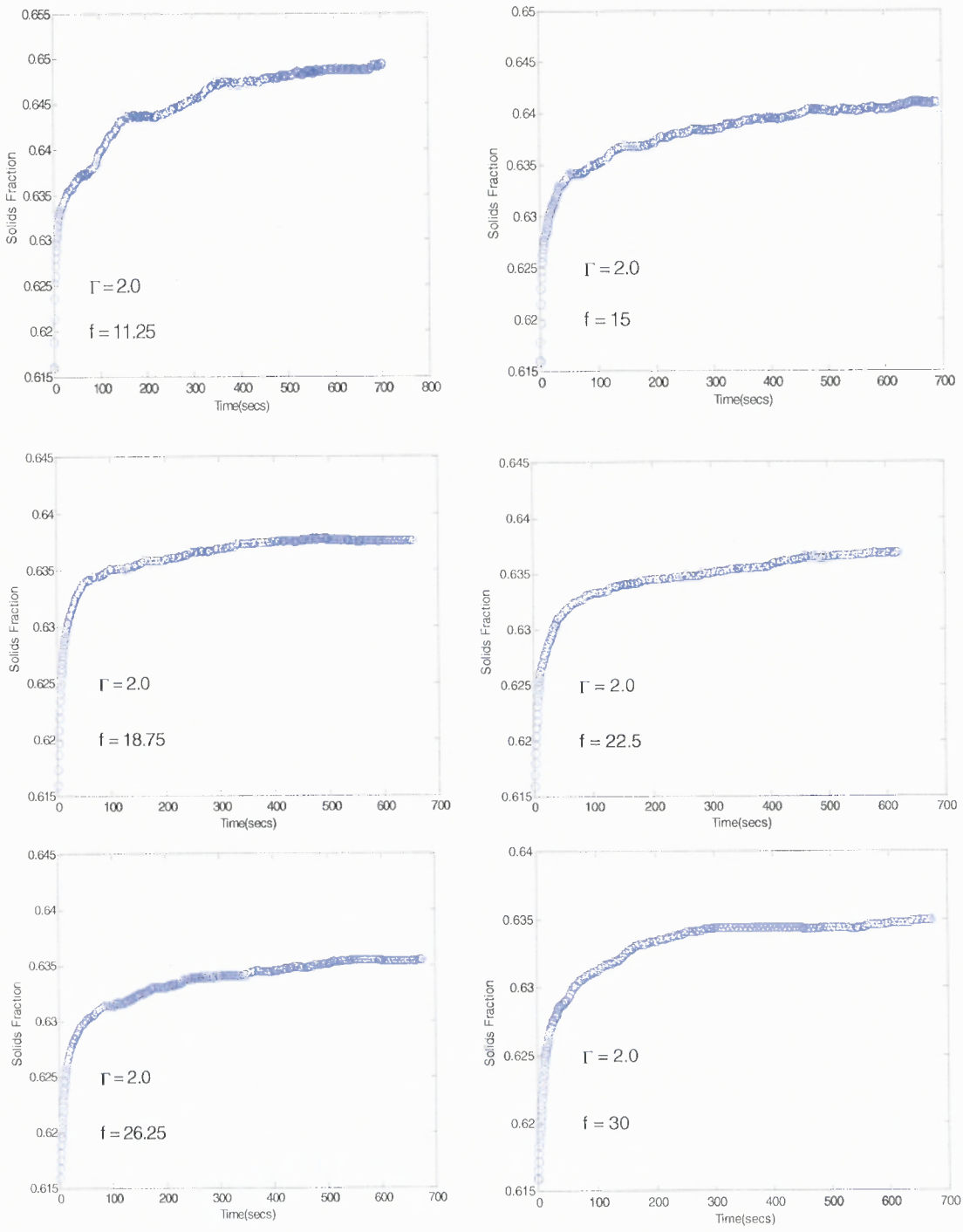

Figure 4.7: Single Realizations for $\Gamma = 2.0$ for frequencies of 11.25, 15, 18.75, 22.5, 26.25, and 30 Hz.

An acceleration of 2.25 is presented in the following results in Figures 4.8 and 4.9. It should be noted that a frequency of 3.75 Hz produces a somewhat noisy density evolution because the system was not quiescent during the long time scale due to the insufficient time that was used for the relaxation phase. Frequencies of 7.5 and 11.15 Hz have gradients that produces increases of the solids fraction as was previously shown.

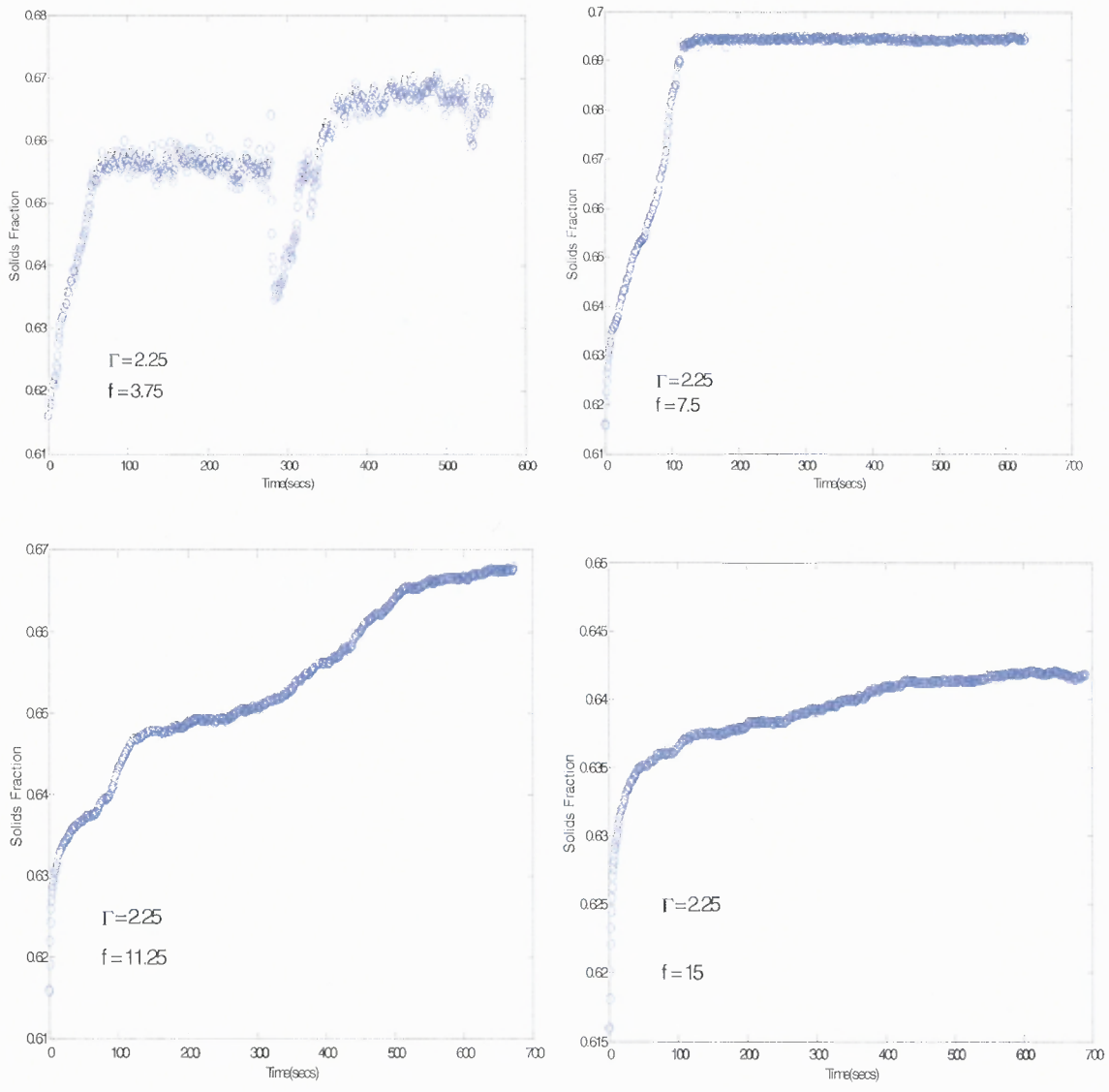

Figure 4.8: Single Realizations for Γ = 2.25 for frequencies of 3.75, 7.5, 11.25 and 15.0 Hz.

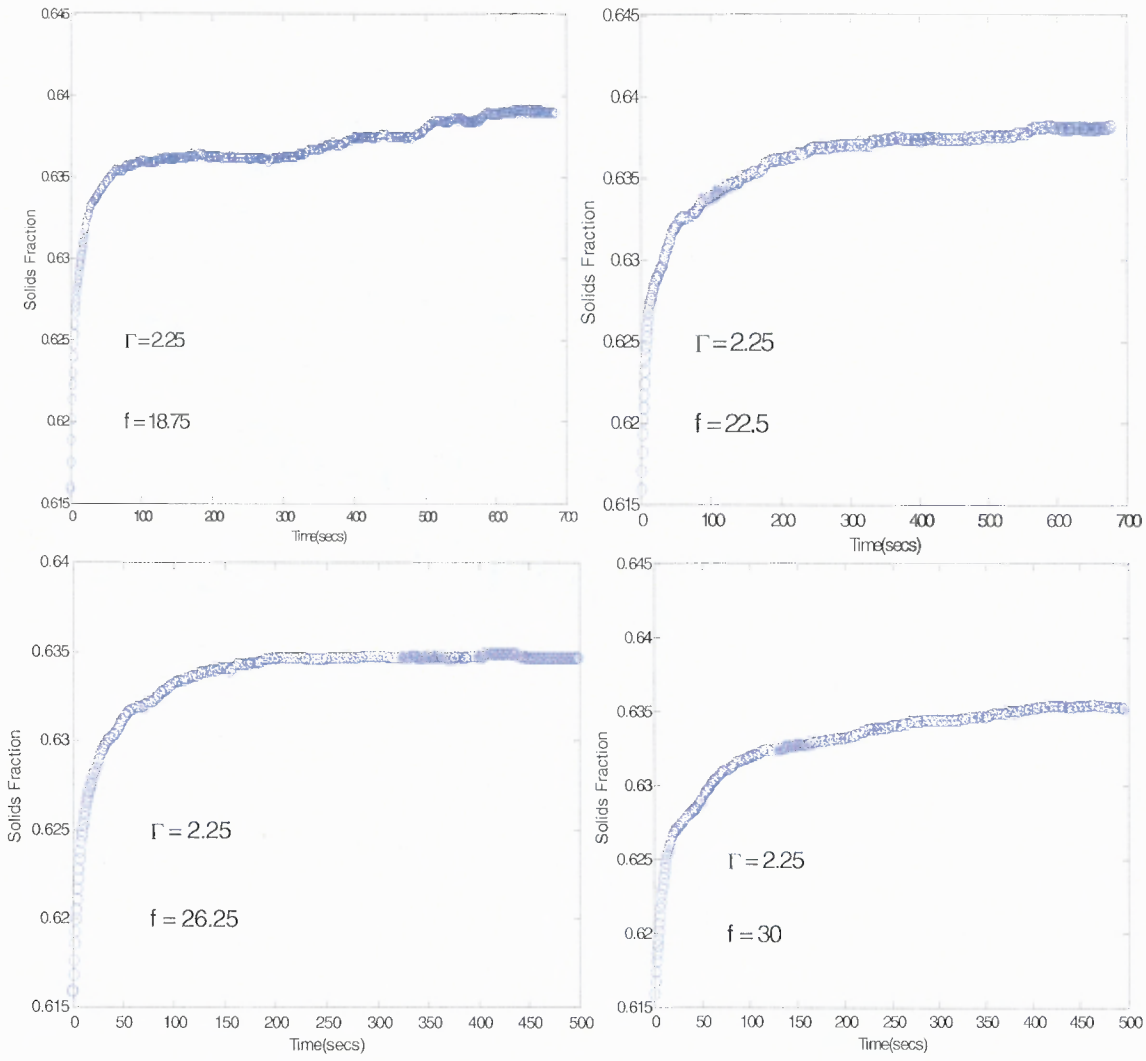

Figure 4.9: Single Realizations for Γ = 2.25 for frequencies of 18.75, 22.5, 26.25 and 30.0 Hz.

An acceleration of 3.0 is presented in the following results in Figures 4.10, 4.11 and 4.12. It should be noted that a frequency of 7.5 Hz produces a somewhat noisy density evolution because the system was not quiescent during the relaxation phase. In addition, a frequency of 11.25 Hz starts to produce a density curve that contains larger gradients in the solids fraction evolution.

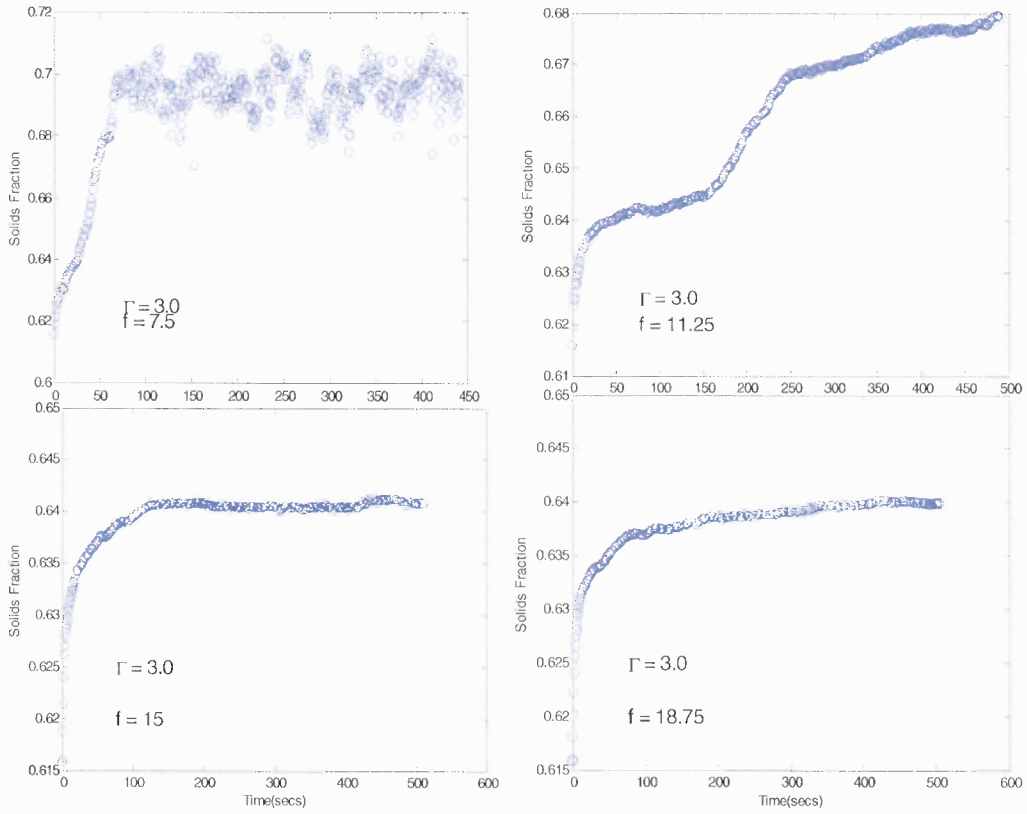

Figure 4.10: Single Realizations for Γ = 3.0 for frequencies of 7.5, 11.25, 15.0 and 18.75 Hz.

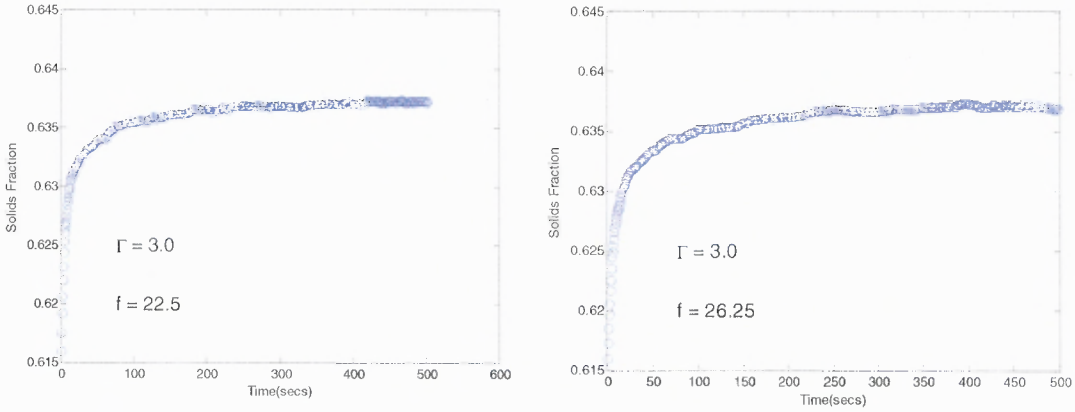

Figure 4.11: Single Realizations for Γ = 3.0 for frequencies of 22.5 and 26.25 Hz.

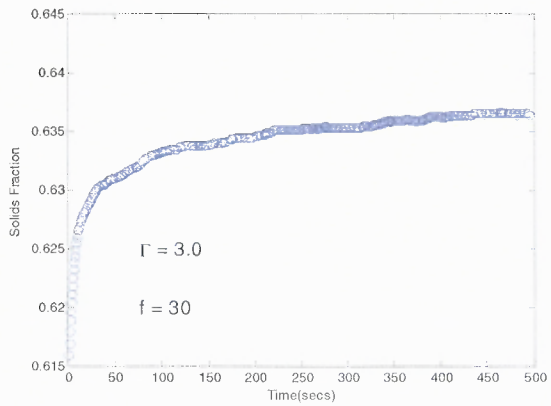

Figure 4.12: Single Realizations for Γ = 3.0 for a frequency of 30 Hz.

An acceleration of 3.5 is presented in the following results in Figures 4.13, 4.14, 4.15 and 4.16. It should be noted that a frequency of 7.5 Hz produces a somewhat noisy density evolution because the system was not quiescent, while frequencies of 11.25, and 15 show sharp increases in the solids fraction. Additionally, a frequency of 18.75 begins to show an onset of gradients in the solids fraction.

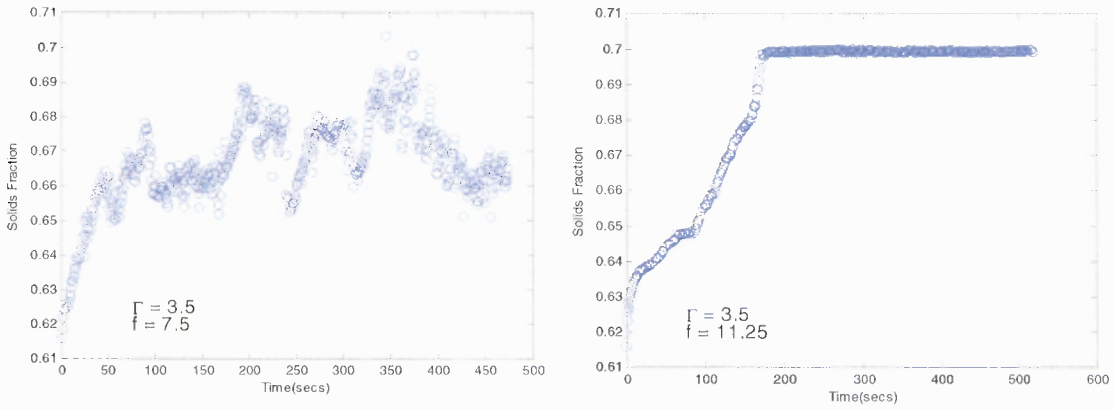

Figure 4.13: Single Realizations for Γ = 3.5 for frequencies of 7.5 and 11.25 Hz.

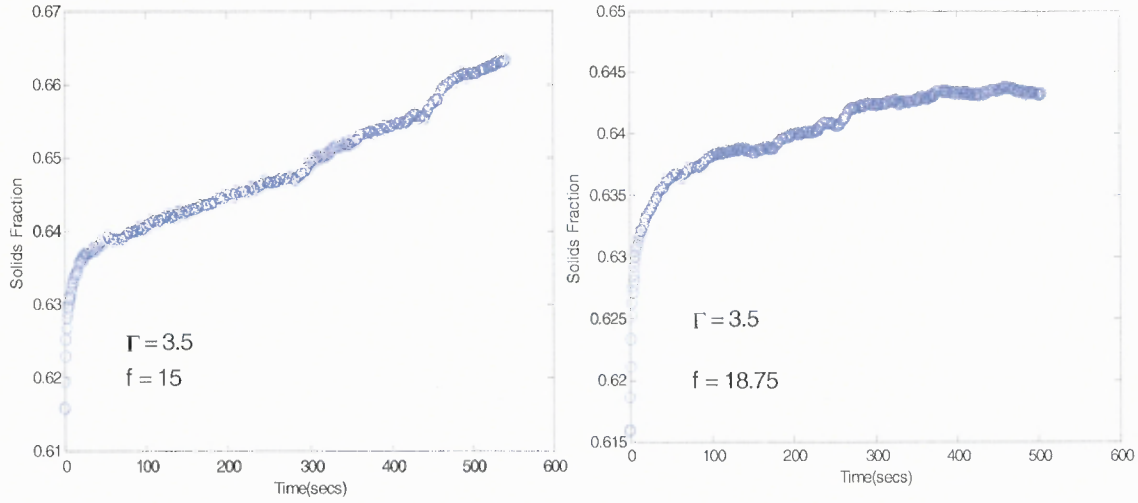

Figure 4.14: Single Realizations for Γ = 3.5 for frequencies of 15 and 18.75 Hz.

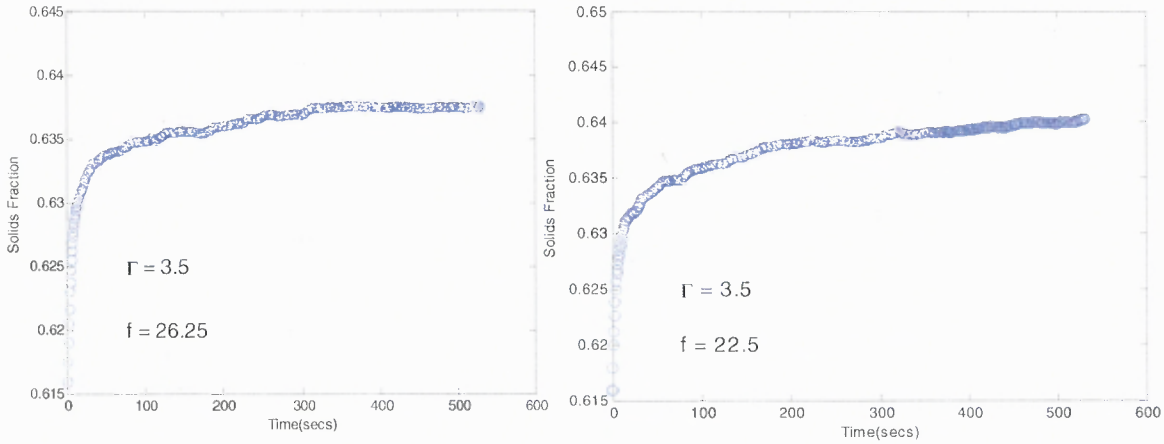

Figure 4.15: Single Realizations for Γ = 3.5 for frequencies of 26.25 and 22.5 Hz.

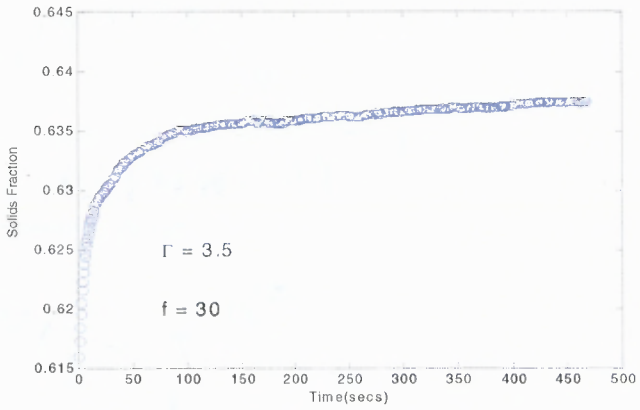

Figure 4.16: Single Realizations for Γ = 3.5 for a frequency of 30 Hz.

An acceleration of 3.75 is presented in the following results in Figures 4.17, 4.18, and 4.19. It should be noted that a frequency of 7.5 Hz produces a somewhat noisy density evolution with large jumps in the solids fraction. Accelerations corresponding to frequencies of 11.25, and 15 show sharp increases in the solids fraction.

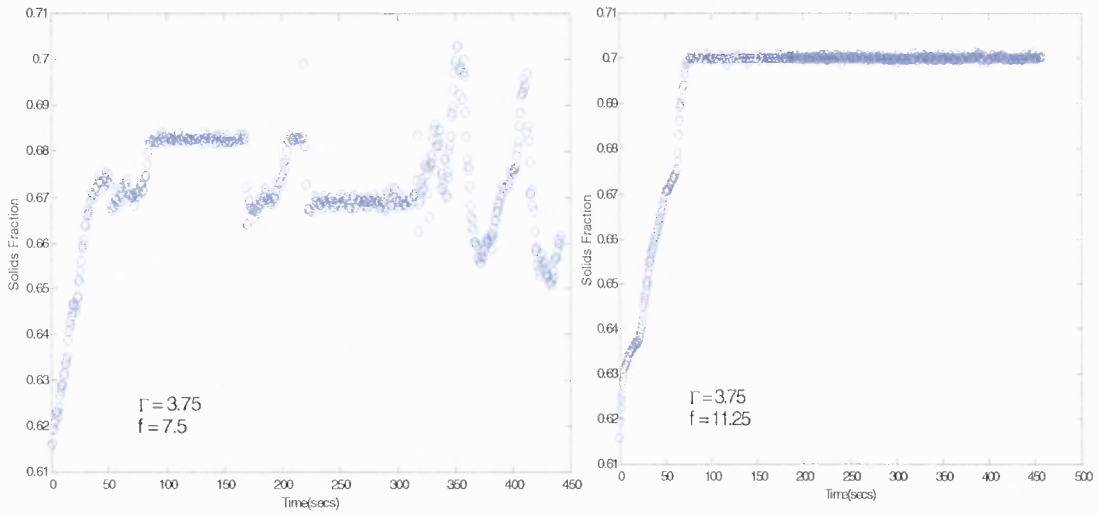

Figure 4.17: Single Realizations for $\Gamma = 3.75$ for frequencies of 7.5 and 11.25 Hz.

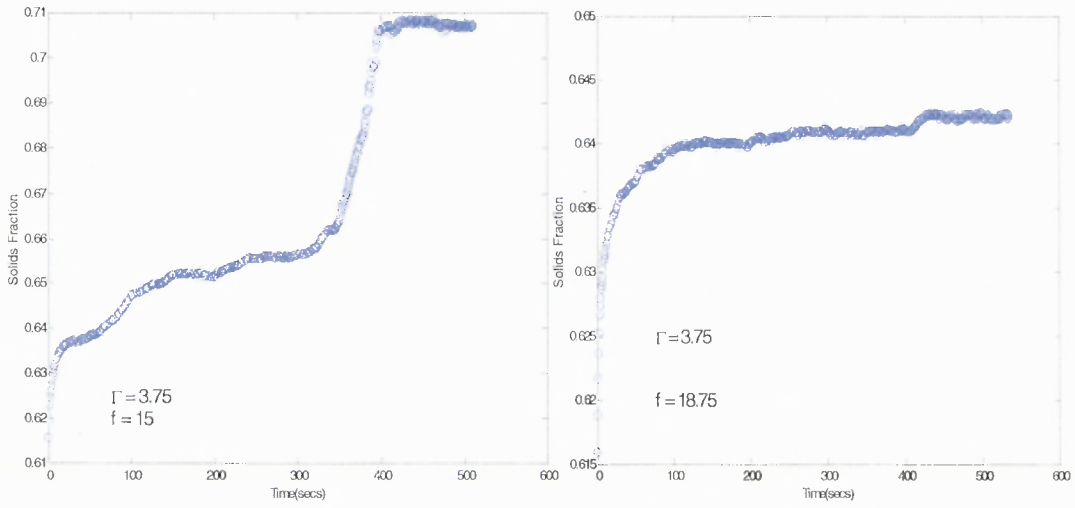

Figure 4.18: Single Realizations for $\Gamma = 3.75$ for frequencies of 15 and 18.75 Hz.

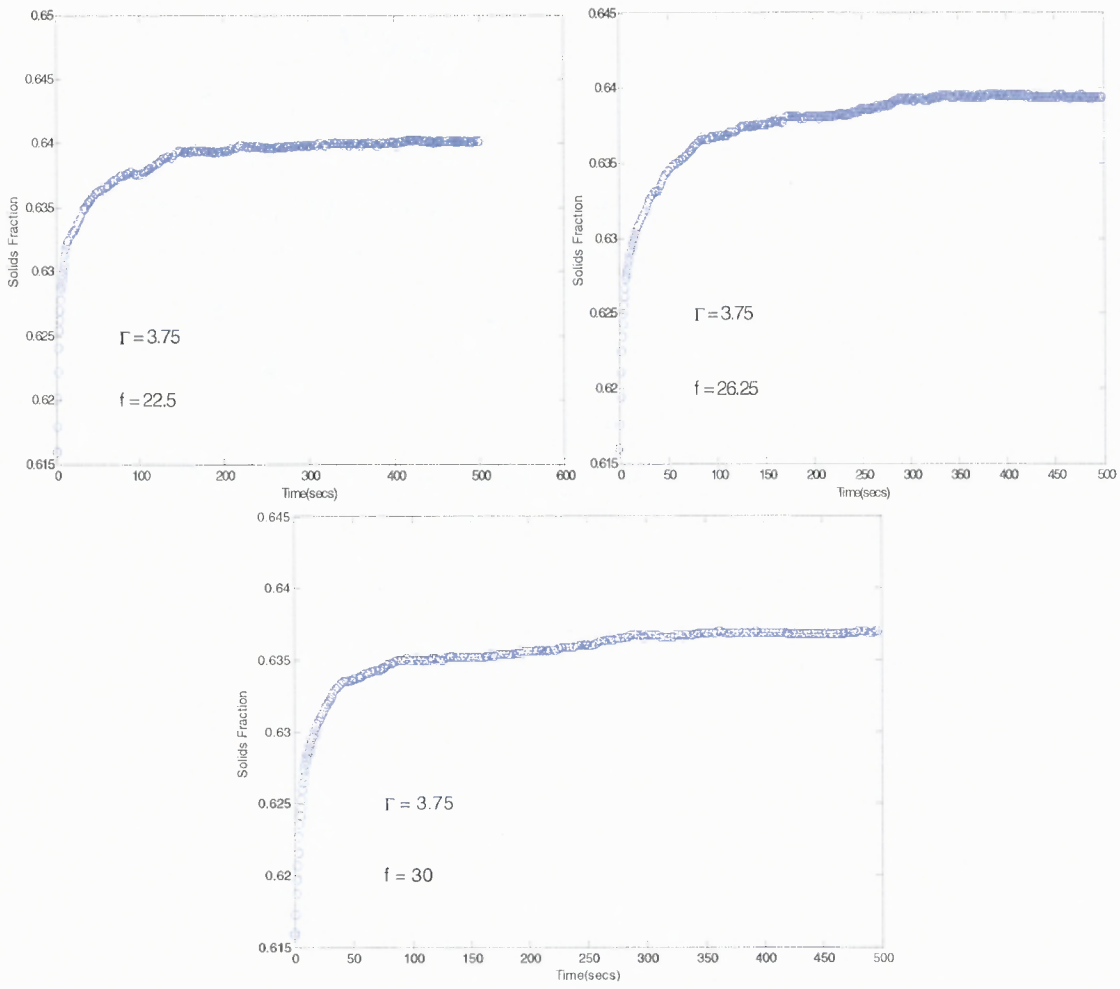

Figure 4.19: Single Realizations for $\Gamma = 3.75$ for frequencies of 22.5, 26.25 and 30 Hz.

An acceleration of 4.5 is presented in the following results in Figures 4.20 and 4.21. It should be noted that a frequency of 11.25 Hz produces a somewhat noisy density evolution because the total kinetic energy of the system hasn't reached a minimum. However, there still are gradients in the evolution of the solids fraction that result in high densities for that frequency. In addition, there are also gradients in the solids fraction for frequencies of 15 and 22.5 Hz.

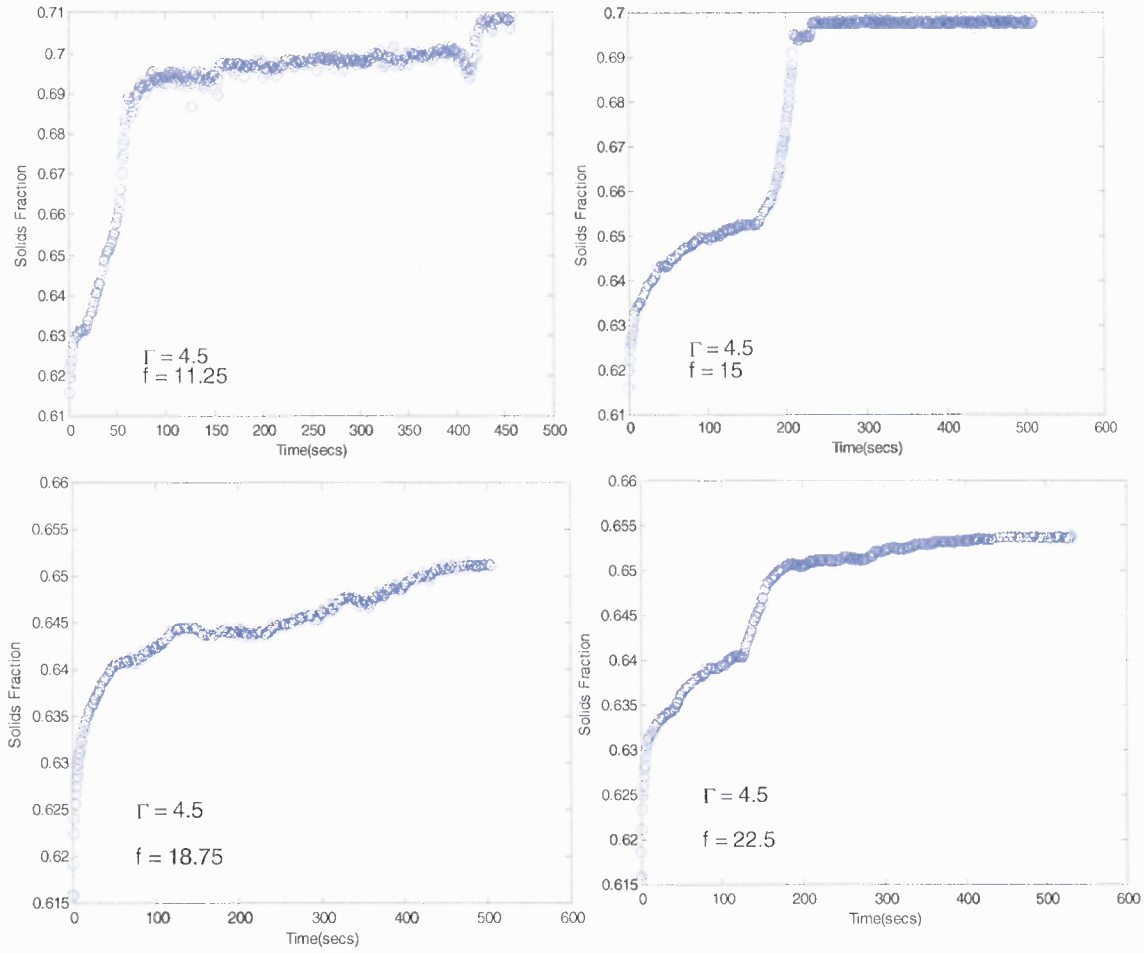

Figure 4.20: Single Realizations for Γ = 4.5 for frequencies of 11.25, 15, 18.75 and 22.5 Hz.

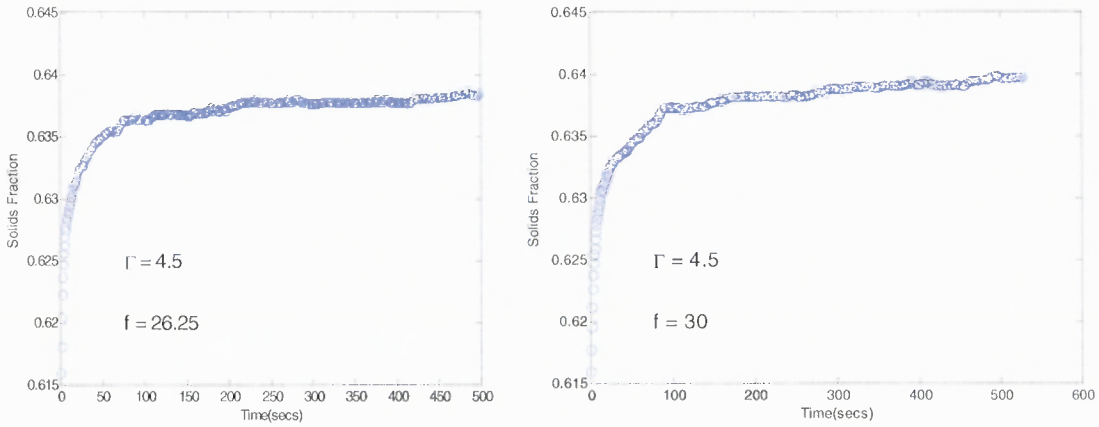

Figure 4.21: Single Realizations for Γ = 4.5 for frequencies of 26.25 and 30 Hz.

An acceleration of 5.0 is presented in the following results in Figures 4.22, 4.23 and 4.4. It should be noted that a frequency of 11.25 Hz and 15 Hz produces a somewhat noisy density evolution because the system was not quiescent during the long time scale due to the insufficient time that was used for the relaxation phase. For this acceleration, a frequency of 18.75 showed sharp increases in the solids fraction.

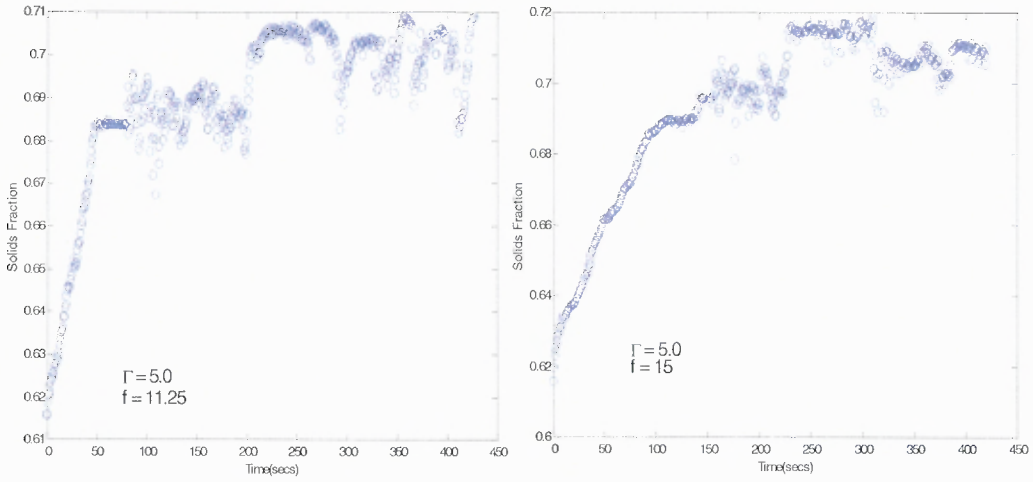

Figure 4.22: Single Realizations for Γ = 5.0 for frequencies of 11.25 and 15.0 Hz.

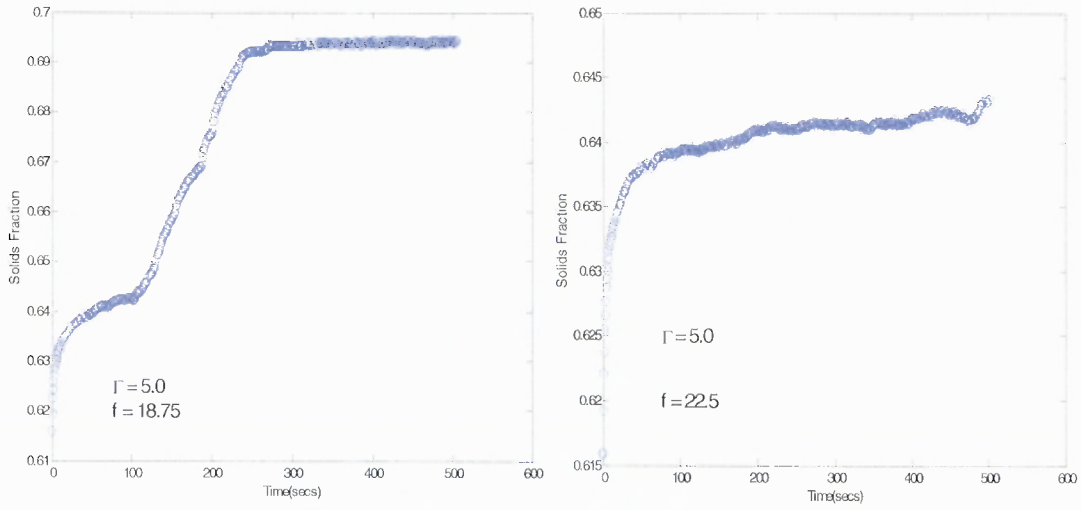

Figure 4.23: Single Realizations for Γ = 5.0 for frequencies of 18.75 and 22.5 Hz.

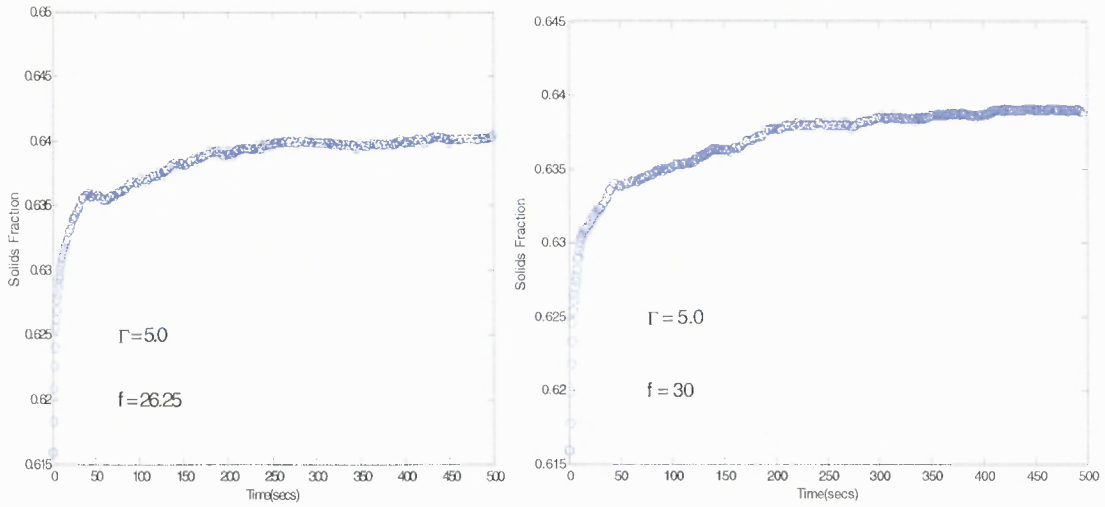

Figure 4.24: Single Realizations for Γ = 5.0 for frequencies of 26.25 and 30 Hz.

An acceleration of 6.0 is presented in the following results in Figs. 4.25 and 4.26. It should be noted that a frequency of 11.25, 15 and 18.75 Hz produces a somewhat noisy density evolution because the system was not quiescent during the long time scale due to the insufficient time that was used for the relaxation phase. The frequency of 22.5 for this acceleration begins to show an onset of gradients in the solids fraction.

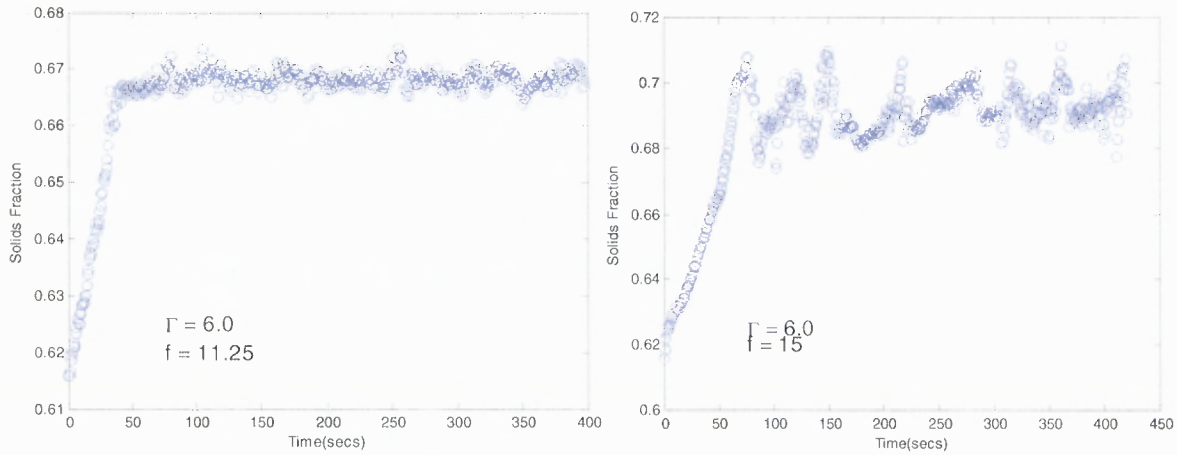

Figure 4.25: Single Realizations for Γ = 6.0 for frequencies of 11.25 and15.0 Hz.

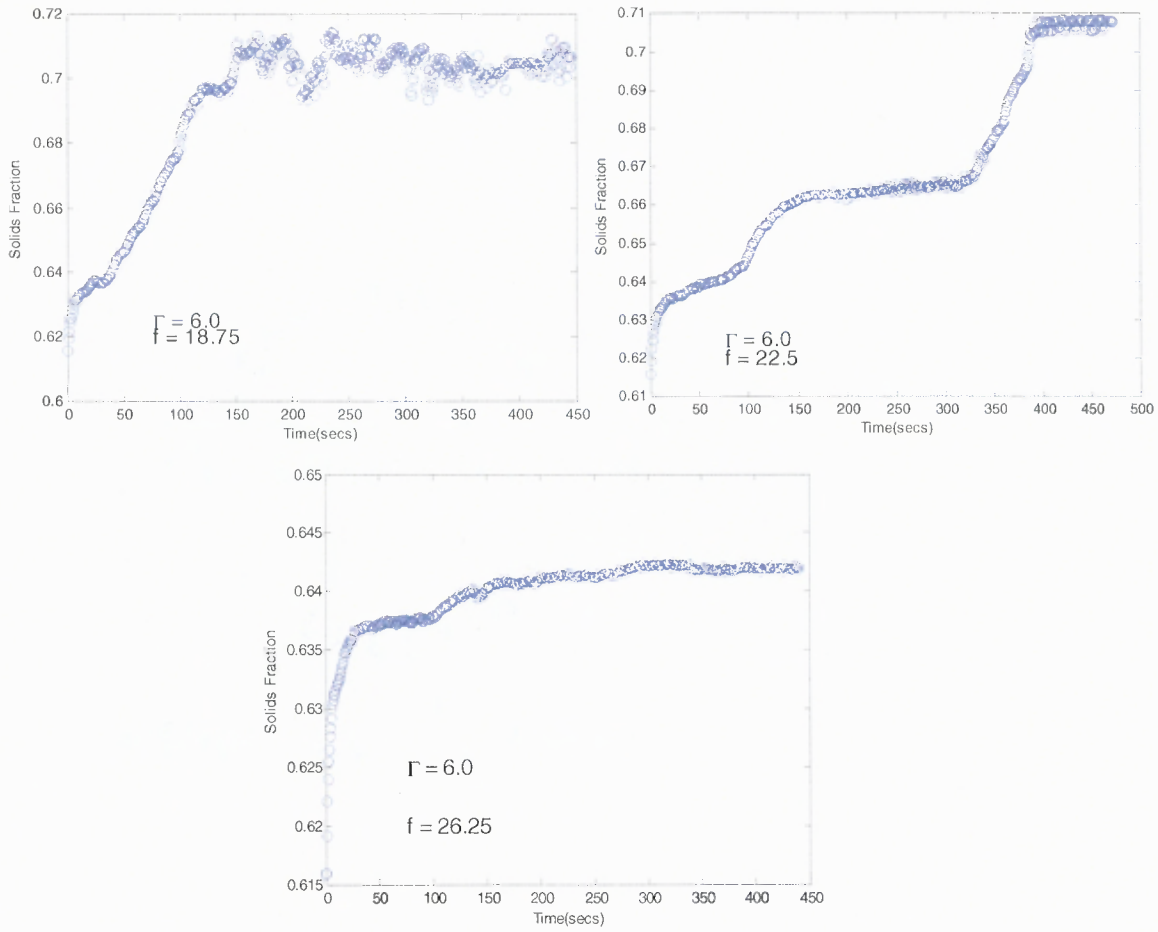

Figure 4.26: Single Realizations for $\Gamma = 6.0$ for frequencies of 18.75, 22.5 and 26.25 Hz.

An acceleration of 6.75 is presented in the following results in Fig. 4.27. It should be noted that a frequency of 15 Hz and 18.75 Hz produces a noisy density evolution because the system was not quiescent during the long time scale due to the insufficient time that was used for the relaxation phase. For the aforementioned acceleration, frequencies of 22.5, and 26.25 show sharp increases in the solids fraction.

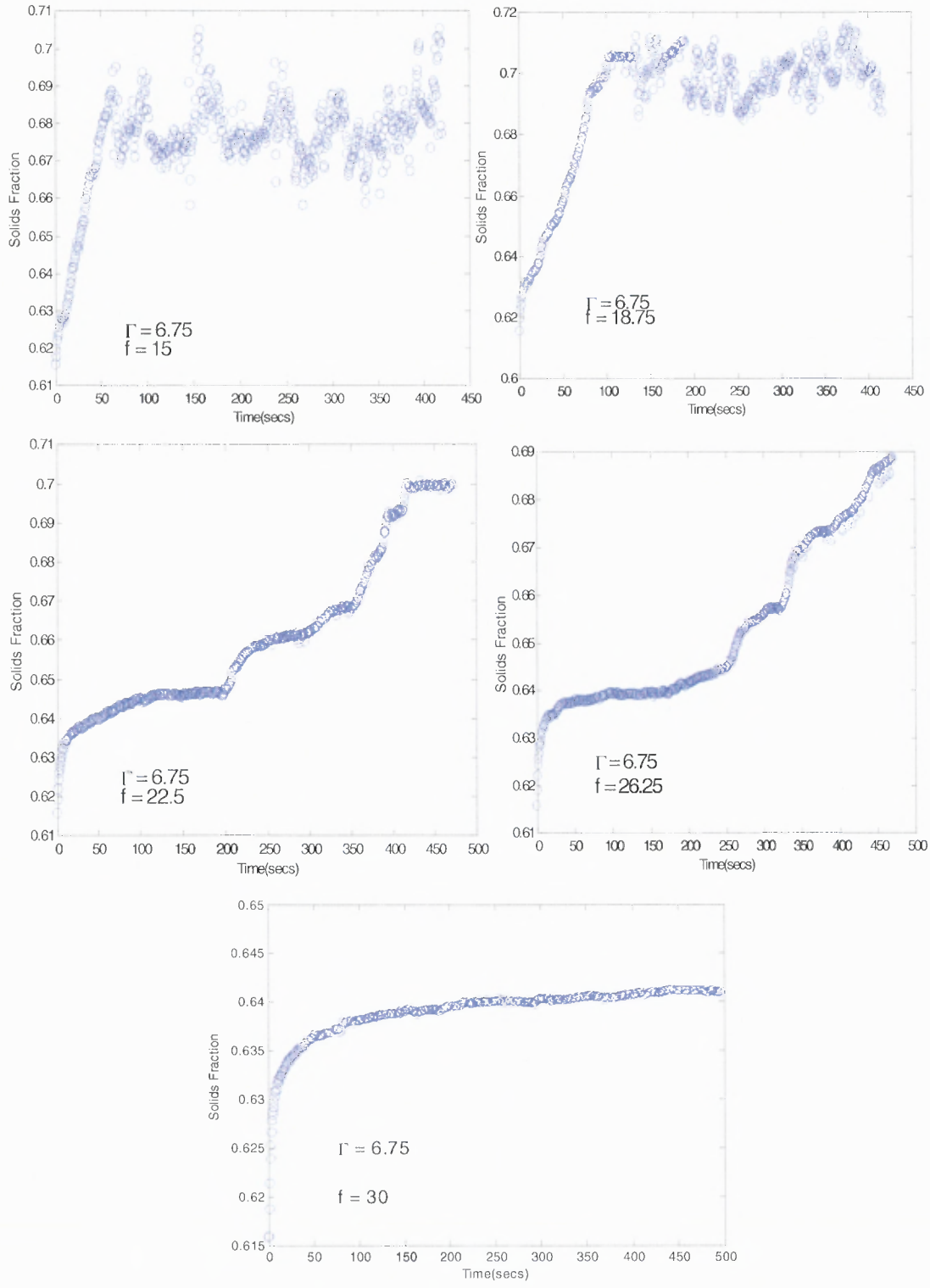

Figure 4.27: Single Realizations for $\Gamma = 6.75$ for frequencies of 315, 18.75, 22.5, 26.25 and 30 Hz.

4.4 Ensemble-Average Bulk Density Evolution

It was found that for poured configurations which are statistically indistinguishable regarding their initial bulk solids fractions and distributions of nearest neighbors and free volume, significant variations in the solids fraction evolutions were observed. This is not surprising since intuition suggests that the details of the microstructure have a dominant influence on how the system advances to a dense configuration. It was demonstrate this with an ensemble of 20 poured realizations with bulk solids fractions in the range 0.6088 $\pm$ 0.0035.

For each realization, the Voronoi diagram was constructed, from which the distribution of nearest neighbors (i.e., coordination number distribution) was obtained. The distributions for all realizations were individually fit ($R^2 \geq 0.9906$) to a normal form in Equation 4.2, with fit parameters of a and b were found for each realization. The mean and standard deviation for these parameters was $a = 7.2713 \pm 0.0558$ and $b = 1.2550 \pm 0.0262$.

$$f(n) = \frac{1}{b\sqrt{2\pi}} \exp\left[-\frac{(n-a)^2}{2b^2} \right] \tag{4.2}$$

Although not shown here, each of these individual distributions was statistically indistinguishable from the coordination number distribution computed from the ensemble average of the distributions (R^2 = 0.9975, a = 7.271, and b = 1.256). Figure 4.28 shows this ensemble average coordination number as well as the normal fit to this data.

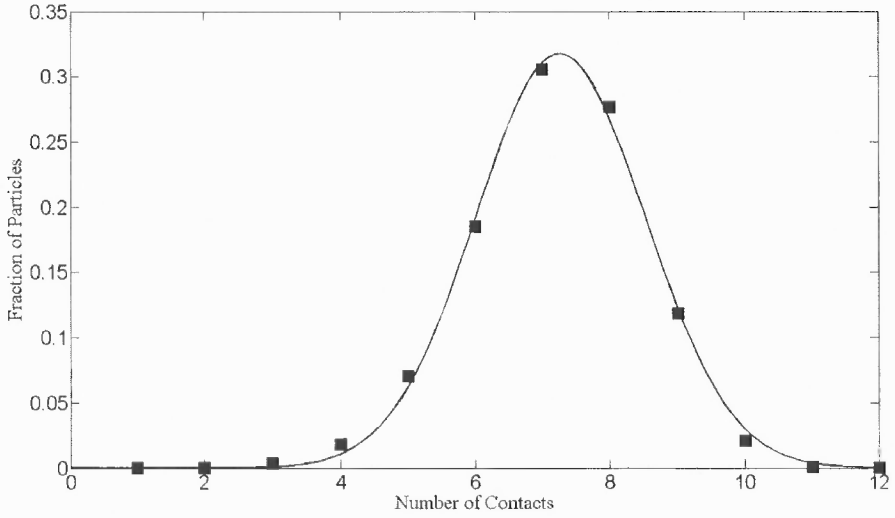

Fig. 4.28. The points are ensemble-averaged coordination numbers for 20 poured realizations. The solid line is a fit (R^2 = 0.9975) to $f(n)=\frac{1}{b\sqrt{2\pi}}\exp\left[-\frac{(n-a)^2}{2b^2}\right]$, where $a=7.271,\ b=1.256$.

Another measure of the microstructure is the free volume, defined here as the difference between the volumes of the polyhedron and the encapsulated sphere. Although not shown in this paper, it was also observed very little visual difference between the free volume distributions of the ensemble of 20 realizations, which were quite similar (both qualitatively and quantitatively) to the ensemble-averaged distribution given in Figure 4.29.

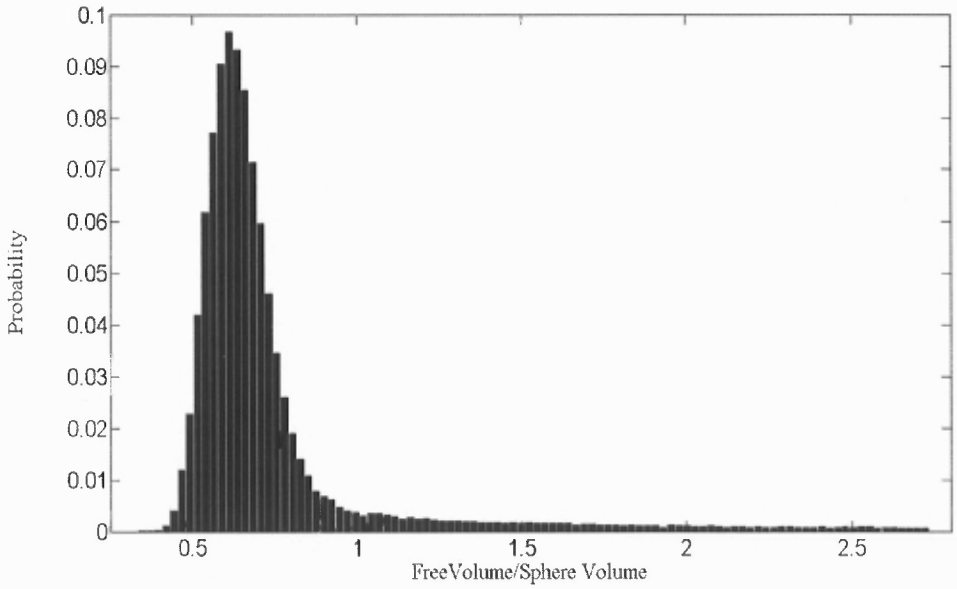

Fig. 4.29. Ensemble-averaged free volume (normalized by the volume of the spherical particle) distribution for 20 poured discrete element realizations.

Thus, from the perspective of bulk density, coordination number, and free volume distribution, each realization in the ensemble was very similar. And yet, the bulk solids fraction trajectories of the realizations were rather different. Taps were applied to each realization for the same time duration using identical vibration parameters, i.e., $a/d = 0.4413$ and $f = 7.5$ Hz, corresponding to $\Gamma = 2$. The ensemble-averaged trajectory of the bulk solids fraction (for which $\langle \nu \rangle\big|_{t\sim 680} = 0.6997 \pm 0.0058$) is given in Figure. 4.30, where the inset shows the standard deviation.

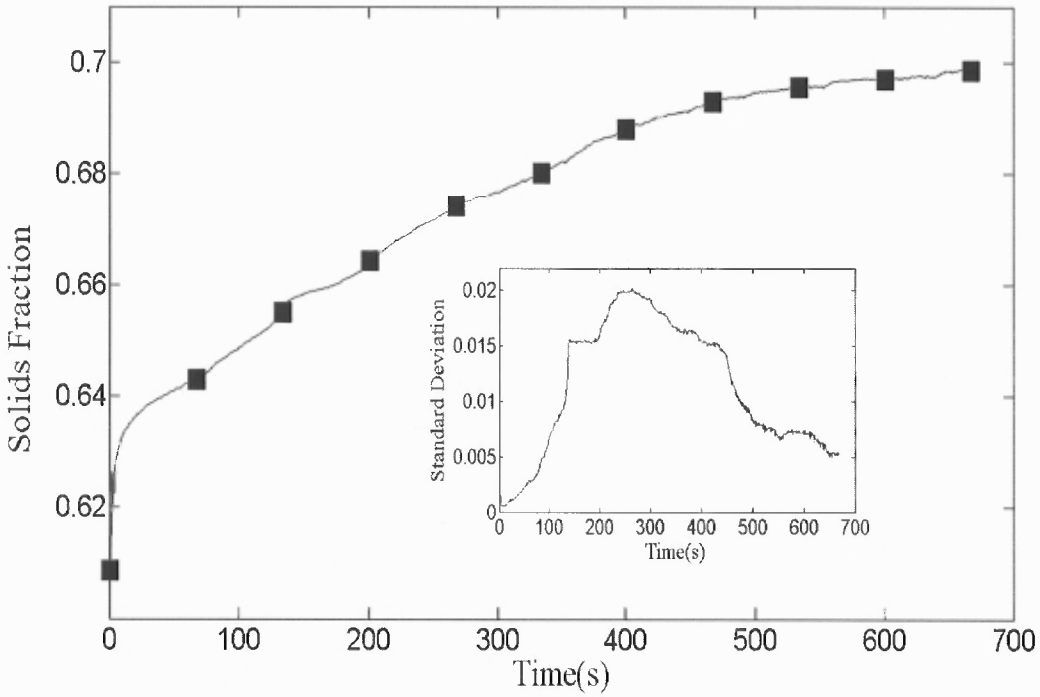

Fig. 4.30. Evolution of the ensemble-averaged bulk solids fraction over 20 discrete element simulations in which f = 7.5 Hz, a/d = 0.4413, Γ =2. The inset shows the standard deviation.

In some of the trajectories, rather dramatic jumps or steep gradients in the solids fraction (see Figure. 4.31) occurred, which at first glance appeared to be spurious. However, further consideration of these trajectories suggested that the jumps were caused by collective reorganizations of the microstructure that took place over small time durations relative to the time of tapping.

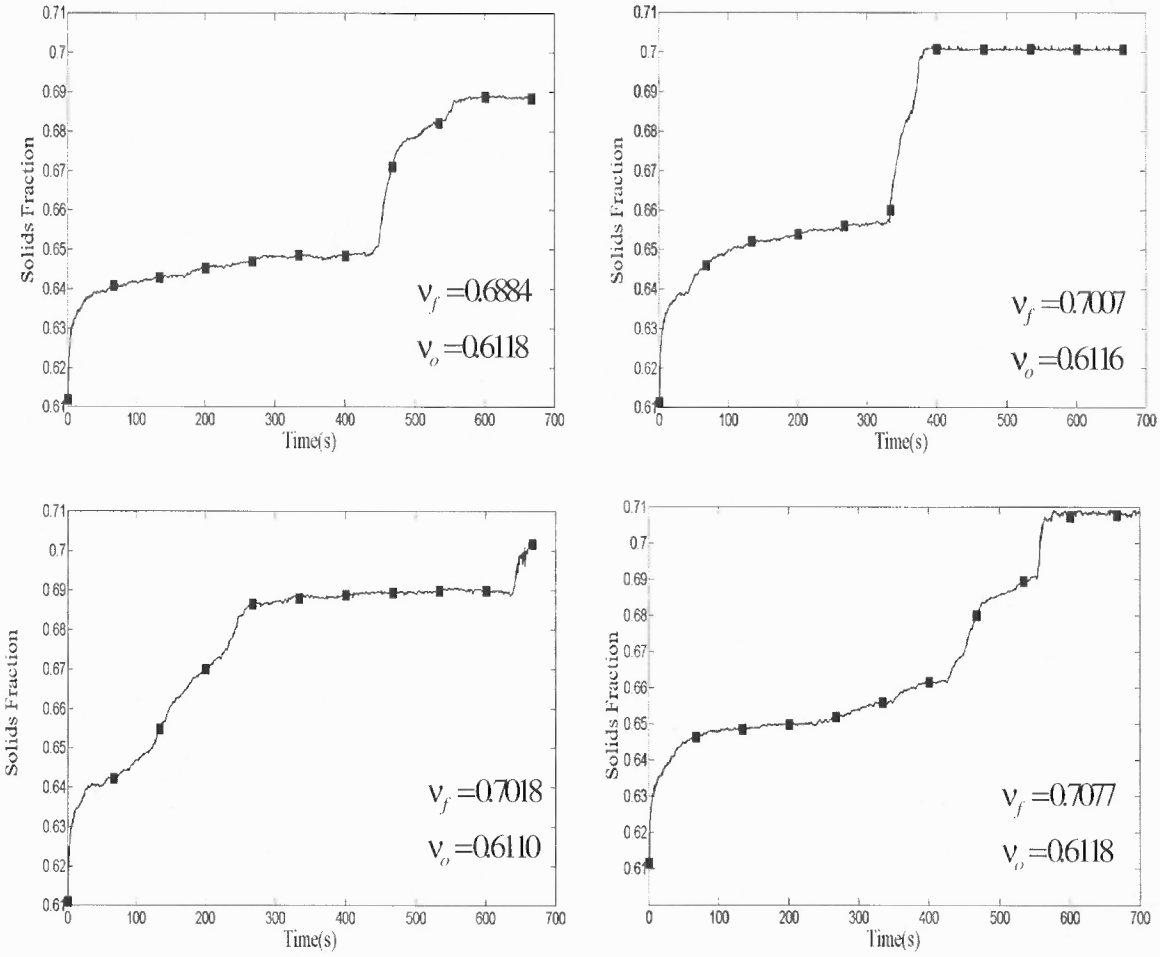

Fig. 4.31. Several trajectories from the ensemble of 20 realizations.

The later study demonstrates the sensitive dependence of the trajectories on the details of the microstructure, and the importance of using ensemble averages (rather than only single realizations) in these simulations to obtain statistically meaningful evolution curves. It is expected (in agreement with [51, 66]) that the equilibrium or final solids fraction of the assembly is not consequent on the initial microstructure. However, the tap parameters do have a significant effect on the final state as will be shown in the next section.

4.5 Dependence on Tap Amplitude and Frequency

After a poured assembly is obtained, the system is tapped by applying harmonic displacement oscillations to the floor consisting of a half-sine wave (amplitude a and period τ), followed by a relaxation time t_r of sufficient duration to ensure that upon collapse a quiescent state of minimal kinetic energy is attained. The occurrence of densification strongly depends on the choice of the tap amplitude; the plot in Figure. 4.32 demonstrates the striking difference between the evolution of bulk solids fraction for $\Gamma = 0.5$ ($f = 7.5$ Hz, $a/d = 0.1103$) and $\Gamma = 2.0$ ($f = 7.5$ Hz, $a/d = 0.4413$).

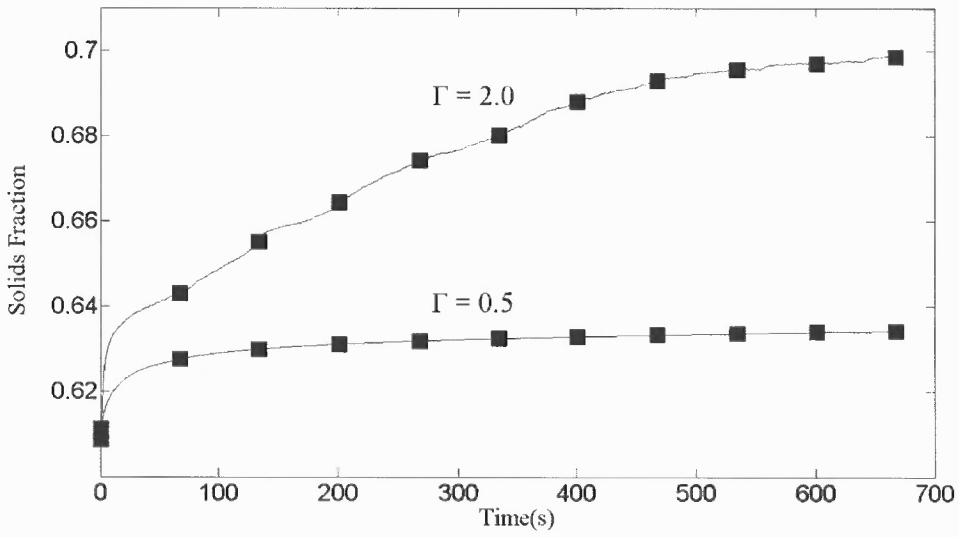

Fig. 4.32. Ensemble averaged solids fraction as a function of time for (a) $\Gamma = 0.5$ ($f = 7.5$ Hz, $a/d = 0.1103$) and (b) $\Gamma = 2$ ($f = 7.5$ Hz, $a/d = 0.4413$).

This is further illustrated in Figure. 4.33, which shows the dependence (as a function of y/d) of the solids fraction at several tap numbers for the two cases of Figure. 4.32. The qualitative behavior of $\bar{n}$ (the number of sphere centers at a given position y/d from the floor) at $\Gamma = 2.0$ shown in Figure. 4.34 is comparable to the MC results

presented in chapter 2; that is, as the taps progress, one observes that the density increases starting from the floor. Moreover, after application of hundreds of taps, the effective height of the system is reduced by approximately two particle diameters (analogous to what took place in the MC simulations).

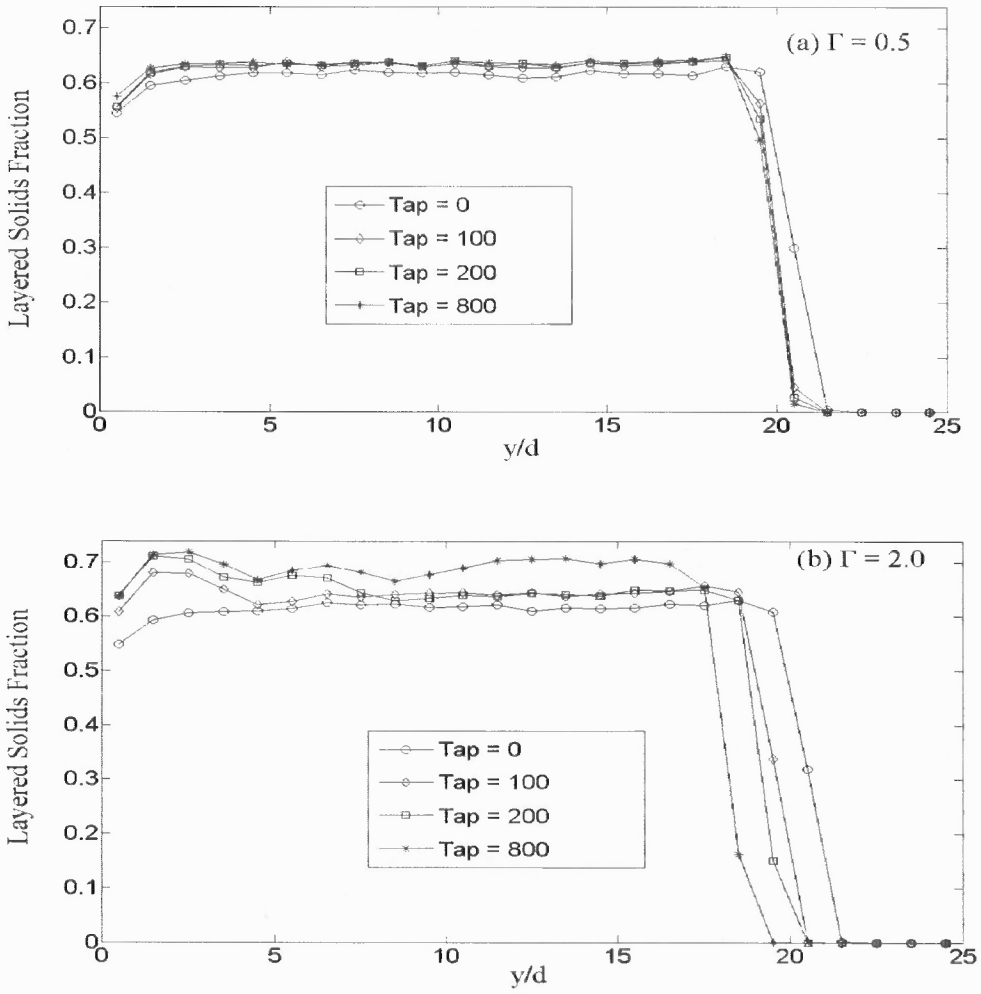

Fig. 4.33. Ensemble averaged solids fraction as a function of *y/d* for the initial configuration, and at tap numbers 100, 200 and 800 for (a) $\Gamma = 0.5$ (f = 7.5 Hz, a/d = 0.1103) and (b) $\Gamma = 2$ (f = 7.5 Hz, a/d = 0.4413).

It is note that formation of ordered structures in shaken granular system was discussed in some detail recently [50], although in that work the authors have found that

more complicated horizontal or horizontal/vertical vibrations were required in order to produce order. Instead, the concentration is focused on the influence of the parameters governing the vibrations, as discussed in what follows.

In order to further illustrate the influence of a reduced amplitude (at constant frequency) on the development of ordered layers and the eventual increase in bulk density of the system with increasing number of taps, and carefully monitored the evolution of particle centers as a function of distance y/d from the floor for the two example cases already discussed, i.e., $f = 7.5$ Hz, $a/d = 0.1103$, $\Gamma = 0.5$ and $f = 7.5$ Hz, $a/d = 0.4413$, $\Gamma = 2.0$. This evolution for the case $\Gamma = 2.0$ is presented in Figure. 4.34, where the vertical axis ($\overline{n}$) represents the ensemble-averaged (over 20 realizations) number of particle centers (normalized by the number of particles in the system) as a function of the position.

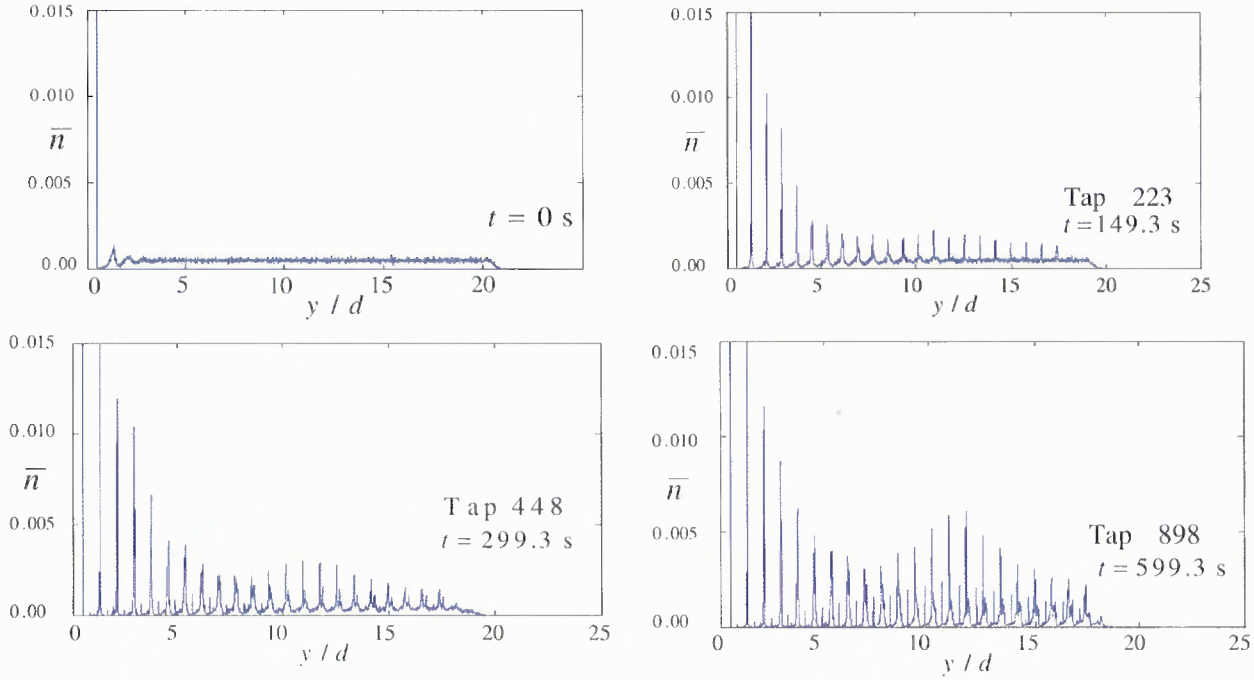

Fig. 4.34. Ensemble-averaged (over 20 realizations) distributions of the particle centers measured from the floor ($y/d = 0$) to the top surface for $a/d = 0.4413$, $f = 7.5$ Hz ($\Gamma = 2.0$) at $t = 0$s, $t = 149.3$s, $t = 299.3$s and $t = 599.3$s.

It is observed that as the number of taps grew, there was an increase in the number of layers (starting from the floor) in which the location of the peaks closely corresponded with those for a hexagonal close-packed structure. Figure 4.35 shows the structural evolution, where $\langle \nu \rangle \approx 0.7$ upon completion of 898 taps.

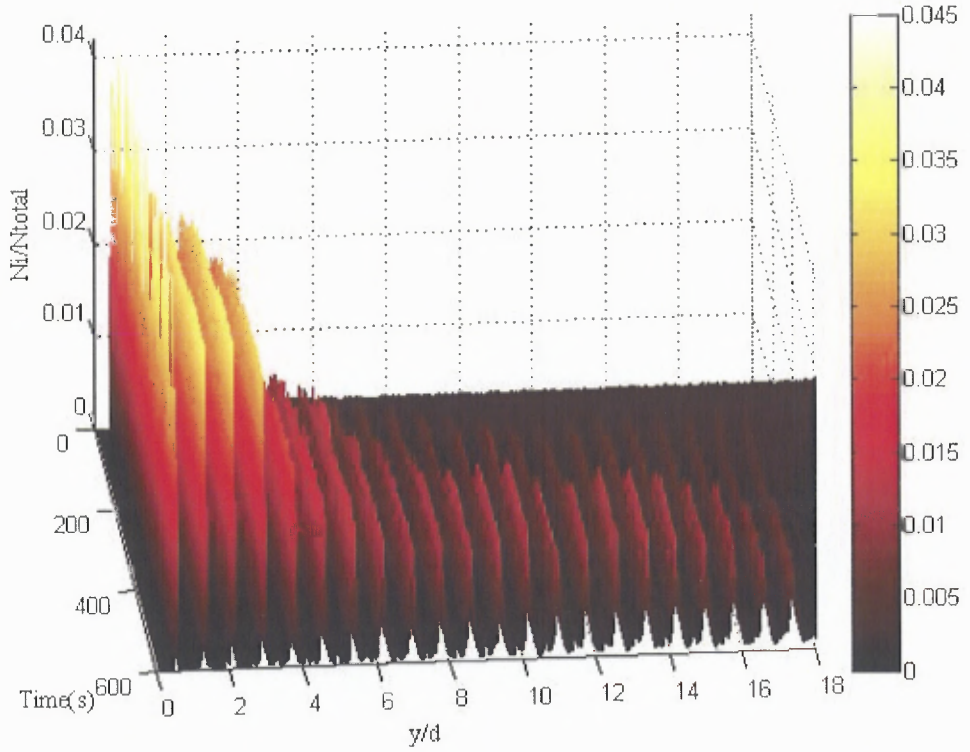

Fig. 4.35. Evolution of the ensemble-averaged distribution of particle centers for $\Gamma = 2$ ($f = 7.5$ Hz, $a/d = 0.4413$).

However, for the case with the smaller amplitude (a/d = 0.1101) no definitive organization was present upon completion of thousands of taps. This behavior supports the finding in the MC simulations of a critical value of the tap amplitude that optimizes the formation of an ordered microstructure. Within the context of the DEM simulations, it is interpreted this amplitude as being related to a peak dilation of the system. Indeed,

one can imagine two extremes that engender no microstructure development or appreciable increase in bulk density: (i) an aggressive, energetic tap that greatly expands the system so that any existing microstructure is destroyed upon contraction and, (ii) a low energy tap that merely transmits a stress wave through the contact network, but does not dislodge or disturb the structure to any appreciable degree. Thus, one can hypothesize that the densification process is regulated by the degree of dilation, and that ordering of the microstructure occurs within some narrow range of values of dilatations. The results of a study to explore this conjecture will be reported in a future paper.

Of particular relevance to the results reported here are the studies of Zhu et al. [50], who report on experiments and discrete element simulations of the density relaxation process through the application of continuous vibrations. In particular, those authors employ a procedure in which very dense structures (solids fraction ~ 0.7 and higher) are built up by vibrating sequentially deposited thin poured layers (of approximately one diameter). This procedure differs from our approach, in which the entire system is exposed to taps, resulting in its evolution to a dense structure ($\langle \nu \rangle \sim 0.7$) as in Figure. 4.30. Their findings are essentially in agreement with our earlier reported discrete element investigation [20] in that high solids fractions (greater than ~ 0.66) were not found in relatively deep systems through the application of continuous vibrations. This can be seen in the phase portrait of Figure. 4.36 (redrawn from [20]) for a system of 8000 particles ($e = 0.9$ and $\mu = 0.1$) within a laterally periodic box (aspect ratio $L/d = 25$), in which the improvement in solids fraction $(\nu_\infty - \nu_0)/\nu_0$ is mapped as a function of the vibration amplitude ($0.02 \leq a.d \leq 0.48$) and frequency ($10 \leq f \leq 90$ Hz).

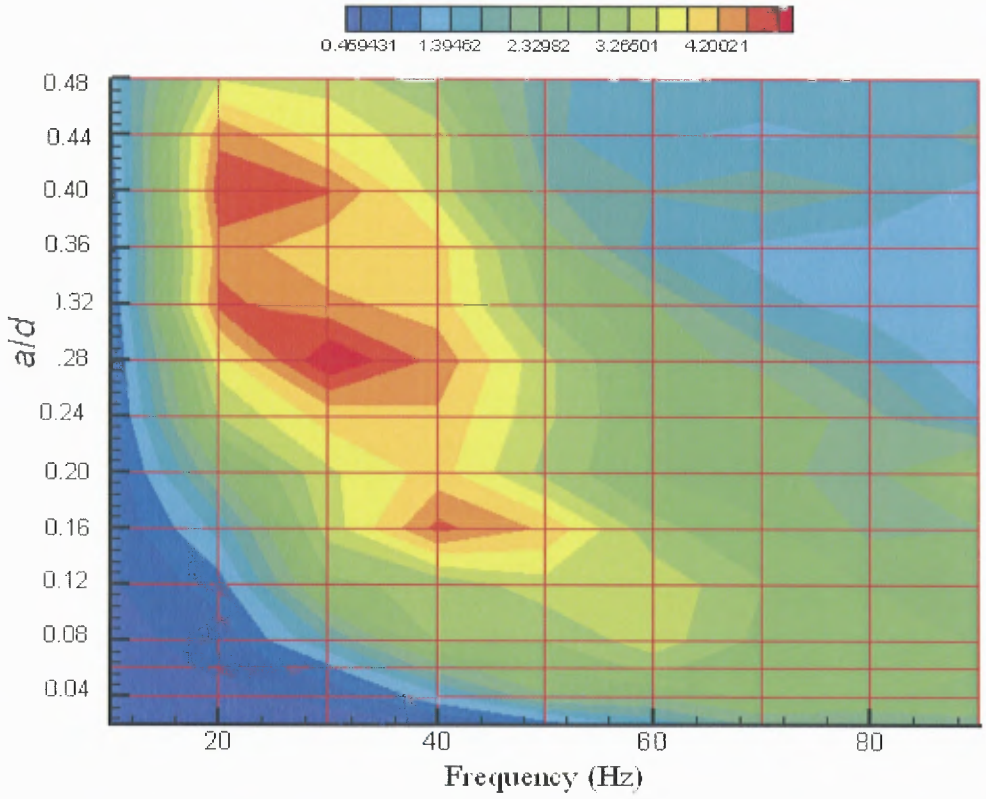

Fig. 4.36. The color scale shows the improvement in bulk solids fraction $(\nu_\infty - \nu_0)/\nu_0$ as a function of amplitude $(0.02 \le a/d \le 0.48)$ and frequency $(10\,\text{Hz} \le f \le 90\,\text{Hz})$ for continuously sinusoidal vibrations applied the floor (taken from [20]).

Distinct regions are visible according to the color scale corresponding to various improvement levels, with a maximum value of only approximately 5%. Although not shown here, results from this study also indicated a correlation between these regions with depth profiles of granular temperature, solids fraction and ratio of the lateral to vertical components of the kinetic energy. Figure 4.28 may represent a typical phase portrait associated with the density relaxation process, albeit quantitative differences are expected based on the mode of energy input (tapping as opposed to continuous vibrations), and on material properties, aspect ratios and mass overburdens.

CHAPTER 5

CONCLUSIONS AND FUTURE WORK

5.1 Conclusions

Density relaxation phenomena were investigated using two different types of methods: Monte Carlo simulations and the Discrete Element Method. For the Monte Carlo method the lift expansion that was used was a uniform expansion where the entire assembly was lifted off the base of the vessel. For such an expansion, many taps were done for various lift expansions.

As a result, the Monte Carlo evolution for each lift expansion was obtained as a function of tap number. The ensembled average curve was calculated and the solids density evolution was obtained. The results were fit well to two phenomenological fits: the inverse natural log fit, and the KWW fit. For the inverse log fit, the data for the low lift intensities were fit well. However, the estimated equilibrium solids fraction obtained from that fit was larger than expected.

Another important result obtained through the MC simulations was that there was evidence to suggest that there might be a critical tap intensity. Even when the estimated equilibrium solids fraction was found from the KWW fit, the behavior of the equilibrated solids fraction vs. the tap intensity still suggested there might be an optimal intensity to produce a dense packing. An important result that the MC simulations pointed is that if one were to lift the system with a large intensity such as $\gamma = 0.4, 0.5$ then there will not be an improvement in the solids fraction of the system of particles. Moreover, if one

were to lift the system with a small tap intensity such as $\gamma = 0.1$, then the density of the system would improve, albeit at a slower rate.

The time that it took for the system to equilibrate the lower lift expansions for $\gamma = 0.1, 0.2, 0.25$ was substantially longer than that of the higher lift expansions. That could be attributed because the nature of the expansion is smaller which would correspond to a system with a less energetic tap. In addition to analyzing the bulk density, the microstructure of the system of particles was analyzed. It was found that for systems where the density was large, such as in the case of the $\gamma = 0.25$, the vertical center distribution found that there was an ordering of the system of particles beginning from the base of the system and progressing upwards through the system as time evolved.

An important result that was verified in Monte Carlo simulations is that the final bulk state is independent of the initial state. That result was tested by starting with one of the most dense packing configurations: an HCP crystal and then applying the same lift expansions. It was found that the equilibrium solids fraction matched up well with the solids fraction corresponding to the same tap that was obtained when one started with a random loose packed system.

In the DEM simulations, the results that were obtained suggested that by changing the inter-particle friction, one could obtain either a denser poured configuration, or a looser poured configuration. In addition to looking at the solids fraction, the kinetic energy of the system of particle could be analyzed to obtain different kinds of behavior. One such behavior is that if one were to increase the H/d ratio of the system, the kinetic energy would change for different accelerations. Other parameters that were investigated were the amplitude of the pulse as well as the frequency of the pulse. It was found that

for higher accelerations, one needed a longer relaxation time to ensure that the system settled down to a quiescent state.

Results that were obtained for the DEM showed that one can obtain different trajectories of the bulk density as a function of time depending on the initial state. However, for each of the realizations, the final bulk density was quite similar thus suggesting that the final state is independent of the initial state as was seen in the Monte Carlo results. In addition, dense packings were obtained for an acceleration of $\Gamma = 2.0$ which gave a solids fraction of approximately 0.69. Additionally, when compared to a case that was run at the same frequency of 7.5 Hz but at a $\Gamma = 0.5$, then density was not as high (~0.63), which also suggested that there might be an optial amplitude corresponding to a frequency that produces a dense packing. In addition, the mass overburden played a role in obtaining high densities as was shown in the DEM results a higher fill height.

Microstructure analysis were also done for the DEM simulations, and there was an ordering of the system starting from the base and progressing upwards as was also seen from the MC results. A new tool that was used to look at the microstructure, the local density analysis, showed that there was an increase in density as time progressed for the system of particles that progressed upwards.

5.2 Future Work

The results that are discussed in this thesis could point to other areas that can be looked into with regard to the density relaxation of granular media. Such areas can also be analyzed using the microstructure tools that have been discussed. Possible areas of future work are mentioned below:

1. Analyze the role of the phase space of the system as well as tap parameters play in influencing the bulk behavior of the system. Such parameters include the restitution coefficient, the aspect ratio, mass overburden, fill height, frequency of the tap, amplitude of the tap, as well as the acceleration.
2. Exploring the dilation of the system of particles to capture the way particles rearrange themselves into denser packings. The dilation analysis should be performed on two time scales: the application of the pulse time scale and the relaxation time scale.
3. An alternative measure of exploring the microstructure of the system by looking at the normal interactions between particles in the relaxed time scale.
4. Reproducing the reversible branch that was obtained by Nowak et al [26] and Ribiere et al [61] for different frequencies using the DEM simulation.
5. Constructing a phase space of the frequency, amplitude and solids fraction to determine which frequencies should be matched to an amplitude to obtain the densest structure.
6. Exploring the role of how the mass overburden comes into play when applying taps to a system of particles, and how the increased mass scales with the solids fraction.

7. Application of the local density distribution during the short time scale to see examine the local phase space of each particle to determine if there are any early indicators of dense structures forming as time increases.

APPENDIX A

MODIFICATIONS TO THE DEM CODE

This appendix documents some of the changes the DEM code has undergone throughout this thesis. Changes are described a brief header that indicates the subroutine, the modification made to the subroutine, and the reason for the modifications.

Main Program *3dshear.f*
The following lines of code initialize parameters for the restarted run. The old values of tmax, istart, tstart, nout, dsump, dtdump, nrun, vamp, frq, vamp, fmu, fmub, dtout are replaced by the new values. These variables are the only ones allowed to change during a restart.

```
c-----initalize parameters for new run
      tcycle = tbump + tpour
      tmax = tpour + nrcg*tcycle
      tbump1 = tbump
      tcycle1 = tcycle
      tmax2 = tmax
      frq2 = frq
      vamp2 = vamp
      dtdump2 = dtdump
      fmu2 = fmu
      fmub2 = fmub
      dtout2 = dtout
```

Subroutine *forces.f*
The following lines of code are for the purpose of extracting the linked list features such as the linked list neighbors, normal forces, overlaps, and tangential forces.

```
open(unit=18,FILE='normalforce.txt',status='unknown', access =
'APPEND')
write(18,17)t, i,jdx1
write(18,22) t,i,jdx,j,idx,nxt,a(jdx),a0(jdx),fn(jdx),tfx(jdx),
     :       tfy(jdx),tfz(jdx),tm(jdx),nbor
```

APPENDIX B

SAMPLE INPUT FILE FOR THE DEM CODE

This appendix gives a sample input file.

```
$var  np =        3203   $Total number of particles in cell
 $var  bdry =      1     $flag for boundry type (1;cubic, 2;tringular)
 $var  nxby0 =     1     $No of boundary particles in x-dir. at y = 0
 $var  nzby0 =     1     $No of boundary particles in y-dir. at y = 0
 $var  nxby1 =     0     $No of boundary particles in x-dir. at ycell
 $var  nzby1 =     0     $No of boundary particles in x-dir. at ycell
 $var  nxbz0 =     0     $
 $var  nybz0 =     0     $
 $var  nxbz1 =     0     $
 $var  nybz1 =     0     $
 $var  nybx0 =     0     $No of boundary particles in y-dir. at x = 0
 $var  nzbx0 =     0     $No of boundary particles in z-dir. at x = 0
 $var  nybx1 =     0     $No of boundary particles in y-dir. at xcell
 $var  nzbx1 =     0     $No of boundary particles in z-dir. at xcell
 $var  nfix =      0    $ number of fixed particles
 $var  nzcyl =     0     $ number of fixed cylinders parallel to z-axis
 $var  nycyl =     1     $ number of fixed cylinders parallel to y-axis
 $var  ncomp =     1     $ the particle used for axial compression
 $var  ncmax =     0     $number of collisions during entire run
 $var  nout =      0    $No. of time to print out results
 $var  nczero =    0     $number of collisions before start cum. ave.
 $var  ntcol =    40     $number of time steps during a collision
 $var  nvel =     20     $number of intervals for vel. distrib.
 $var  nyzone =    5      $number of y zones
 $var  mzcell =    4      $number of z cells
 $var  nycell =    1     $numner of y cells
 $var  itervm =    1     $max iterations per time step
 $var  icoord =    0     $flag for coordinates print out
 $var  itty =      0    $flag for tty interaction
 $var  ixyz =      0     $flag to read init coords of fxd & bnd particles
 $var  istart =    0    $to restart the code rename d3ds to d3ds1000 and set istart=1000
 $var  tmax =  30.00       $max time for calculation
 $var  tpour = 0.5         $time for pouring
 $var  dt =    0.         $time step
 $var  dtout =  0.5        $time interval for printing out results
 $var  dtdump =  30.0      $time interval for dumping
 $var  tzero =   10.0      $restart long-term cum. ave.
 $var  search =  0.05      $search distance for near neighbors
```

```
$var  ycell =   3.00       $cell height (m)
$var  xyrat =   100.0      $ratio used to compute xcell
$var  zyrat =   100.0      $ratio used to compute zcell
$var  vave =    0.0        $average deviatoric transl. velocity
$var  vseed =   0.9        $seed for random initial particle velocities
$var  vxzero =  0.0        $initial velocity in the x-direction (ave)
$var  vyzero =  0.0        $initial velocity in y-direction (ave)
$var  vzzero =  0.0        $loading stiffness K1
$var  skn1 =    2.8e+06    $normal force coefficient
$var  elast =   0.971      $coefficient of restitution
$var  slope =   0.         $alternative parameter for unloading
$var  ratk =    0.8        $ratio of tangential/normal stiffness
$var  fmu =     0.1        $coefficient of friction
$var  fmub =    0.00       $friction for boundary and fixed particles
$var  power =   0.3333333  $tangential force exponent
$var  rmassz =  10891      $mass of unit sphere
$var  tstart=   0.1        $time to initialize long term averages
$var  gravx =   0.0        $acceleration of gravity in x direction
$var  gravy =   -9.81      $acceleration of gravity in y direction
$var  gravz =   0.0        $acceleration of gravity in z direction
$var  vxby0 =   0.0        $x velocity of real boundary at y = zero
$var  vxby1 =   0.0        $x velocity of real boundary at y = ycell
$var  vyby0 =   0.0        $y velocity of real boundary at y = zero
$var  vyby1 =   0.0        $y velocity of real boundary at y = ycell
$var  t2move = 70.0        $time to start moving the floor/wall
$var  t2stop = 2000.0      $time to stop the floor from moving
$var  vyfloor = 0.0001     $velocity of the floor/wall when moving
$var  draddt =  20.        $rate of increase of particle radii
$var  compforce = 0.00001  $axial force to be applied (N)
$var  number(1) = 3200     $number of particles in group 1
$var  radius(1) = 0.05     $particle radii for group 1
$var  number(2) = 1        $number of particles in group
$var  radius(2) = 0.05     $radius of particles in group
$var  number(3) = 1        $number of particles in group
$var  radius(3) = -0.6667  $radius of cylindrical boundry
$var  number(4) = 1        $number of particles in group
$var  radius(4) = 0.05     $radius of large particle
$var  skn1b = 2.8e+06      $
$var  elastb= 0.83         $
$var  slopeb= 0.           $
$var  vamp =  0.115080997  $velocity amplitude of boundary
$var  frq =   30.          $frequency of bump
$var  tbump =   0.0166667  $duration of one bump
$var  nrcg =  5            $number of bumps to be processed
$var  finis =   1.         $end
```

APPENDIX C

SCRIPT FILES IMPLEMENTED ON THE OPEN SCIENCE GRID

This appendix details the files that are needed to run the DEM code on the Open Science Grid.

The following lines of code are for the first file called the "job-wrapper."

```
#!/bin/bash

set -x

function create_work_dir()
{
   TARGETS="$OSG_WN_TMP $OSG_DATA"
   if [ "x$TMPDIR" != "x" ]; then
      TARGETS="$TMPDIR $TARGETS"
      unset TMPDIR
   fi
   echo "Possible targets for work dir: $TARGETS"
   for DER in $TARGETS; do
      WORKDIR=`/bin/mktemp -d -p $DER engage.XXXXXXXXXX`
      if [ $? = 0 ]; then
         echo "Created workdir in $DER"
         export WORKDIR
         return 0
      fi
      echo "Failed to create workdir in $DER"
   done
   return 1
}


function cleanup()
{
   cd $STARTDIR
   rm -rf $WORKDIR || /bin/true
}

# run id is the first argument
RUNID=$1
```

```
# job id
JOBID=$2

# keep the exit code to the end
EXITCODE=1

# remember start dir
STARTDIR=`pwd`

# output file (so staging always works)
touch $STARTDIR/../$JOBID.tar.gz

# we need a local temp directory to do the actual work in
# it is important to try to use local filesystems as much as
# possible during jobs, instead of using the shared $OSG_DATA
create_work_dir
if [ $? != 0 ]; then
   exit 1
fi

# is it very important to do the cleanup in case of failure
trap cleanup 1 2 3 6

# copy inputs to work directory
cd $WORKDIR
cp $STARTDIR/mds .
cp $STARTDIR/i3ds .
cp $STARTDIR/poured.txt .

chmod 755 mds
time ./mds >mds.output 2>&1
EXITCODE=$?

if [ "x$EXITCODE" != "x0" ]; then
   tail -n 100 mds.output
fi

# create output tar
mkdir $JOBID
for FILE in `find . -type f -maxdepth 1`; do
   mv $FILE $JOBID/
done
tar cvzf $STARTDIR/../$JOBID.tar.gz $JOBID

# cleanup
cleanup
```

```
# signal the sucess/failure of the job
if [ "x$EXITCODE" = "x0" ]; then
   # give the all good signal to the post-job script
   echo "=== RUN SUCCESSFUL ==="
else
   echo "Job failed with exit code $EXITCODE"
fi
```

The second file is the "pre-job" file.

```
#!/bin/sh

set -e

RUN_DIR=$1
JOB_ID=$2

mkdir -p $RUN_DIR/logs/$JOB_ID
touch $RUN_DIR/alljobs.log
chmod 644 $RUN_DIR/alljobs.log
```

The following lines of code are for the first file called the "post-job."

```
#!/bin/sh

set -e

RUN_DIR=$1
JOB_ID=$2

TIMESTAMP=`/bin/date +'%y%m%d_%H:%M'`

LOG_DIR=$RUN_DIR/logs/$JOB_ID

if grep "=== RUN SUCCESSFUL ===" $LOG_DIR/job.out; then
   cd $RUN_DIR
   mv $JOB_ID.tar.gz $RUN_DIR/outputs/tars/
   cd $RUN_DIR/outputs/untarred
   tar xzf ../tars/$JOB_ID.tar.gz
   exit 0
else
   # keep copies
   cp $LOG_DIR/job.out $LOG_DIR/job.out.checked.$TIMESTAMP
   cp $LOG_DIR/job.err $LOG_DIR/job.err.checked.$TIMESTAMP
   exit 1
fi
```

The following lines of code are used to submit the jobs to run on the OSG system for the first file called the "submit."

```
#!/bin/bash

set -e

##############################################################################
#####
#
#  SETTINGS
#

# number of jobs to run
NUMBER_JOBS=1

# max runtime (in minutes)
MAX_RUN_TIME=1000

##############################################################################
#####


# top dir
TOP_DIR=`pwd`

# runid
RUN_ID=`/bin/date +'%F_%H%M%S'``pwd | sed 's:/home/[a-z0-9]*::' | sed 's:/:_:g'`
echo "Run id is $RUN_ID"

# run dir
RUN_DIR=$TOP_DIR/runs/$RUN_ID
mkdir -p $RUN_DIR/logs

# output dir
OUTPUT_DIR=/scratch/scratch1/users/$USER/osg-output/$RUN_ID
mkdir -p $OUTPUT_DIR/tars
mkdir -p $OUTPUT_DIR/untarred
ln -s $OUTPUT_DIR $RUN_DIR/outputs

for JOB_ID in `seq 1 $NUMBER_JOBS`; do

   echo "Generating job $JOB_ID"
   mkdir -p $RUN_DIR/logs/$JOB_ID
```

```
   # create a self extractable executable - this makes stage in easy
   cd $RUN_DIR
   mkdir $JOB_ID
   cp ../../job-wrapper $JOB_ID/
   cp ../../mds $JOB_ID/
   cp ../../i3ds $JOB_ID/
   cp ../../poured.txt $JOB_ID/
   makeself --nox11 --gzip --notemp $JOB_ID $JOB_ID.sh \
         "Job Run: $RUN_ID Job: $JOB_ID" \
         ./job-wrapper >logs/$JOB_ID/makeself.out 2>&1
   rm -rf $JOB_ID

   # condor submit file
   cd $RUN_DIR
   cat >$JOB_ID.condor <<EOF
universe       = grid
grid_type      = gt2
globusscheduler = \$\$(GlueCEInfoContactString)
globusrsl      = (maxWallTime=$MAX_RUN_TIME)
requirements   = ( (TARGET.GlueCEInfoContactString =!= UNDEFINED) && \\
                 (TARGET.Rank > 300) && \\
                 ( isUndefined(TARGET.OSGMM_Success_Rate_$USER > 75) \\
                   || (TARGET.OSGMM_Success_Rate_$USER > 75) ) \\
               )

# when retrying, remember the last 5 resources tried
match_list_length = 5
Rank           = (TARGET.Rank) - \\
                 ((TARGET.Name =?= LastMatchName0) * 1000) - \\
                 ((TARGET.Name =?= LastMatchName1) * 1000) - \\
                 ((TARGET.Name =?= LastMatchName2) * 1000) - \\
                 ((TARGET.Name =?= LastMatchName3) * 1000) - \\
                 ((TARGET.Name =?= LastMatchName4) * 1000)

# make sure the job is being retried and rematched
periodic_release = (NumGlobusSubmits < 5)
globusresubmit = (NumSystemHolds >= NumJobMatches)
globus_rematch = True

# only allow for the job to be queued for a while, then try to move it
#  GlobusStatus==16 is suspended
#  GlobusStatus==32 is submitting
#  JobStatus==1 is pending
#  JobStatus==2 is running
periodic_hold = ( (GlobusStatus==16) || \\
                ( (GlobusStatus==32) && (Matched==True) && \\
```

```
                ((CurrentTime - EnteredCurrentStatus) > (15*60)) ) || \\
              ( (JobStatus==1) && \\
                ((CurrentTime - EnteredCurrentStatus) > (60*60)) ) || \\
              ( (JobStatus==2) && \\
                ((CurrentTime - EnteredCurrentStatus) > ($MAX_RUN_TIME*60)) ) )

# stay in queue on failures
on_exit_remove = (ExitBySignal == False) && (ExitCode == 0)

executable = $JOB_ID.sh
arguments = $RUN_ID $JOB_ID

stream_output = False
stream_error  = False

WhenToTransferOutput = ON_EXIT
TransferExecutable = true
transfer_output_files = $JOB_ID.tar.gz

output = logs/$JOB_ID/job.out
error = logs/$JOB_ID/job.err
log = alljobs.log

notification = NEVER

queue
EOF

   # keep a list of all the jobs we want in the dag
   JOB_LIST="$JOB_LIST $JOB_ID"
done

# generate condor dagman to manage jobs
echo
cd $RUN_DIR
for JOB_ID in $JOB_LIST; do
   echo "JOB    job_$JOB_ID $JOB_ID.condor" >>master.dag
   echo "SCRIPT PRE   job_$JOB_ID $TOP_DIR/pre-job $RUN_DIR $JOB_ID"
>>master.dag
   echo "SCRIPT POST  job_$JOB_ID $TOP_DIR/post-job $RUN_DIR $JOB_ID"
>>master.dag
   echo "RETRY  job_$JOB_ID 5" >>master.dag
done
condor_submit_dag -notification Never master.dag
```

REFERENCES

1. Aste, T., *Variations around disordered close packing.* J. Phys.: Condens. Matter, 2005. **17**: pp. S2361-S2390.

2. Adams, D.J. and A.J. Matheson, *Computation of dense random packings of hard spheres.* J. Chem. Phys., 1972. **56**: p. 1989-1994.

3. Arthur, J.R.F. and T. Dunstan, *Radiography measurements of particle packing.* Nature, 1969. **223**(2): p. 464-468.

4. Bernal, J.D. and J. Mason, *Co-ordination of randomly packed spheres.* Nature, 1960. **188**: p. 910-911.

5. Cumberland, D.J. and R.J. Crawford, *The Packing of Particles.* Handbook of Powder Technology, ed. J.C. Williams and T. Allen. Vol. 6. 1987: Elsevier.

6. Hilbert, D. and S. Cohn-Vossen, *Anschauliche Geometrie.* 1932, Berlin: Springer Verlag.

7. Onoda, G.Y. and E.G. Liniger, *Random loose packing of uniform spheres and the dilantancy onset.* Physical Review Letters, 1990. **64**: p. 2727-2731.

8. Scott, G.D. and D.M. Kilgour, *The density of random close packing of spheres.* British Journal of Applied Physics, 1969. **2**: p. 863-864.

9. Silbert, L.E., D. Ertas, G.S. Grest, T.C. Halsey, and D. Levine, *Geometry of frictionless and frictional sphere packings.* Phys. Rev. E 2002. **65**(3): p. 031304.

10. Smith, W.O., P.D. Foote, and P.F. Bussang, *Packing of homogeneous spheres.* Physical Review E, 1929. **34**(2): p. 1271-1274.

11. Torquato, S. and F.H. Stillinger, *New Conjectural Lower Bounds on the Optimal Density of Sphere Packings.* Experimental Mathematics, 2006. **15**(3): p. 307-332.

12. Tory, E.M., B.H. Church, M.K. Tan, and M. Ratner, *Simulated random packing of equal spheres.* Can. J. Chem. Eng., 1973. **51**: p. 484-493.

13. Berg, T.G.O., R.L. McDonald, and R.J.T. Jr., *The Packing of Spheres.* Powder Technology, 1969/70. **3**: p. 183-188.

14. Cundall, P.A. and O.D.L. Strack, *A discrete numerical model for granular assemblies.* Geotechnique, 1979. **29**(1): pp. 47-65.

15. Stewart, D.A., *High Quality Concrete.* 1951, London: Spon Publishers.

16. Evans, P.E. and R.S. Millman, *The Vibratory Packing of Powders.* Powder Met., 1964. **7**: p. 50-52.

17. Ayer, J.E. and F.E. Soppet, *Vibratory Compaction: I, Compaction of Spherical Shapes.* J. Am. Ceram. Soc., 1965. **48**(4): pp. 180-181.

18. D'Appolonia, D. and E. D'Appolonia. *Determination of the maximum density of cohesionless soils.* in *3rd Asian Regional Conference on Soil Mechanics and Foundation Engineering.* 1967: Jerusalem Academic Press.

19. Dobry, R. and R.V. Whitman, *Compaction of Sand on a Vertically Vibrated Table.* 1973, American Society of Testing Materials: Philadelphia. p. 156-170.

20. Zhang, N. and A.D. Rosato, *Experiments and Simulations on Vibration Induced Densification of Bulk Solids.* KONA, 2006. **24**: p. 93-103.

21. Macrae, J.C., W.A. Gray, and P.C. Finlason, *Vibration packing of dry granular solids.* Nature, 1957. **179**: p. 1365-1367.

22. Takahashi, M. and S. Suzuki, *Numerical analysis of tapping behavior of ceramic powders.* Ceramic Bulletin, 1986. **65**: p. 1587-1590.

23. Kawakita, K. and K.-H. Ludde, *Some considerations on powder compression equations.* Powder Technology, 1971. **4**(2): p. 61-68.

24. Knight, J.B., C.G. Fandrich, C.N. Lau, H.M. Jaeger, and S.R. Nagel, *Density relaxation in a vibrated granular material.* Phys. Rev. E, 1995. **51**: p. 3957-3963.

25. Jaeger, H.M. and S.R. Nagel, *Granular solids, liquids, and gases.* Rev. Mod. Phys., 1996. **68**: p. 1259-1273.

26. Jaeger, H.M., S.R. Nagel, and R.P. Behringer, *The physics of granular materials.* Physics Today, 1996. **49**(4): p. 32-38.

27. Nowak, E.R., J.B. Knight, E.B. Naim, H.M. Jaeger, and S.R. Nagel, *Density fluctuation in vibrated granular materials.* Physical Review E., 1998. **57**: p. 1971-1982.

28. Nowak, E.R., J.B. Knight, M.L. Povinelli, H.M. Jaeger, and S.R. Nagel, *Reversibility and irreversibility in the packing of vibrated granular material.* Powder Technology, 1997. **94**(1): p. 79-83.

29. Nicolas, M., P. Duru, and O. Pouliquen, *Compaction of granular material under cyclic shear.* Europhysics Letters, 2002. **60**: p. 677-683.

30. Rosato, A.D., K.J. Strandburg, F. Prinz, and R.H. Swendsen, *Why the Brazil nuts are on top: Size segregation of particulate matter by shaking.* Phys. Rev. Lett., 1987. **58**: p. 1038-1042.

31. Tobochnik, J. and P.M. Chapin, *Monte Carlo simulation of hard spheres near random closest packing using spherical boundary conditions.* Journal of Chemical Physics, 1988. **88**(9): p. 5824-5830.

32. Metropolis, N., A.W. Rosenbluth, M.N. Rosenbluth, A.H. Teller, and E. Teller, *Equation of state calculations by fast computing machines.* J. Chem. Phys., 1953. **21**(6): p. 1087-1092.

33. Rosenbluth, M.N. and A.W. Rosenbluth, *Further Results on Monte Carlo Equations of State.* Journal of Chemical Physics, 1954. **22**(5): p. 881-884.

34. Mehta, A. and G.C. Barker, *Vibrated powders: a microscopic approach.* Physical Review Letters, 1991. **67**(3): p. 394-397.

35. Barker, G.C. and A. Mehta, *Vibrated powders: structure, correlations and dynamics.* Phys. Rev. A, 1992. **45**(6): p. 3435-3446.

36. Barker, G.C. and A. Mehta, *Transient phenomena, self-diffusion, and orientational effects in vibrated powders.* Physical Review E, 1993. **47**(1): p. 184-188.

37. Coniglio, A., *Clusters and frustration in glass forming systems and granular materials.* Progress of Theoretical Physics Supplement, 1997(126): p. 281-287.

38. Coniglio, A., A. Fierro, M. Nicodemi, M.P. Ciamarra, and M. Tarzia, *Statistical mechanics of dense granular media.* Journal of Physics Condensed Matter, 2005. **17**(24): p. S2557-S2572.

39. Coniglio, A. and H.J. Herrmann, *Phase transitions in granular packings.* Physica A, 1996. **225**: p. 1-6.

40. Coniglio, A. and M. Nicodemi, *A statistical mechanics approach to the inherent states of granular media.* Physica A: Statistical Mechanics and its Applications, 2001. **296**(3-4): p. 451-459.

41. Nicodemi, M. and A. Coniglio, *Aging in out-of-equilibrium dynamics of models for granular media.* Phys. Rev. Letters, 1999. **82**: p. 916-919.

42. Nicodemi, M., A. Coniglio, and H.J. Hermann, *Density fluctuations in a model for vibrated granular media.* Phys. Rev. E, 1999. **Vol.59, N6**: p. 6830-6837.

43. Nicodemi, M., A. Coniglio, and H.J. Herrmann, *The compaction in granular media and frustrated ising models.* Journal of Physics A: Mathematical and General, 1997. **30**(11): p. L379-L385.

44. Walton, O.R., *Numerical simulation of inelastic, frictional particle-particle interactions*, in *Particulate Two-Phase Flow*, M.C. Roco, Editor. 1992, Butterworth: Boston. p. 884-911.

45. Schafer, J., S. Dippel, and D.E. Wolf, *Force schemes in simulations of granular materials.* J. Phys. I France, 1996. **6**: p. 5-20.

46. Luding, S., *Models and simulations of granular materials*, in *Theoretische Polymerphysik.* 1994, Albert-Ludwigs-Universitat: Freiburg. p. 125-138.

47. Liu, L.F., Z.P. Zhang, and A.B. Yu, *Dynamic Simulation of the Centripetal Packing of Mono-Sized Spheres.* Physica A, 1999. **268**: p. 433-453.

48. Cheng, Y.F., S.J. Guo, and H.Y. Lai, *Dynamic simulation of random packing of spherical particles.* Powder Tech, 2000. **107**: p. 123-130.

49. Rosato, A.D., D.L. Blackmore, N. Zhang, and Y. Lan, *A perspective of vibration-induced size segregation of granular materials.* Chemical Engineering Science, 2002. **57**: p. 265-275.

50. An, X.Z., R.Y. Yang, K.J. Dong, R.P. Zou, and A.B. Yu, *Micromechanical simulation and analysis of one-dimensional vibratory sphere packing.* Physical Review Letters, 2005. **95**: p. 205502.

51. A.B. Yu, An, X.Z., R.P. Zou, R.Y. Yang, and K.J. Kendall, *Self-Assembly of Particles for Densest Packing by Mechanical Vibration.* Physical Review Letters, 2006. **97**: p. 265501.

52. Arsenovic, D., S.B. Vrhovac, Z.M. Jaksic, L. Budinski-Petkovic, and A. Belic, *Simulation Study of Granular Compaction Dynamics under Vertical Tapping.* Physical Review E, 2006. **74**: p. 061302-1-14.

53. Linz, S.J., *Phenomenological Modeling of the Compaction Dynamics of Granular Systems.* Phys. Rev. E, 1996. **54**: p. 292501-292504.

54. Peng, G. and T. Ohta, *Logarithmic density relaxation in compaction of granular materials.* Phys. Rev. E, 1998. **57**: p. 829-833.

55. Brey, J.J. and A. Prados, *Linear response of vibrated granular systems to sudden changes in the vibration intensity.* Physical Review E, 2001. **63**: p. 061301-1.

56. Brey, J.J., A. Prados, and B. Sanchez-Rey, *Thermodynamic description in a simple model for granular compaction.* Physica A: Statistical Mechanics and its Applications, 2000. **275**(3): p. 310-324.

57. Round, G.F. and R. Newton, *Random Packing of Equal Spheres on a Plane Surface.* Nature, 1963. **198**(4882): p. 747-750.

58. Josserand, C., A.V. Tkahenko, D.M. Mueth, and H.M. Jaeger, *Memory effects in granular materials.* Physical Review Letters, 2000. **85**(17): p. 3632-3635.

59. Rosato, A.D., D.L. Blackmore, N. Zhang, and Y. Lan, *A perspective on vibration-induced size segregation of granular materials.* Chemical Engineering Science, 2002. **57**(2): p. 265-275.

60. Powell, M.J., *Distribution of Near Neighbors in Randomly Packed Hard Spheres.* Powder Technology, 1980. **26**: p. 221-223.

61. Luding, S., E. Clement, A. Blumen, J. Rajchenbach, and J. Duran, *Studies of columns of beads under external vibrations.* Physical Review E, 1994. **49**(2): p. 1634-1641.

62. Ribiere, P., P. Philippe, P. Richard, R. Delannay, and D. Bideau, *Slow compaction of granular systems.* J. Phys.: Condens. Matter, 2005. **17**: p. S2743-S2754.

63. Ribiere, P., P. Richard, R. Delannay, and D. Bideau, *Importance of convection in the compaction mechanisms of anisotropic granular media.* Physical Review E, 2005. **71**: p. 011304.

64. Ribiere, P., P. Richard, R. Delannay, D. Bideau, M. Toiya, and W. Losert, *Effect of rare events on out-of-equilibrium relaxation.* Physical Review Letters, 2005. **95**(26): p. 1-4.

65. Ribiere, P., P. Richard, P. Phillipe, D. Bideau, R. Delannay, *On the existence of stationary states during granular compaction.* European Physics Journal E, 2007. **22**(3): p. 249-253.

66. Knight, J.B., C.G. Frandrich, C.N. Lau, H.M. Jaeger, and S.R. Nagel, *Density relaxation in a vibrated granular material.* Physical Review E, 1995. **51**: p. 3957-3963.

67. Jaeger, H.M., S.R. Nagel, and R.P. Behringer, *Granular Solids, Liquids and Gases.* Reviews of Modern Physics, 1996. **68**: p. 1259 - 1273.

68. Linz, S. and A. Dohle, *Minimal relaxation law for compaction of tapped granular matter.* Phys. Rev. E, 1999. **60**(5): p. 5737-5741.

69. Lumay, G., F. Ludewig, and N. Vandewalle, *Compaction of granular materials: Experiments and contact dynamics simulations.* Journal of Physics: Conference Series, 2006. **40**(1): p. 133-143.

70. Ciamarra, M.P., A. Coniglio, and M. Nicodemi, *Thermodynamics and statistical mechanics of dense granular media.* Physical Review Letters, 2006. **97**(15).

71. Ciamarra, M.P., M. Nicodemi, and A. Coniglio, *Granular Packs under Vertical Tapping: Structure Evolution, Grain Motion and Dynamic Heterogeneities.* Physical Review E, 2007. **75**: p. 021303-1-10.

72. Ciamarra, and A. Coniglio, *Random Very Loose Packings.* Physical Review Letters, 2008. **101**: p. 128001.

73. Nolan, G.T. and P.E. Kavanagh, *Octahedral Configurations in Random Close Packing.* Powder Technology, 1995. **83**: p. 253-258.

74. Bratberg, I., K.J. Maloy, and A. Hansen, *Validity of the Janssen law in narrow granular columns.* European Physical Journal E, 2005. **18**: p. 245-252.

75. Cargill, G.S., *Dense Random Packing of Hard Spheres as a Structural Model for Noncrystalline Metallic Solids.* J of Appl Physics, 1970. **41**(5): p. 2248-2250.

76. Beresford, R.H., *Statistical Geometry of Random Heaps of Equal Hard Spheres.* Nature, 1969. **224**: p. 550-553.

77. Torquato, S., T.M. Truskett, and P.G. Debenedetti, *Is Random Close Packing of Spheres Well Defined?* Phys. Rev. Lett., 2000. **84**: p. 2064-2067.

78. He, D., N.N. Ekere, and L. Cai, *New Statistic Techniques for Structure Evaluation of Particle Packing.* Materials Science and Engineering, 2001. **A298**: p. 209-215.

79. Gotoh, K. and J.L. Finney, *Statistical geometrical approach to random packing density of equal spheres.* Nature, 1974. **252**: p. 202-205.

80. Iwata, H. and T. Homma, *Distribution of Coordination Numbers in Random Packing of Homogeneous Spheres.* Powder Technology, 1974. **10**: p. 79-83.

81. Mueller, G.E., *Numerically Packing Spheres in Cylinders.* Powder Technology, 2005. **159**: p. 105-110.

82. Kumar, V.S. and V. Kumaran, *Voronoi neighbor statistics of hard-disks and hard-spheres.* Journal of Chemical Physics, 2005. **123**: p. 074502.

83. Kumar, V.S. and V. Kumaran, *Voronoi cell volume distribution and configurational entropy of hard-spheres.* J. Chem. Phys., 2005. **123**(11): p. 114501-114503.

84. Levine, M.M. and J. Chernick, *A Numerical Model of Random Packing of Spheres.* Nature, 1965. **208**: p. 68-69.

85. Suzuki, M., K. Makino, M. Yamada, and K. Linoya, *A Study on the Co-ordination Number in a System of Randomly Packed, Uniform-Sized Spherical Particles.* International Chemical Engineering, 1981. **21**: p. 482-485.

86. Rumpf, J., *Grundlagen und Methoden des Granulierens.* Chemie-Ingenieur-Technik, 1958. **3**: p. 144–158.

87. Ridgway, K. and K.J. Tarbuck, *The Random Packing of Spheres.* British Chemical Engineering, 1967. **12**: p. 384-385.

88. Ouchiyama, N. and T. Tanaka, *Estimation of the average number of contacts between randomly mixed solid particles.* Industrial and Engineering Chemical Fundamentals, 1980. **19**: p. 338-340.

89. Hill, T., *Statistical Mechanics.* 1956, New York: McGraw-Hill.

90. Powell, M.J., *Computer-simulated random packing of spheres.* Powder Technology, 1980. **25**: p. 45-52.

91. Rosato, A.D. and D. Yacoub, *Microstructure evolution in compacted granular beds.* Powder Technology, 2000. **109**: p. 255-261.

92. Sweetman, M., *Addition of a chain-cell search method and a van der Waals force model to a particle dynamics code*, in *Mechanical Engineering*. 2003, New Jersey Institute of Technology: Newark, NJ.

93. Dybenko, O. M., *Density Relaxation of Granular Matter through Monte Carlo and Granular Dynamics Simulations*, in *Mechanical Engineering*. 2008, New Jersey Institute of Technology: Newark, NJ.

94. Allen, M.P. and D.J. Tildesley, *Computer Simulation of Liquids.* 1989: Oxford University Press. 385-387.

95. Haile, J.M., *Molecular Dynamics Simulation: Elementary Methods.* 1992: J. Wiley and Sons. 489-492.

96. Walton, O.R. and R.L. Braun, *Stress calculations for assemblies of inelastic spheres in uniform shear.* Acta Mechanica, 1986. **63**: p. 73-86.

97. Mindlin, R.D. and H. Deresiewicz, *Elastic spheres in contact under varying oblique forces.* J. Appl. Mech., 1953. **20**: p. 327-328.

98. Alcocer, F.J., V. Kumar, and P. Singh, *Permeability of Periodic Porous Media.* Physical Review E, 1999. **59**(1): p. 711-714.

99. Singh, P. and D.D. Joseph, *Dynamics of fluidized suspensions of spheres of finite size.* Int. J. Multiphase Flows, 1995. **21**: p. 1-26.